SLAC – 300
UC – 34D
(E)

A MEASUREMENT OF THE AVERAGE LIFETIME OF HADRONS CONTAINING BOTTOM QUARKS*

Daniel Edward Klem

Stanford Linear Accelerator Center
Stanford University
Stanford, California 94305

June 1986

Prepared for the Department of Energy
under contract number DE-AC03-76SF00515

Printed in the United States of America. Available from the National Technical Information Service, U.S. Department of Commerce, 5285 Port Royal Road, Springfield, Virginia 22161. Price: Printed Copy A07, Microfiche A01.

* Ph.D. Thesis

Abstract

This thesis reports a measurement of the average lifetime of hadrons containing bottom quarks. It is based on data taken with the DELCO detector at the PEP e^+e^- storage ring at a center of mass energy of 29 GeV. The decays of hadrons containing bottom quarks are tagged in hadronic events by the presence of electrons with a large component of momentum transverse to the event axis. Such electrons are identified in the DELCO detector by an atmospheric pressure Čerenkov counter assisted by a lead/scintillator electromagnetic shower counter. The lifetime measured is $1.17^{+0.27}_{-0.22}$ (stat.) $^{+0.17}_{-0.16}$ (sys.) psec, consistent with previous measurements. This measurement, in conjunction with a limit on the non-charm branching ratio in b-decay obtained by other experiments, can be used to constrain the magnitude of the V_{cb} element of the Kobayashi-Maskawa matrix to the range $0.042^{+0.005}_{-0.004}$ (stat.) $^{+0.004}_{-0.002}$ (sys.), where the errors reflect the uncertainty on τ_b only and not the uncertainties in the calculations which relate the b-lifetime and the element of the Kobayashi-Maskawa matrix.

Acknowledgments

It goes with out saying that an experiment of this size requires the efforts of a great many people. I particularly wish to thank the 38 other physicists who worked on DELCO: W.B. Atwood, P.H. Baillon, B.C. Barish, G.R. Bonneaud, A. Courau, H. DeStaebler, G.J. Donaldson, R. Dubois, M.M. Duro, E.E. Elsen, S.G. Gao, Y.Z. Huang, G.M. Irwin, R.P. Johnson, H. Kichimi, J. Kirkby, D.E. Koop, J. Ludwig, G.B. Mills, A. Ogawa, T. Pal, D. Peret-Galix, R. Pitthan, D.L. Pollard, C.Y. Prescott, L.Z. Rivkin, L.S. Rochester, W. Ruckstuhl, M. Sakuda, S.S. Sherman, E.J. Siskind, R. Stroynowski, R.E. Taylor, S.Q. Wang, S.G. Wojcicki, H. Yamamoto, W.G. Yan, and C.C. Young; as well as the technical staffs of Caltech and SLAC groups A and G. The lifetime measurement reported here would not have been possible without the electron analysis which is described in Chapter 3. The people primarily responsible for this work are D.E. Koop, T. Pal, and M. Sakuda. I also wish to give particular thanks to Richard Dubois and Charlie Young for their help in the early stages of this work; to my advisor Charlie Prescott for his guidance over the last several years; to Bill Atwood for his many helpful suggestions, and to John Jaros for several helpful discussions. The preparation of this manuscript was aided by the Psizzl macros written by Art Ogawa.

Finally, I would like to thank my father who sparked my interest in the physical sciences, and most of all I would like to thank my wife Karen for her careful proofreading of the manuscript and her support and companionship over the last few years.

Table of Contents

List of Tables

List of Figures

1. INTRODUCTION

This thesis reports a measurement of the average lifetime of hadrons containing bottom quarks. It is based on the data taken with the DELCO detector at the PEP e^+e^- storage ring during the years 1982 to 1984. Hadrons containing bottom quarks (B-hadrons) are produced by electron positron annihilation at the storage ring with a cross section of approximately $3 \cdot \frac{4\pi\alpha^2}{3s} e_q^2$ ($e_q = -\frac{1}{3}$ is the b-quark charge).[1] At a center of mass energy of $\sqrt{s} = 29$ GeV this amounts to 34.4 pb. This production of B-hadrons is understood to be the result of the production of a $b\bar{b}$ quark pair (or quark pairs plus gluons, $b\bar{b}g$), followed by the subsequent "fragmentation" of this system into hadrons. Two of the subsequent hadrons will contain one of the original b-quarks. The properties of these hadrons are dominated by the characteristics of the b-quark. Because of this, while the hadron is thought to be a spin-0 boson, its decays are in some ways characteristic of a heavy spin-$\frac{1}{2}$ fermion. Among these characteristics is a large branching fraction ($\approx 10 - 15\%$) into the light leptons (e, μ) with a momentum spectrum characteristic of a V-A interaction. This is typical for a decay which proceeds through the production of a virtual $W^{\pm}$ (the intermediate vector boson). The copious production of electrons in the decays of B-hadrons makes it possible to tag these events with reasonable efficiency. Fig. 1.1 shows an example of such an event recorded by the DELCO detector. Because B-hadrons decay by way of the weak interaction, their lifetime is comparatively long. This makes it possible to measure the average lifetime of these particles by looking at the displacement of the tracks from the decay products relative to the point where the hadrons were first produced. The remainder of this thesis discusses the many details involved.

1.1 THEORETICAL CONSIDERATIONS

The Standard Model [$SU(2) \times U(1) \times SU(3)_{color}$], which appears to provide an adequate[2] description of the decay of heavy (bottom and charmed) hadrons, is briefly summarized in Fig. 1.2. It contains three "generations" of quarks and

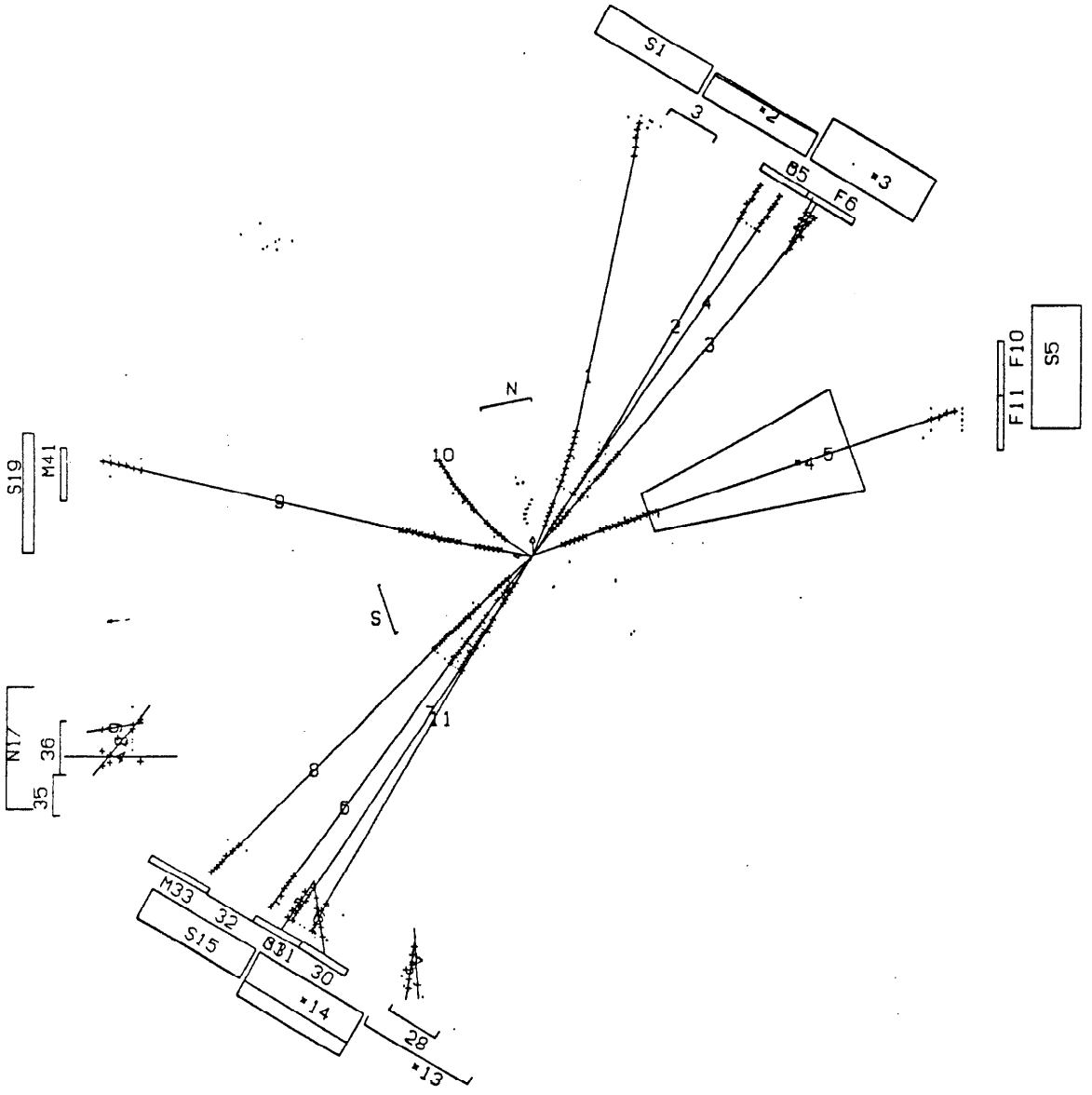

Figure 1.1. A high p_t electron in a hadronic event logged by the DELCO detector at PEP. The electron is identified by the Čerenkov counter (the large trapezoid in the first quadrant of the figure) in conjunction with the lead/scintillator shower counters (the rectangles around the periphery). The Čerenkov counters provide efficient electron identification at low momentum. The electron in this event has a p_t relative to the sphericity axis greater than 1 GeV and is probably from the decay of a B-hadron. See the next chapter for a more complete discussion of the detector.

SPIN $\frac{1}{2}$ FERMIONS

Quarks

$u_r \;\; d_r$	$c_r \;\; s_r$	$t_r \;\; b_r$	← singlets
$\begin{pmatrix} u \\ d \end{pmatrix}_l$	$\begin{pmatrix} c \\ s \end{pmatrix}_l$	$\begin{pmatrix} t \\ b \end{pmatrix}_l$	← doublets

Leptons

e_r^-	μ_r^-	τ_r^-	← singlets
$\begin{pmatrix} \nu_e \\ e^- \end{pmatrix}_l$	$\begin{pmatrix} \nu_\mu \\ \mu^- \end{pmatrix}_l$	$\begin{pmatrix} \nu_\tau \\ \tau^- \end{pmatrix}_l$	← doublets

GAUGE BOSONS

$$\gamma \, , \; W^{\pm} \, , \; Z^o \, , \; g$$

Figure 1.2. A summary of the Standard Model. Quarks and leptons are subscripted l or r for the left-handed and the right-handed components respectively.

leptons. For instance the lightest generation consists of the leptons e^- and ν_e and the quarks u and d. Within a generation the quarks and leptons are further grouped according to their weak interactions. In the first generation the left-handed part of the u and the d quarks form a weak isodoublet as do the left-handed parts of the e^- and the ν_e. The right-handed parts of the u and d quarks as well as the right-handed part of the e^- are all in weak isosinglets. Transitions within the doublets are mediated by the charged vector boson $W^{\pm}$. For our present purposes the effects of the photon (γ) and the neutral vector boson (Z^o) will be neglected. This is possible because firstly neither one changes the "flavor" of the particle with which it interacts and therefore it is not possible for it to be responsible for a decay,

Table 1.1. Quark composition of some hadrons containing bottom quarks. An asterisk in the mass column indicates that the particle is expected to exist, but has not yet been observed.

HADRON	quarks	mass (GeV)
B^-	$b\bar{u}$	5.271
$\bar{B}^o$	$b\bar{d}$	5.274
B_s	$b\bar{s}$	*
Λ_B	bdu	*

and secondly, to the accuracy with which these calculations are done, neither one introduces a significant radiative correction. The remaining gauge boson, the gluon (g), is also not capable of initiating the decay of heavy quarks, but it produces a correction to the decay rate. The gluon couples only to the quarks which carry the SU(3) color charge (hence the distinction between quarks and leptons). These QCD corrections are not necessarily small and it is not possible to calculate them in all the cases where it would be useful. This difficulty is ameliorated by the availability of measurements of the ratio of $B \rightarrow Xe$ to $B \rightarrow X$† (the semileptonic branching ratio).

The B-hadrons, whose lifetimes are reported on in this thesis, are composed of a single b-quark and some other combination of quarks so that the total color charge of the hadron is zero. Some of the possibilities are shown in Table 1.1. The simplest model of heavy quark decay ignores the presence of these so called "spectator quarks" and computes the decay rate as if the heavy quark were an isolated free object. This is shown schematically by the diagram in Fig. 1.3. Since $m_t > m_b$ it is clear that in the absence of mixing between the generations the decay rate would be exactly zero. Because heavy quarks (including the bottom quark) do decay, it must be that the weak interaction eigenstates are not the same as the mass eigenstates.

† The symbol X stands for anything.

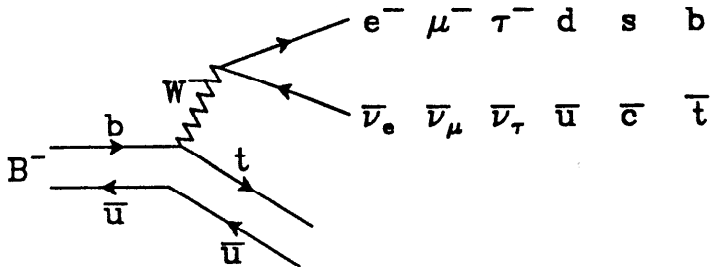

Figure 1.3. Contributions to B-meson decay in the spectator model assuming no mixing between the generations. Multiple labels on the top two fermion lines represent the six different diagrams which could in principle contribute to the decay.

This mixing is described by the Kobayashi-Maskawa[3] (K-M) matrix:

$$\begin{pmatrix} d' \\ s' \\ b' \end{pmatrix} = \begin{pmatrix} V_{ud} & V_{us} & V_{ub} \\ V_{cd} & V_{cs} & V_{cb} \\ V_{td} & V_{ts} & V_{tb} \end{pmatrix} \cdot \begin{pmatrix} d \\ s \\ b \end{pmatrix}, \tag{1.1}$$

where the primed quarks are now eigenstates of the weak interactions. Constraints of unitarity and the ability to remove unphysical phases from the matrix by redefining the phases of the quark states can be used to restrict the K-M matrix. For the case of three families of quarks, which is being considered here, it is possible to reduce the number of parameters in the matrix from 18 to 4. A typical parameterization in terms of 3 angles (ϕ, θ, ψ) and a phase (δ) is

$$\begin{pmatrix} c_\phi & s_\phi\, c_\psi & s_\phi\, s_\psi \\ -s_\phi\, c_\theta & c_\phi\, c_\theta\, c_\psi - e^{i\delta} s_\theta\, s_\psi & c_\phi\, c_\theta\, s_\psi + e^{i\delta} s_\theta\, c_\psi \\ s_\phi\, s_\theta & -c_\phi\, s_\theta\, c_\psi - e^{i\delta} c_\theta\, s_\psi & -c_\phi\, s_\theta\, s_\psi + e^{i\delta} c_\theta\, c_\psi \end{pmatrix}. \tag{1.2}$$

In this expression $c_\phi = \cos\phi$, $s_\phi = \sin\phi$ and so forth. The mixing introduced by the K-M matrix results in the single diagram in Fig. 1.3 being replaced by the

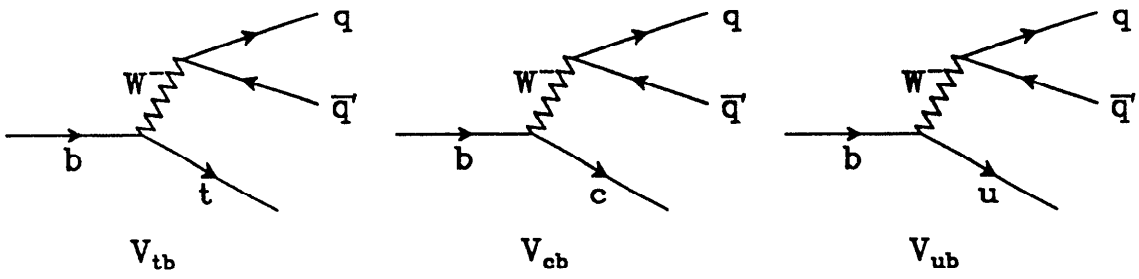

Figure 1.4. Contributions to b-quark decay in the presence of mixing. Each diagram has an amplitude proportional to the element of the K-M matrix shown directly beneath it. The fermion pair labeled $q\bar{q}'$ can be any of the six pairs of fermions shown in Fig. 1.3.

three diagrams in Fig. 1.4. As before the diagram involving a $b \rightarrow t$ transition does not contribute. The amplitude of each diagram is proportional to the corresponding element of the mixing matrix. The total decay rate can then be written in the form:

$$\Gamma_{tot} = \Gamma(b \rightarrow cX) + \Gamma(b \rightarrow uX), \tag{1.3}$$

where $\Gamma(b \rightarrow cX)$ and $\Gamma(b \rightarrow uX)$ are presumably calculable in the standard model and proportional to $|V_{cb}|^2$ and $|V_{ub}|^2$ respectively. It is possible to calculate $\Gamma(b \rightarrow cX)$ and $\Gamma(b \rightarrow uX)$ by summing all of the various decay modes represented by the $q\bar{q}'$ in Fig. 1.4.[4,5] This involves calculating the amplitudes for the diagrams where $q\bar{q}'$ is a pair of quarks. Because of QCD effects these calculations are more uncertain than the calculations for the semileptonic decays. This difficulty can be avoided by making use of the measured semileptonic branching ratio for the decay of B-hadrons:

$$BR(b \rightarrow Xe\bar{\nu}_e) = \frac{\Gamma(b \rightarrow ce\bar{\nu}_e) + \Gamma(b \rightarrow ue\bar{\nu}_e)}{\Gamma(b \rightarrow cX) + \Gamma(b \rightarrow uX)}. \tag{1.4}$$

Plugging this expression into equation 1.3 gives

$$\Gamma_{tot} = \frac{1}{BR(b \rightarrow Xe\bar{\nu}_e)} \left[\Gamma(b \rightarrow ce\bar{\nu}_e) + \Gamma(b \rightarrow ue\bar{\nu}_e)\right]. \tag{1.5}$$

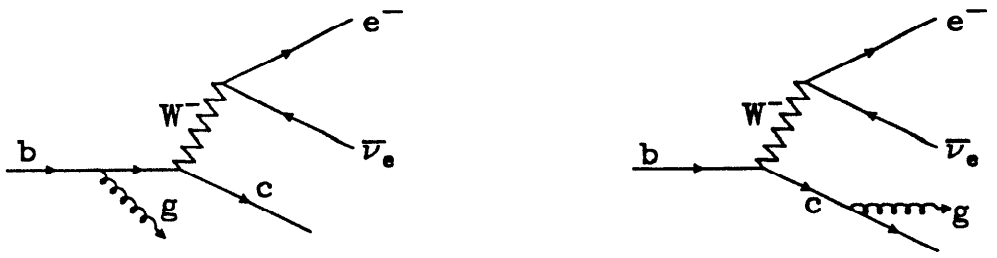

Figure 1.5. QCD corrections due to soft gluon radiation from either the initial or the final quark leg.

One is then left with the job of calculating $\Gamma(b \to ce\bar{\nu}_e)$ and $\Gamma(b \to ue\bar{\nu}_e)$. The relevant matrix element is

$$M = \frac{G}{\sqrt{2}} V_{qb} \bar{e}\gamma_\mu(1+\gamma_5)\nu_e \bar{q}\gamma^\mu(1+\gamma_5)b. \tag{1.6}$$

The task of squaring this and integrating over the appropriate phase space is left to Appendix D. The result is

$$\Gamma(b \to qe\bar{\nu}_e) = |V_{qb}|^2 \frac{G^2 m_b^5}{192\pi^3}\left[1 - 8z^2 + 8z^6 - z^8 - 24z^4 \ln z\right], \tag{1.7}$$

where q is c or u and $z = \frac{m_q}{m_b}$. The $\frac{G^2 m_b^5}{192\pi^3}$ term is the well known expression for the muon lifetime with the muon mass replaced by the bottom quark mass. The term in the parenthesis is a correction due to the not necessarily negligible mass of the final state quark and will be referred to as $g(z)$.

There are also small modifications to the above expressions due to radiative QCD corrections. To the lowest order in α_s, two sets of graphs contribute. The first, which corresponds to the radiation of a gluon off either the initial or the final quark leg, is shown in Fig. 1.5. The second set, which represents the radiation and subsequent reabsorption of a gluon is shown in Fig. 1.6. The matrix elements for these processes have been calculated[6] and integrated first

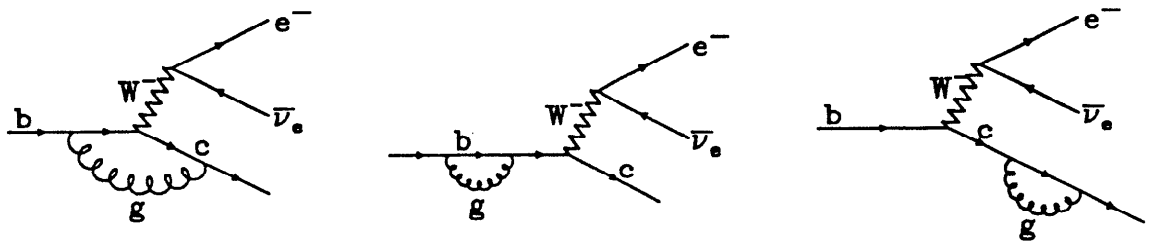

Figure 1.6. QCD corrections due to radiation and subsequent reabsorption of a gluon from one of the two quark legs of the graph.

numerically[6] and then analytically[7,8] to obtain the electron spectrum. This, in turn, can be integrated to obtain the total rate. For the case at hand parts of this procedure can be by-passed. It was observed some time ago that the QCD corrections to heavy quark decay are simply related to the QED corrections to muon decay.[9] Therefore it is possible to obtain the corrections to the decay rate for heavy quarks by integrating the electron spectrum from muon decay after making the substitution:

$$\alpha \rightarrow \frac{1}{4}\alpha_s \sum_{i=1}^{8} \lambda^i \lambda^i = \frac{4}{3}\alpha_s, \tag{1.8}$$

where

$$\alpha_s = \frac{12\pi}{(33 - 2n_f)\ln\left(\frac{m_b^2}{\Lambda^2}\right)}. \tag{1.9}$$

In the above n_f is the number of flavors, m_b is the mass of the bottom quark, and $\Lambda = 0.2$ GeV. This produces $\alpha_s = 0.28$. The electron spectrum from muon decay has been calculated as a function of $\frac{m_e}{m_\mu}$.[10,11,12] This spectrum (which corresponds to the momentum spectrum of the charmed quark in b-decay) has been integrated in ref. 9 for various values of $\frac{m_c}{m_b}$. The result is to modify the previous expression

for $\Gamma\left(b \rightarrow qe\bar{\nu}_e\right)$ to

$$\Gamma(b \rightarrow qe\bar{\nu}_e) = |V_{qb}|^2 \frac{G^2 m_b^5}{192\pi^3} g(z) \left[1 - \frac{2}{3\pi}\alpha_s f(z)\right]. \tag{1.10}$$

The function f(z) is tabulated in ref. 9 and is plotted in Fig. 1.7 along with the phase space correction which appears in equation 1.7. Taking $m_b = 4.7$ GeV, $m_c = 1.5$ GeV, and $m_u = 0.15$ GeV gives $g(z) = 0.48$ and $f(z) = 2.5$ for $b \rightarrow c$ and $g(z) = 0.99$ and $f(z) = 3.5$ for $b \rightarrow u$. The total semileptonic rate is then

$$\Gamma(b \rightarrow Xe\bar{\nu}_e) = \frac{G^2 m_b^5}{192\pi^3} \left[0.41 \cdot |V_{cb}|^2 + 0.79 \cdot |V_{ub}|^2\right]. \tag{1.11}$$

This calculation suffers from a large uncertainty due to the factor of m_b^5. While the masses of the B-mesons are well known, the m_b which appears in the expression is the mass of the "bare" quark and is uncertain at least at the level of 0.2 to 0.4 GeV. This produces an uncertainty on Γ which is comparable to that due to the error on τ_b.

The difficulty associated with the m_b^5 term can be alleviated (albeit in a model dependent way) by using some of the information which can be obtained from the momentum spectrum of electrons produced in the decay of B-mesons. The end point of the electron spectrum is sensitive to the mass of the bottom quark as well as to the mass of the charmed quark. B-mesons are produced copiously in e^+e^- annihilations at the $\Upsilon(4S)$. Two experiments at CESR have reported results on the lepton spectrum.[14,15] In fitting the momentum spectrum from the decay $b \rightarrow ce\bar{\nu}_e$ it is necessary to account for the effect of the binding of the bottom quark to the spectator quark. The model used here is due to Altarelli *et. al.*[13] It accounts for the Fermi motion within the meson in a way which respects kinematic constraints. In particular, if the B-meson has a mass of M_B and the spectator quark has a mass of m_{sp}, then the b-quark mass is taken to be

$$m_b^2 = M_B^2 + m_{sp}^2 - 2M_B\sqrt{\vec{p}^2 + m_{sp}^2}, \tag{1.12}$$

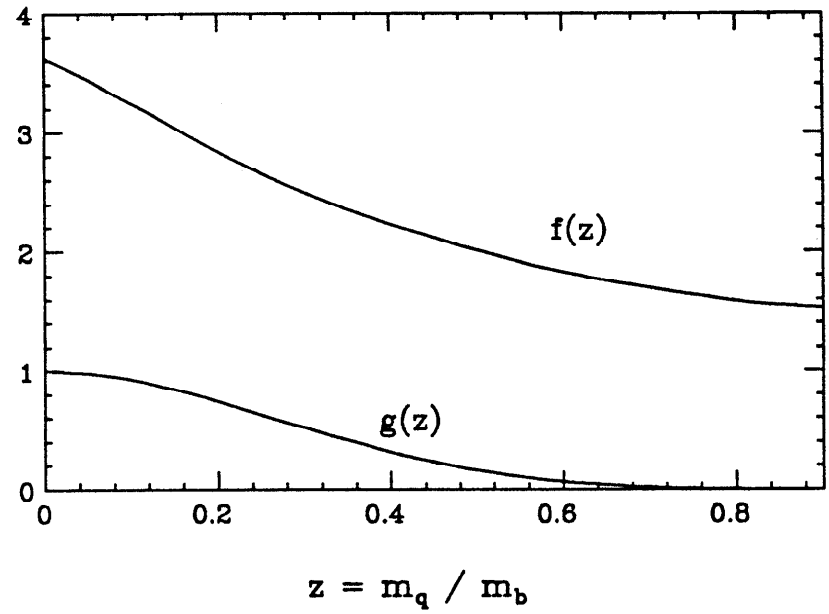

Figure 1.7. Corrections to the leptonic decay rate of B-hadrons. The lower curve labelled g(z) is simply a phase space correction caused by the non-negligible mass of the charmed quark in the final state. The upper curve is due to lowest order QCD corrections to the simple spectator model calculations (see equation 1.10). This analysis uses $z = 0.34$.

where $\vec{p}$ is the spectator momentum which is randomly distributed according to

$$P(p)p^2dp = \frac{4}{\sqrt{\pi}p_F^3}\exp\left(-\frac{|p|^2}{p_F^2}\right)p^2dp. \tag{1.13}$$

In this expression p_F is a parameter which describes the Fermi motion. J. Lee-Franzini has used this procedure to fit the CUSB electron data taken at the $\Upsilon(4S)$.[16] The fit takes into account gluon corrections as calculated in ref. 8 and accounts for the initial velocity of the B-meson, detector resolution, and other sources of electrons. She finds $m_b \approx 5.0$ GeV and $m_c \approx 1.7$ GeV. Acceptable fits are obtained using various values of m_{sp} and p_F in the range of 0 to 300 MeV. The uncertainty on m_b and m_c associated with this is apparently small (≈ 0.05 GeV) compared to the uncertainty on τ_b. While this model has an obvious intuitive appeal, it is not clear how large the systematic uncertainties associated with it are. Using the

values of m_b and m_c obtained above and $m_u = 0.15$ GeV, the total semileptonic decay rate is

$$\Gamma(b \to Xe\bar{\nu}_e) = \frac{G^2 m_b^5}{192\pi^3}\left[0.37 \cdot |V_{cb}|^2 + 0.79 \cdot |V_{ub}|^2\right]. \tag{1.14}$$

For $m_b = 5.0$ GeV the $\frac{G^2 m_b^5}{192\pi^3}$ term becomes $1.08 \cdot 10^{24}$ sec^{-1} so that the total rate can be written as

$$\Gamma(b \to Xe\bar{\nu}_e) = \left[0.40 \cdot |V_{cb}|^2 + 0.85 \cdot |V_{ub}|^2\right] \cdot 10^{14}\text{sec}^{-1}. \tag{1.15}$$

An alternative approach is to calculate the semileptonic decay rates of B-mesons into specific decay products and to then sum the different channels to get the total rate.[17,18] This requires a model for the B-meson involved as well as for its weak interactions. The matrix element is modified so that it has the form (for $B \to X_q e\bar{\nu}_e$; q = b, c):

$$M = \frac{G}{\sqrt{2}} V_{qb} \bar{e}\gamma_\mu(1+\gamma_5)\nu_e \ \langle X_q(p_x, s_x)|j^\mu_{qb}|B(p_B)\rangle. \tag{1.16}$$

The new object on the right hand side describes the hadronic part of the decay. In refs. 17 and 18 the hadrons are described by a non-relativistic quark potential model. Within this model the quarks are given masses of $m_u = m_d = 0.33$ GeV, $m_s = 0.55$ GeV, $m_c = 1.82$ GeV, and $m_b = 5.12$ GeV. The authors find that for the decay $B \to X_c e\bar{\nu}_e$ the decays to D and D* account for nearly the entire rate. They find the contribution to the total rate from b → c decays to be $0.58 \cdot 10^{14}|V_{cb}|^2$ sec^{-1}. The uncertainty on this, which comes from varying the wave functions in the quark model, is estimated to be less than 20%. This compares with a rate of $0.49 \cdot 10^{14}|V_{cb}|^2$ sec^{-1} which is obtained for free quarks with the masses used in this model. For the case of $B \to X_u e\bar{\nu}_e$, they find that the total rate is not saturated by the decays to the lowest lying states and that the absolute normalization of their answer is quite sensitive to the wave functions used. They suggest using a free

quark rate of $1.18 \cdot 10^{14}|V_{ub}|^2$ sec^{-1} for the b $\rightarrow$ u decays. This results in a total semileptonic rate given by

$$\Gamma(b \rightarrow Xe\bar{\nu}_e) = \left[0.58 \cdot |V_{cb}|^2 + 1.18 \cdot |V_{ub}|^2\right] \cdot 10^{14}\text{sec}^{-1}. \qquad (1.17)$$

This differs substantially from equation 1.15. For the b $\rightarrow$ u transition this difference stems partially from the larger value of m_b ($\approx 10\%$) and partially from the lack of a QCD correction ($\approx 20\%$). Since the b $\rightarrow$ u transition makes only a negligible contribution to the total rate (see Chapter 6), this difference does not affect the constraints on $|V_{cb}|$. The difference for the b $\rightarrow$ c transition is larger than for the b $\rightarrow$ u transition and directly affects the constraints on $|V_{cb}|$. The factor of 0.58 in equation 1.17 is approximately 20% larger than the corresponding free quark factor of 0.49. This is within the 20% uncertainty claimed by the authors in ref. 17. The free quark factor of 0.49 is approximately 20% larger than what appears in equation 1.15. This difference is due to the different quark masses and the lack of a QCD correction.

2. THE DELCO DETECTOR

This thesis is based on data taken with the DELCO† detector at the PEP e^+e^- storage ring. Fig. 2.1 shows a cross section of the detector and Fig. 2.2 shows an end-on view. DELCO ran at interaction region 8 until the spring of 1984. It logged data corresponding to a total luminosity of 214 pb^{-1}. All of this data was taken at a center of mass energy of 29 GeV. The DELCO detector emphasizes the identification of electrons at relatively low momenta. The detector combines charged particle tracking from drift chambers in a magnetic field with particle identification from an atmospheric pressure Čerenkov counter. Since one of the principle aims of the detector was to study the production of electrons from the decay of heavy (charm and bottom) quarks, particular attention was given to the problem of detecting electrons in hadronic events. The major backgrounds come from the production of real electrons by gamma conversions and Dalitz decays. Particular effort has been made to minimize the amount of material before the Čerenkov counters and thereby minimize the number of conversion electrons produced. The material between the beams and the beginning of the gas volume in the Čerenkov counter amounts to only 3% of a radiation length for the final configuration of the detector. This material is summarized in Table 2.1. There is a second set of drift chambers outside the Čerenkov counters. In addition to providing tracking information, gamma conversions which are not detected in the inner tracking chambers can sometimes be tagged by the presence of track stubs in these chambers.

2.1 Charged Particle Tracking

The direction and momentum of charged particles are measured by three sets of drift chambers in a magnetic field. The magnetic field is produced by a set of coils and an iron flux return. The field (which is far from uniform) is 3.3 kG at the center of the detector and has a total integrated bending strength of 1.8 kG-m. The momentum resolution is $\frac{\sigma_p}{p} = (0.02^2 + 0.06^2 p^2)^{\frac{1}{2}}$, where the first term comes from

† DELCO is an acronym for the Direct ELectron COunter.

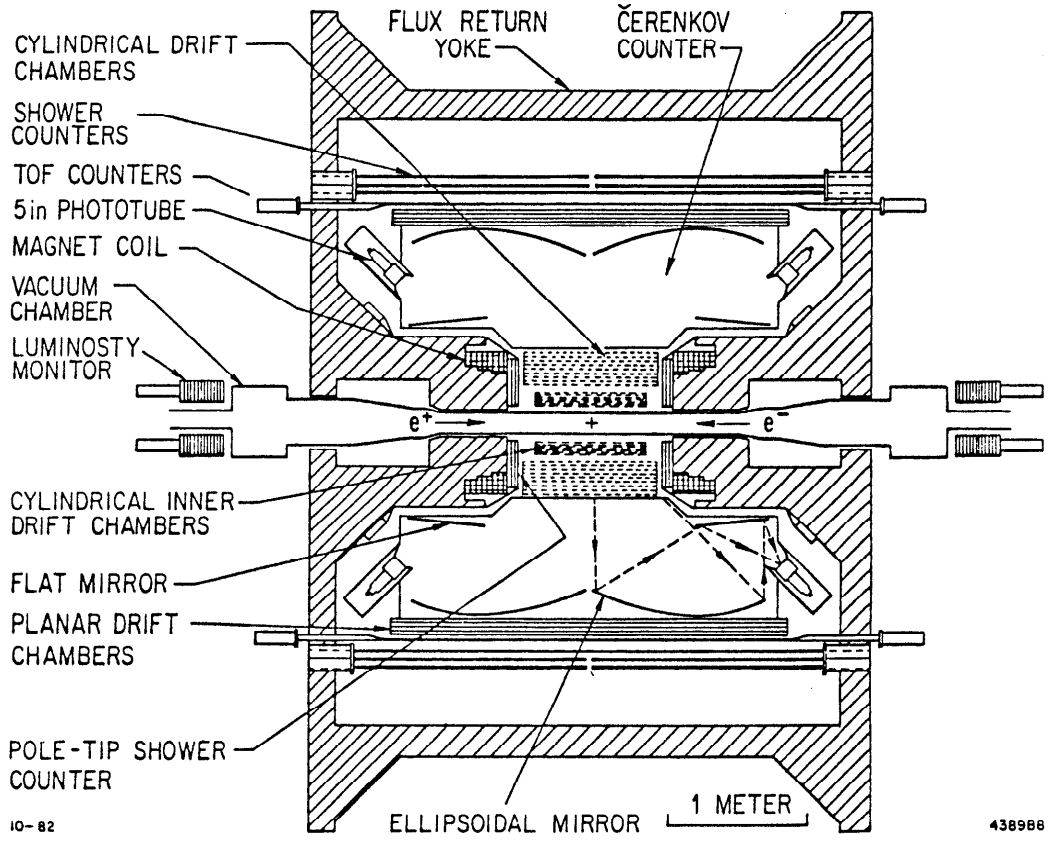

Figure 2.1. A cross section of the DELCO detector. Limited material between the interaction point and the gas volume of the Čerenkov counter reduces the number of electrons produced by gamma conversions in hadronic events. This allows the efficient identification of low momentum electrons from heavy quark decay.

multiple Coulomb scattering and the second from the limited resolution of the drift chambers. The drift chamber closest to the beam pipe is the Inner Drift Chamber (IDC). Immediately outside the IDC is the Central Drift Chamber (CDC). The last drift chambers, the Planar Drift Chambers (PDC's), are the ones mentioned above which are outside the Čerenkov counter. All of the drift chambers ran on a mixture of 50% argon and 50% ethane in 1982, and 90% argon, 8.5% carbon dioxide, and 1.5% methane in 1983 and 1984. The drift chambers were read out

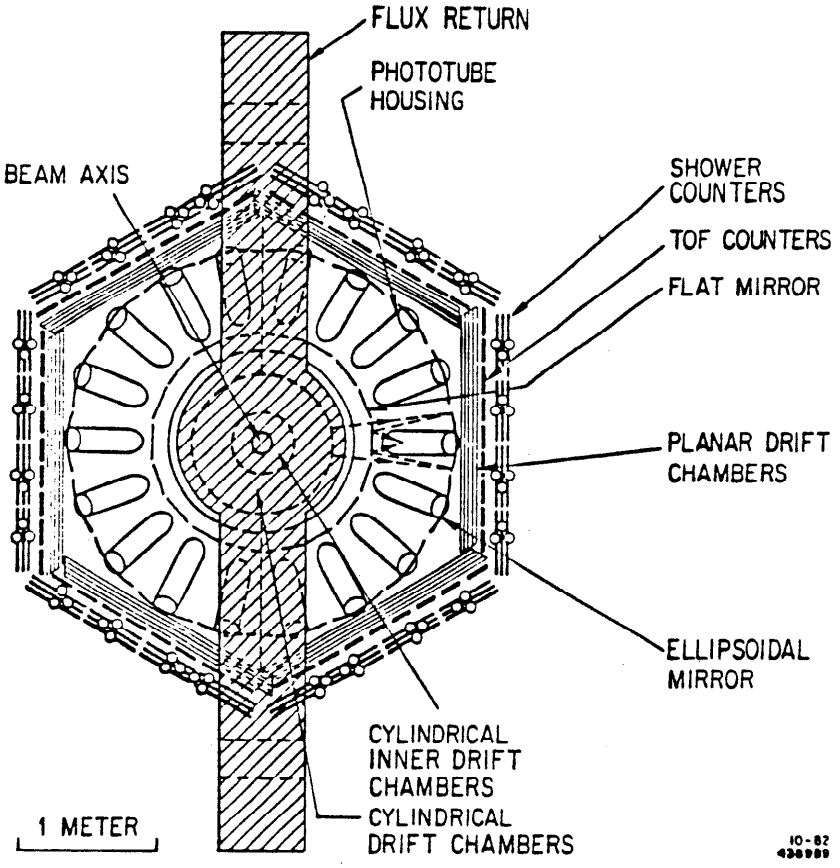

Figure 2.2. An end-on view of the DELCO detector. The fine segmentation in the Čerenkov counter (36 cells) is necessary in order to identify electrons in hadronic events.

using multi-hit TDC's with 4 nsec bins.[19] These drift chambers provide solid angle coverage over approximately ± 0.8 in $\cos\theta$ (θ is the polar angle) and very nearly 2π in ϕ (ϕ is the azimuthal angle). Because of the importance of minimizing the material in the detector before the Čerenkov counter gas volume, the walls of the drift chambers and the beam pipe were made from a hexagonal cell core material sandwiched between two thin skins of aluminum.[20,21] As stated previously, this technique made it possible to reduce the material before the Čerenkov counter to only 3% of a radiation length.

Table 2.1. A summary of the material in DELCO. The numbers given are for tracks at normal incidence. Two numbers separated by a slash indicate changes to the detector. The original thick beam pipe and the entrance wall of the Čerenkov counter were replaced between '83 and '84. The two numbers given for the Čerenkov gas correspond to isobutane and nitrogen respectively.

Material in DELCO	
What	# of radiation lengths
beam pipe	0.0225 / 0.0059
IDC - entrance	0.0070
- gas + wires	0.0033
- exit	0.0019
CDC - entrance	0.0035
- gas + wires	0.0041
- exit	0.0035
Čerenkov - entrance	0.0040 / 0.0014
- gas	0.0047 / 0.0026
- mirrors	0.0540
- exit	0.0710

2.1.1 The inner drift chamber

The IDC consists of 6 layers of sense wires with 64 cells per layer in a cylindrical geometry. The active volume of the chamber is 62 cm in length. The wire pattern and a typical residual distribution are shown in Fig. 2.3 for one layer. The other layers are similar. The sense wires were operated at ground potential, the field wires at approximately -2.4 kV and the guard wires at approximately -1.2 kV. These voltages varied from year to year depending on the gas used and on the amount of background radiation produced by the storage ring. The sense wire pattern at z=0 is shown in Fig. 2.4. The inner layer of the IDC is at a radius of 12.07 cm and the spacing between the layers is 1.71 cm. Alternate layers are offset in ϕ by one half

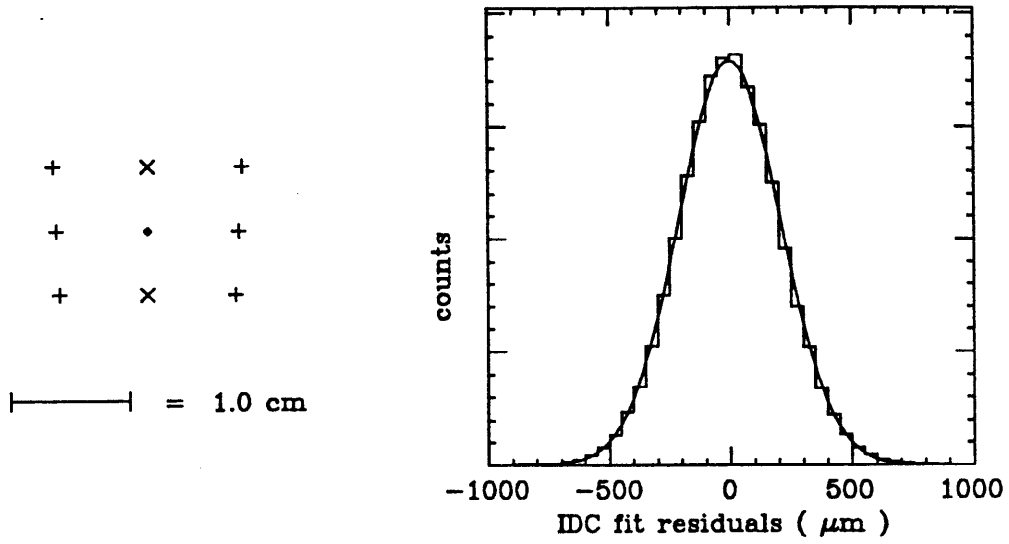

Figure 2.3. Wire pattern for one cell and residuals in the IDC for layer 3. The sense wire appears as a small diamond, the field wires as vertical crosses and the guard wires as diagonal crosses. The curve is a Gaussian fitted to the residual distribution.

of a cell width so that the left/right ambiguity can be resolved. In layers 3 and 4 the wires run parallel to the z-axis. The wires in the remaining layers are tipped at a small angle relative to the z-axis to provide information on the z-coordinate of the track origin and the track's dip angle. This small "stereo angle" is achieved by displacing the wires by two cells in the end plate of the drift chamber. This displacement results in a stereo angle of $\theta_s \approx 2.9°$. Layers 1 and 2 are tipped in the same direction and layers 5 and 6 are tipped in the opposite direction. Because the precision obtained in this drift chamber is central to the lifetime measurement, special care has been taken in locating the wires. The mechanism used is shown schematically in Fig. 2.5.[22] It results in wire location errors less than 60 μm. This chamber achieved the best resolution of the three tracking chambers in DELCO. The resolution obtained for each year and layer is shown in Table 2.2.

2.1.2 The central drift chamber

The CDC consists of 10 layers of wires with 64 cells per layer in layers 1 to 6 and 96 cells per layer in layers 7 to 10. The active volume of the chamber is 100 cm

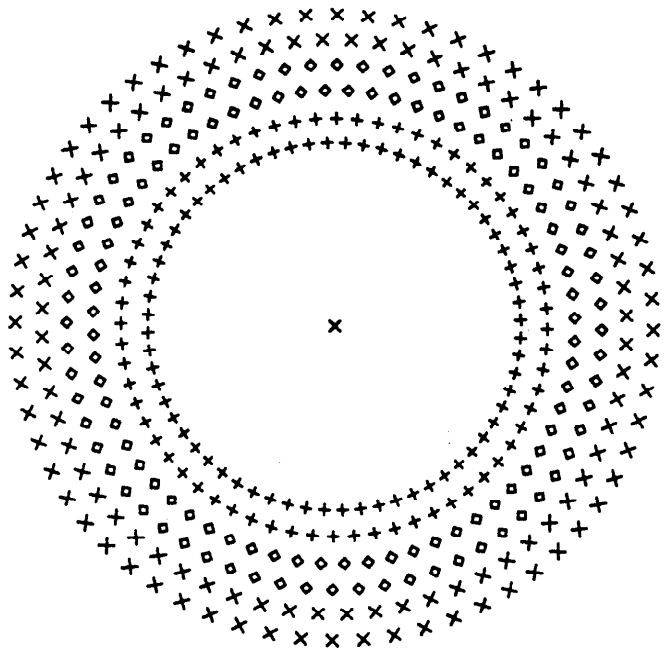

Figure 2.4. Sense wire pattern in the IDC. This figure shows the wire locations in the z=0 plane (the z-axis is oriented along the beam line). The first two layers and the last two layers are at small angles relative to the z-axis. Alternate layers are staggered to allow for the resolution of left-right ambiguities. Only sense wire locations are shown in this figure. For the location of the field and guard wires relative to the sense wires, see the cell in Fig. 2.3.

in length. The wire pattern is similar to that in the IDC and a typical cell is shown in Fig. 2.6 along with a typical residual distribution. The sense wires were operated at ground potential, the field wires at approximately -2.8 kV and the guard wires at approximately -1.4 kV. These voltages varied from year to year. As in the IDC alternate layers are offset by one half of a cell width. In the CDC layers 1,2,5,6,9, and 10 have their wires parallel to the z-axis. Layers 3 and 4 have a stereo angle in one direction and layers 7 and 8 have a stereo angle in the opposite direction. In the CDC the stereo angle results from a displacement of one cell width which produces a stereo angle of $\theta_s \approx 1.7°$. The resolution obtained for each year and layer is shown in Table 2.2.

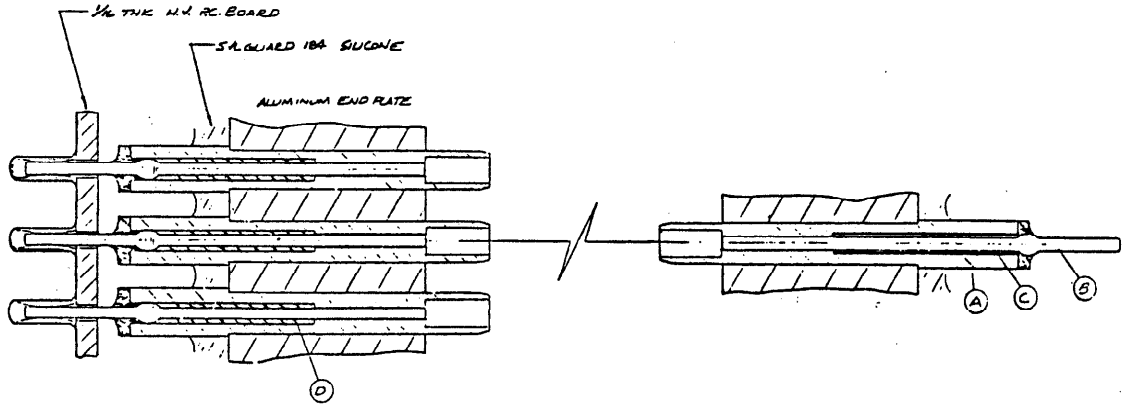

Figure 2.5. Drift chamber feedthroughs. This figure shows a cross section of the mechanism used to locate the wires in the IDC. In each end plate there are plastic (Delrin) feedthroughs (A) which provide high voltage insulation between the wires and the end plate. The wire is located and held in the feedthrough by means of a hollow stainless steel crimp pin (B). The crimp pin is retained in the feedthrough by means of the crimp in conjunction with either a metal sleeve (C) or a spring (D). The springs serve to maintain a constant tension on the wires during the stringing process. A gas seal is provided by a drop of epoxy around the crimp pin and a layer of cast silicon rubber between the plastic feedthroughs and the aluminum end plate.

2.1.3 The planar drift chambers

The PDC's consist of six sets of planar chambers with six layers in each set. Each set covers approximately one side of a hexagon around the outside of the Čerenkov counter. Fig. 2.7a shows a schematic representation of the construction of one layer of the PDC. Layers 1,2,5, and 6 run parallel to the z-axis and layers 3 and 4 are at large stereo angles of ±30°. The residual distribution for layer 3 is shown in the same figure. The resolution obtained by layer and year is shown in Table 2.2. The ribs are operated at -3.2 kV and the wire at 2.0 kV. These voltages also varied from year to year.

2.2 THE ČERENKOV COUNTERS

Electron identification in the DELCO detector is provided principally by a large

Table 2.2. Drift chamber resolution by layer and year. Numbers given are obtained from a least squares fit of Gaussians to the residual distributions. They represent averages over all the cells in a layer.

IDC resolution (μm)	Year		
	1982	1983	1984
layer 1	142	221	141
layer 2	137	212	142
layer 3	165	209	180
layer 4	159	213	186
layer 5	127	199	155
layer 6	131	205	135

CDC resolution (μm)	Year		
	1982	1983	1984
layer 1	194	280	228
layer 2	149	206	185
layer 3	162	223	191
layer 4	175	244	210
layer 5	151	215	155
layer 6	151	224	170
layer 7	170	231	186
layer 8	184	238	198
layer 9	173	201	178
layer 10	214	257	253

PDC resolution (μm)	Year		
	1982	1983	1984
layer 1	505	571	464
layer 2	536	595	512
layer 3	441	505	396
layer 4	460	529	448
layer 5	554	647	540
layer 6	600	683	660

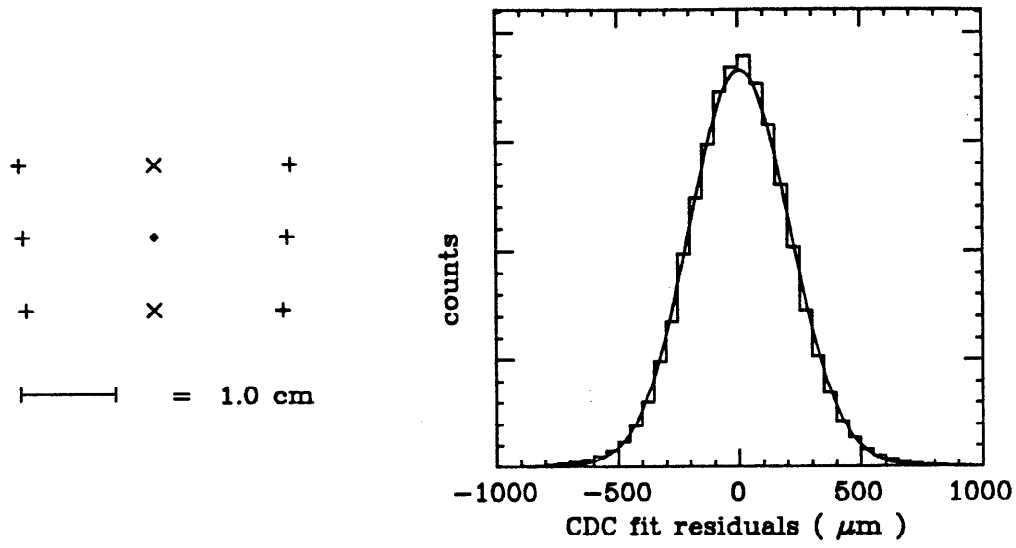

Figure 2.6. Wire pattern for one cell and residuals in the CDC for layer 2. The sense wire appears as a small diamond, the field wires as vertical crosses and the guard wires as diagonal crosses. The curve is a Gaussian fitted to the residual distribution.

solid angle Čerenkov counter. This counter covers from +0.62 to -0.62 in $\cos\theta$ and nearly all of 2π in ϕ. The counter system is segmented in both ϕ and θ. Each cell of the counter covers from 0 to 0.62 (or -0.62) in $\cos\theta$ and 20° in ϕ. A cross section of one cell of the Čerenkov counter is shown in Fig. 2.8. The ellipsoidal first mirror in the Čerenkov counter provides for a constant path length between the interaction point and the phototube face independent of the initial direction of the particle producing the radiation. Because of this all light produced by particles originating from the interaction point arrives at the phototube face at the same time. The faces of the phototubes (5 inch diameter RCA 8854 Quantacons) are coated with p-terphenyl, a wavelength shifter. This improves the total light yield since a substantial part of the Čerenkov radiation is in the UV where the glass window of the phototube is absorptive. The p-terphenyl absorbs the short wavelength light and re-emits it at a longer wavelength which can be transmitted through to the

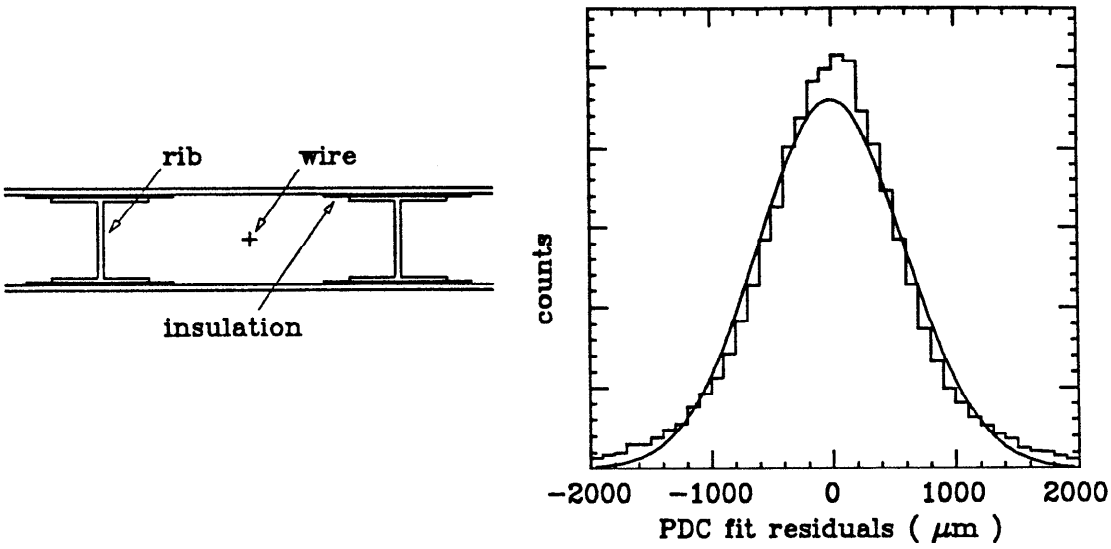

Figure 2.7. A cross section and the residuals for a layer in the PDC. The curve is a Gaussian fitted to the residual distribution.

photocathode. As in most of the counter systems at DELCO, the phototubes in the Čerenkov counter are "read out" in three separate ways. For each tube there is a latch to indicate the presence of a signal, a TDC (Lecroy 2228A) which gives the time of the signal relative to the beam crossing, and an ADC (Lecroy 2249A) to record the amplitude. Fig. 2.9 shows a scatter plot of the pulse height in the Čerenkov counter versus momentum for isolated tracks in hadronic events. The quantity plotted here is the "corrected number" of photoelectrons. This is obtained from the "raw number" (ADC information after pedestal subtractions and gain corrections) by making corrections for the path length in the radiator, the curvature of the track, and the Čerenkov light spot size on the phototube. A separate band is clearly visible for pions above threshold. Isobutane was used as the radiator for the data in this figure. Two different gases where used as radiators. A total of 147 pb^{-1} of data was taken with isobutane and 67 pb^{-1} with nitrogen. The indices of refraction and corresponding minimum momenta to produce Čerenkov radiation

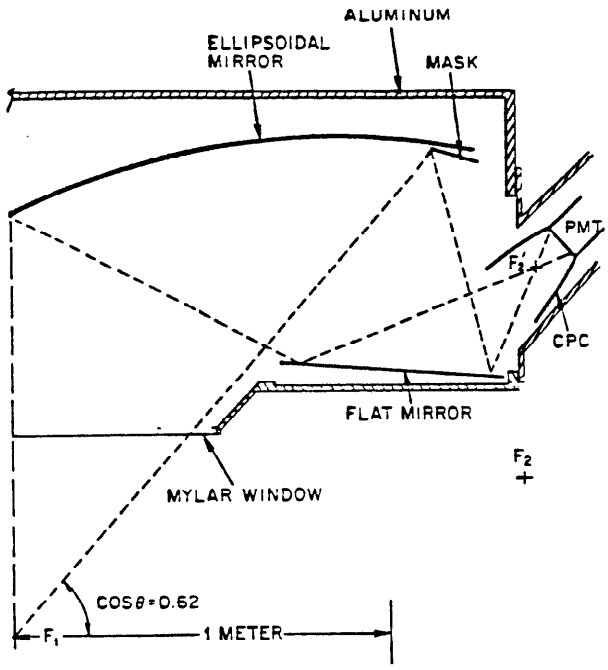

Figure 2.8. A cross section of the Čerenkov counter showing the optics involved. The mask restricts the Čerenkov solid angle to be the same as that of the PDC's.

are given in Table 2.3. This counter system suffers from a single photoelectron background in hadronic events. This is believed to be due to photons from very low momentum electrons which can be reflected repeatedly between the mirrors of the counter before finally entering a phototube. [23]

2.3 The Time of Flight Counters

Additional particle identification is provided in the DELCO detector by a time of flight system. This system consists of 52 plastic scintillators each approximately 3.2 m long, 2.5 cm thick, and 20 cm wide. They are located outside of the PDC's and run parallel to the beam line. They are read out by 2 inch diameter phototubes on each end. Both timing and pulse height information is digitized for each phototube. (The pulse height information is used to perform slewing corrections.) A time residual distribution for these counters is shown in Fig. 2.10. These counters are

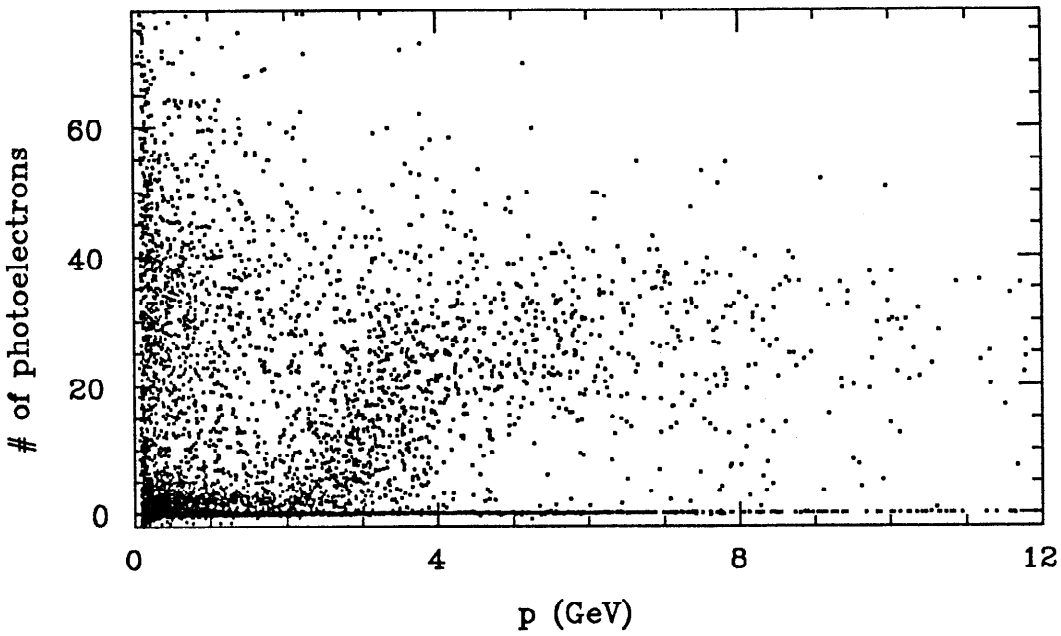

Figure 2.9. Pulse height in the Čerenkov counter versus momentum for isolated tracks from hadronic events. This data was taken with isobutane as a radiator. The pulse heights shown have been corrected (see the text).

Table 2.3. Characteristics of gases used as radiators in the Čerenkov counter. The index of refraction (n) and the minimum momentum to produce Čerenkov radiation for pions (p_π) and kaons (p_K) are given for the two gases.

GAS	n	p_π	p_K
isobutane	1.00144	2.7	9.4
nitrogen	1.000295	5.6	20.0

not directly used in this analysis.

2.4 The Shower Counters

The DELCO detector contains three sets of lead/plastic-scintillator shower counters. These shower counters obtain only a modest resolution in both energy and angle and are used primarily for tagging or to confirm particle identification

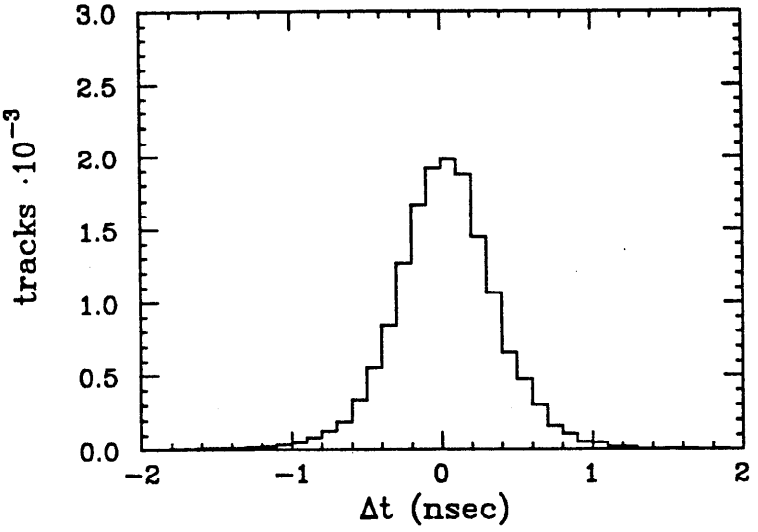

Figure 2.10. Residual distribution for the T.O.F. system. The tracks are electrons in two-gamma events. Quantity plotted is the difference between the counter time and the time expected for a $\beta = 1$ particle.

already made in the Čerenkov counter.

2.4.1 The barrel shower counters

The largest system of shower counters is the barrel shower counter which is located just behind the TOF system. The counters are made up of three layers of lead and plastic scintillator. Each layer of lead or scintillator is 1.25 cm thick for a total of 6 radiation lengths. These counters are used in the electron analysis to provide confirmation of the particle identification provided by the Čerenkov counter. In solid angle they cover approximately ± 0.62 in $\cos\theta$ and most of 2π in ϕ. There are small gaps in ϕ at the corners of each sextant. This system is broken into 48 segments in ϕ. Position resolution in the z-direction is obtained by timing information on the first layer and by segmentation (0 to +0.62 and 0 to -0.62 in $\cos\theta$) in the other two layers.

2.4.2 The pole tip shower counters

The magnet pole tips are covered with a system of shower counters which provides tagging for events in which some number of particles strike the pole tips.

These counters cover from 0.79 to 0.98 and from -0.79 to -0.98 in $\cos\theta$ and essentially 2π in ϕ. They are segmented in ϕ with each section covering 20° and have a total thickness of 5 radiation lengths. The scintillator is read out by BBQ bars which run radially along each section. They are used only indirectly in the electron analysis to tag (and remove) hadronic events in which a large part of the energy missed the tracking volume of the detector.

2.4.3 The luminosity monitors

These counters provide tagging at very small angles relative to the beam. They cover from 0.025 to 0.068 and from -0.025 to -0.068 in $\cos\theta$ and essentially 2π in ϕ. Each segment covers an interval of 60° in ϕ and has a thickness of 16 radiation lengths. They are used for luminosity measurements and to tag two-photon events.

2.5 The Beam Position Monitor

The position of the interaction point is determined on an event by event basis by the beam position monitors (BPM's). They consist of two sets of four "beam buttons" located 3.7 meters on either side of the interaction point. The "buttons," which are small electrical probes which intrude into the beam pipe, are shown in Fig. 2.11. The passing beam bunch induces a signal in them which depends on the current in the ring and on the position of the beam relative to the buttons. The signals from these probes are first processed in a "stretcher" where the signal is rectified and broadened, and then the total integrated charge is measured in a Lecroy 2249A ADC. The raw signals for one set of buttons are given by v_i $(i = 1,4)$ and gain and pedestal corrections are applied by

$$a_i = g_i \cdot (v_i - p_i). \tag{2.1}$$

These quantities are proportional to the current in the storage ring. Due to the symmetry of the buttons, for small displacements about the center, the changes in

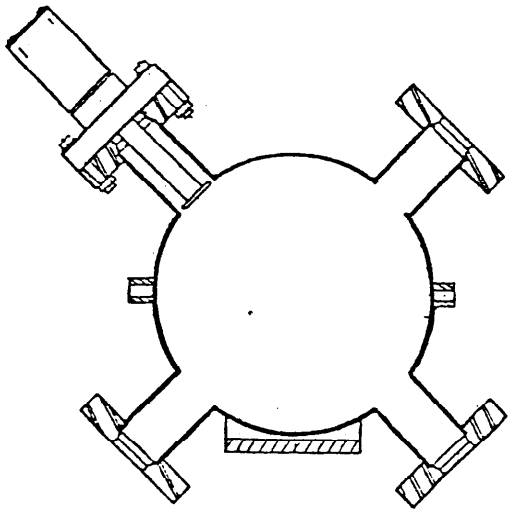

Figure 2.11. Cross section of a beam position monitor. Only the upper left hand assembly is shown complete. The other three are similar. The probe extends 0.5 mm beyond the inner circumference of the beam pipe.

the signals induced in the buttons will cancel each other so that

$$A = \sum_{i=1}^{4} a_i \tag{2.2}$$

is independent of the position of the beam and proportional to the current in the ring. Dividing by A removes the current dependence so that the quantities

$$x = c_x \cdot \frac{a_2 + a_3 - a_1 - a_4}{A} \tag{2.3}$$

and

$$y = c_y \cdot \frac{a_1 + a_2 - a_3 - a_4}{A} \tag{2.4}$$

give the position of the beam at the BPM. The constants c_x and c_y are determined prior to installation for each set of buttons by pulsing a probe placed between the buttons and observing the change in the signals induced as the probe in moved. The c's are all approximately 5 cm. The position of the beam at the interaction point is interpolated from the position of the beam at the two BPM's. The location

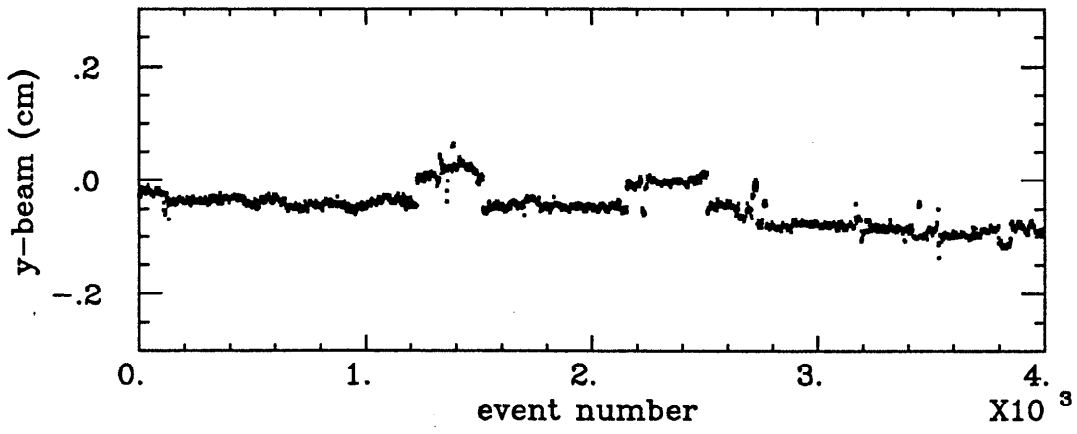

Figure 2.12. The y-coordinate of the beam position as a function of time as determined by the beam position monitor. The particular data shown here is from early 1983.

of the BPM system relative to the detector is determined using tracks from Bhabha events.

This measurement is sensitive to pedestal errors. For instance, if e_i is the pedestal error for the i'th channel, then (assuming $g_i = 1$) the error in x is

$$\Delta x = c_x \cdot \frac{e_2 + e_3 - e_1 - e_4}{A}. \tag{2.5}$$

As a result, if a_i is typically 500 ADC counts, then a one-count pedestal error produces a position error of 25 μm. The average value of this error is taken out in the process of surveying the BPM's relative to the detector; however, since A is proportional to the current in the ring, part of the error will remain. Fig. 2.12 shows the y-coordinate of the beam position as a function of time for a particular run block. Prior to correct pedestal subtractions, this distribution had a pronounced saw-tooth shape due to an interaction between the pedestals and the changing current in the storage ring during a run.

2.6 THE TRIGGER

The DELCO detector employs a collection of triggers which will be described

below. Because the lifetime analysis does not involve measuring cross sections, questions of trigger efficiency are not important and therefore only a brief discussion of the trigger will be given. Because hadronic events have many tracks and because they generally deposit a fair amount of energy in the shower counters, there is a high probability that they will satisfy more than one of the triggers.

The high rate at which beam crossings occur at the PEP storage ring (417 khz) requires the use of a two stage trigger. The first stage employs only information from the various shower counters and the Čerenkov counter. If these counters indicate that an event has occurred, then a second stage is employed which uses information from the tracking chambers (the IDC and the CDC only). The hardware tracker involved has been described previously.[24] It uses the drift chamber information (hits only without regard to time) to detect the presence of a "track" pointing to a latched shower counter. If such a "track" is present, then the event is read out. More specifically, the following collection of counters is sufficient to produce a trigger if the hardware tracker finds a track:

- Two barrel shower counters latched in two different sextants of the detector.
- A latched Čerenkov counter and a latched barrel shower counter in the same sextant.
- A latched barrel shower counter plus a poletip counter with a minimum energy.
- A latched barrel shower counter plus a luminosity monitor with a minimum energy.

In addition to these triggers which require the presence of a charged track in the detector, there are several neutral triggers which do not require a charged track. These are:

- Two barrel shower counters latched in two different sextants plus a minimum total energy deposited in the barrel shower counter.
- Four barrel shower counters latched in four different sextants.
- A latched barrel shower counter and a latched Čerenkov counter in the same

sextant. This trigger is scaled by 128.

- Two pole tip counters opposite each other with sufficient energy. (This trigger is intended to catch Bhabha events where the tracks go into the poletips.)
- Two luminosity monitors opposite each other with sufficient energy. (This trigger is intended to catch Bhabha events where the tracks go into the luminosity monitors.) This trigger is prescaled by 128.

3. THE ELECTRON ANALYSIS

It is clear from the proceeding chapter that the DELCO detector was designed with an eye toward the analysis which will be described in this chapter. This chapter logically breaks into two halves. The first describes the filters which are used to separate out events which contain an "electron." Because not all tracks identified as "electrons" are in fact really electrons and because there are various sources of real electrons in the data, it is necessary to fit the data to a model in order to extract the physics from it. This fit is described in the second half of this chapter. The results of this fit are used in the subsequent chapters which deal specifically with the lifetime measurements.

3.1 THE PASS1 FILTER

The PASS1 filter described here is the first step in the off-line analysis. Its purpose is to separate the triggers caused by real physics events from those caused by various sorts of noise in the detector. These "noise events" make up the majority of the triggers. This separation is not difficult for hadronic events because of the large number of charged tracks they typically contain and because they produce a total visible energy which is of the order of the beam energy. For this reason and because questions of overall efficiency are irrelevant for the bottom lifetime analysis, this filter will not be described in great detail. There are two principal paths by which a hadronic event can pass this filter.[25] The first requires only that the event produce a sufficient response in the barrel shower counter. Specifically, there must exist at least two clusters of energy in the shower counters. Each cluster must have an energy of at least 40 gap crossings.[26] The second requires that there be at least two charged tracks in the event. At least one of these tracks must have produced a consistent response in either a time of flight counter or in a barrel shower counter. In either case a hadronic event in which the jet axis points into the detector acceptance will almost certainly pass.

3.2 THE HADRON FILTER

The first step in the electron analysis is to select a hadronic data set from the output of the first pass. Hadronic events produced in e^+e^- annihilation at 29 GeV are distinguished by large multiplicities and large visible energies. The filter described below cuts on these quantities to separate the hadronic events present at the output of the PASS1 from the obvious non-hadronic events (i.e. $e^+e^- \rightarrow e^+e^-, \mu^+\mu^-, \tau^+\tau^-$, and low multiplicity two-gamma events). These cuts are followed by other cuts which remove the more hadron-like backgrounds which remain. To minimize the use of computer time, the filter is divided into two steps. These two steps correspond to the two stages of track reconstruction. At the first stage various combinations of drift chamber hits are compared to a particle path which is based on a simple parameterization in order to "recognize" the tracks. The cuts applied to each event after this stage are:

- The total number of tracks found must be at least 5.
- The sum of the momenta of all the tracks must be at least 2.5 GeV. For this cut and all cuts involving track momentum (p), tracks with $p > 14.5$ GeV (the beam energy) are assumed to be mismeasured. Such tracks are given a momentum of $p = 14.5$ GeV.
- The total energy (E_t) in the event must be greater than 5.0 GeV. The total energy is defined as the sum of: (1) the sum of all track momenta, (2) the sum of all the energy in the barrel shower counter and, (3) the sum of all the energy in the pole tip counters. (For the last two the energies are corrected to minimize double counting of charged energy. This is done by subtracting the expected counter response assuming minimum ionizing particles.)
- At least three of the tracks in the event must have at least two hits from PDC wires which run parallel to the beam line. This cut helps remove "noise events." In such events the drift chambers in the center of the detector will have a great many hits which are erroneously identified as tracks. Such "tracks" will seldom contain hits in the PDC's because the PDC's, which

are located outside the Čerenkov counters, are distant from the other drift chambers and not usually affected by the noise.

These cuts are followed by two more which remove events which originate in the interaction of an electron from the beam with a residual gas molecule in the beam pipe. Such events are characterized by a large asymmetry because the total momentum of the beam-gas system is equal to the beam momentum (as opposed to zero for beam-beam interactions), and by initial z-coordinates which have a flat distribution. (The beams are parallel to the z-axis.) The cuts which remove such events are:

- The energy asymmetry (E_{asym}) of the event must be

$$E_{asym} < 0.224 \cdot \sqrt{E_t - 5.0}, \tag{3.1}$$

  where energy is measured in GeV. The asymmetry is defined as $E_{asym} = (E_c + P_c)/E_t$ where $E_c = \sum E_i \cdot \cos\theta_i$. The sum is over shower counters and θ_i is the polar angle. The quantity P_c is defined similarly for charged tracks.
- The difference between the average z-coordinate of the origin of all the tracks and the z-coordinate of the beam center must be less than 4.5 cm.

The second stage of track reconstruction consists of another fit of the track to the drift chamber hits. At this stage a full "swim" of the particle through the nonuniform magnetic field is employed. Drift chamber hits may also be added or deleted, based on the improved information from this "swim". In the following a "good" track is one which: (1) has at least twelve drift chamber hits, (2) has a distance of closest approach to the beam of less than 2 cm and, (3) had a good χ^2, etc. during this second stage of track reconstruction. The following cuts are just tighter versions of the previous cuts:

- There must be at least five "good" tracks.
- The sum of the momenta of the "good" tracks must be at least 6 GeV.
- The average z-coordinate of the origins of the "good" tracks must be within 4.5 cm of the z-coordinate of the beam.

The last two cuts in the hadron filter are used to ensure that most of the event went into the part of the detector which is well instrumented. Hadronic events which clip the edge of the tracking chambers can produce events which are asymmetric and/or deposit a lot of energy into the poletip counters.

- There must be at least two tracks in each event hemisphere. The event is divided into two hemispheres by a plane perpendicular to the sphericity axis. This cut also removes certain two-gamma backgrounds.
- The total energy in the pole tip counters must be less than 20.0 GeV (corrected for charged energy as above).

3.3 THE ELECTRON FILTER

The PASS1 filter (which separates real events from "junk" events) and the hadron filter (which separates hadronic events from all other events) are followed by one more filter which identifies events which contain electrons. The particle identification in this filter is provided by the Čerenkov counters in conjunction with the shower counters. These systems were described in the previous chapter. The electron filter logically breaks into four parts. The first part attempts to define a "good" Čerenkov cell; the second removes identifiable backgrounds; the third decides which of the tracks in the cell could have produced the Čerenkov and barrel shower counter responses associated with it; and the last (which is used only in the case where there are multiple tracks in the cell, all of which are consistent with the barrel shower and Čerenkov responses) applies a minimum χ^2 selection criterion to the tracks in a cell in order to select the one which is most likely to be an electron. The first part of the filter, which defines a good Čerenkov cell, consists of the following cuts:

- The time for the cell must be within ± 1 nsec (± 1.5 nsec if nitrogen was used as the radiator) of the expected time. Early times are often the result of particles striking the phototube. Such particles may be produced by beam-beam interactions and travel directly from the interaction point to the

phototube or they may be degraded beam particles which strike the detector from the outside.

- The number of charged tracks which pass through the cell must be less than six. The probability of correctly identifying the electron in a group of six or more particles is very small. Most events only have one or two tracks in a cell.
- The momentum of all the tracks in the cell must be less than 2.5 GeV (5.5 GeV for nitrogen). These numbers are slightly below the threshold for the production of Čerenkov radiation by pions in isobutane and nitrogen respectively.
- The raw pulse height recorded for the phototube in this cell of the Čerenkov counter must correspond to more than 1.75 photoelectrons. This removes the 1 photoelectron background mentioned in the previous chapter.

These cuts are followed by another set which is aimed at removing backgrounds. Since a pion with momentum less than pion threshold never turns on a Čerenkov counter, backgrounds are always caused by electrons. These backgrounds either take the form of an electron from a gamma conversion (or from a π^o Dalitz decay) appearing directly, or of an electron from a background source which is missed by the tracking program, but which turns on a Čerenkov cell which is occupied by a pion. The following cuts are aimed at eliminating events in which the electron was not tracked in the central tracking chambers (the IDC and the CDC):

- There must not be any track stubs found in the drift chambers behind the Čerenkov cell (the PDC's). This cut removes events in which a gamma converted in the outer parts of the drift chambers or in the Čerenkov counters so that no recognizable tracks were left in the IDC or CDC. Electrons from such gamma conversions may produce track stubs in the PDC's.
- There must not be any adjacent empty Čerenkov cells fired. Such cells can be produced by gamma conversions in which the produced electron crosses more than one cell.

The following cuts are aimed at picking up gamma conversions which occurred early enough in the detector for all or part of the products to have been successfully reconstructed by the track-finding programs:

- Every track in the cell must have a hit on the first or second layer of the IDC. This cut removes events in which a gamma converted inside the central drift chambers. Likely places for such a conversion are the walls separating the IDC and the CDC.
- Every track in the cell must have a distance of closest approach to the beam of less than 0.3 cm. Electrons from gammas which convert in the beam pipe will appear to have originated away from the beam because of their curvature in the magnetic field. The 0.3 cm cut is as tight as can be used without introducing a significant bias into the lifetime measurement.
- Every track in the cell is paired with other tracks in the event to look for pairs consistent (on the basis of kinematic cuts) with their having come from a gamma conversion. Any cell which contains a track identified as coming from a gamma conversion is dropped.
- Each event is visually scanned for the presence of gamma conversions. In a certain fraction of the gamma conversions, one of the electrons receives most of the momentum from the original gamma. This results in a soft track which curls up inside the central tracking chambers. Such tracks are difficult to find using the tracking programs, but easy to see on the single event display. Events with such tracks, where the soft track could be paired up with the electron, are dropped.

After these cuts a further set of cuts is applied to the individual tracks in the Čerenkov cell. It is not necessary for all the tracks in the cell to pass the following cuts, but in order to be considered as an electron, the track in question must pass them:

- The track must use at least 16 drift chamber hits. Of these at least two must be from wires that are parallel to the beam and in the drift chambers which

are located outside the Čerenkov counters (the PDC's). These two cuts ensure that the track is well measured in the drift chambers.

- The track must strike a barrel shower counter module and the energy measured in that module must be large enough to be consistent with the track having been produced by an electron. No upper limit is placed on the shower counter response because of the possibility of more energy being deposited in that counter by other particles.
- The number of photoelectrons in the Čerenkov counter must be consistent with their having been produced by the track in question. (Because of the small number of photoelectrons produced in the nitrogen data, this cut is not used there.)

In about 25% of the cases, there is more than one track in the Čerenkov cell which passes all of these cuts. In this situation the "electron" is selected based on the barrel shower and Čerenkov responses. For each possible assignment of particle types the expected counter responses are calculated along with their errors and a χ^2 is calculated based on the difference between the measured and calculated response. The combination with the lowest χ^2 is accepted. These situations, which typically involve just two tracks, occur mostly at low p and p_t and therefore have only a small influence on the b-lifetime measurement. A scatter plot of the resulting distribution in p and p_t in shown in Fig. 3.1.

3.4 The Fit to the Electron Spectrum

The "electrons" identified by this filter are produced by several different processes. The ones of interest to this analysis are from the semileptonic decay of heavy (bottom and charm) hadrons. In addition to these "direct electrons" there are background contributions to the signal from misidentified pions and from electrons produced by gamma conversions and π^0 and η Dalitz decays. These sources of electrons are summarized here:

- The semileptonic decay of hadrons containing bottom quarks (b $\rightarrow$ e). The

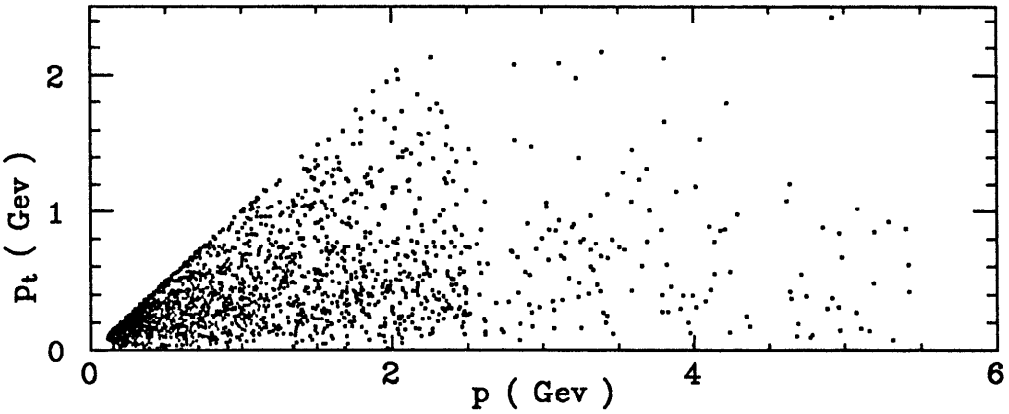

Figure 3.1. The distribution of the electrons in p and p_t. This figure combines both the nitrogen and the isobutane data.

number of electrons from this source is clearly proportional to the branching ratio for $B \rightarrow eX$. The distribution of electron transverse momentum (p_t) is determined qualitatively by the mass of the hadron (5.2 GeV). The distribution of electron momentum (p) is determined by the hadron's mass and its momentum after the fragmentation process. The latter is parameterized in a simple form (the fragmentation function) and is included in the fit.

- The semileptonic decay of hadrons containing charmed quarks produced in the decay of hadrons containing bottom quarks (b $\rightarrow$ c $\rightarrow$ e). The number of electrons from this source is proportional to the branching ratio for $C \rightarrow eX$. The distribution in p and p_t of electrons from this source is soft because of the two sequential decays involved. These distributions are clearly affected by both m_b and m_c as well as by the B-hadron momentum after fragmentation.
- The semileptonic decay of hadrons containing charmed quarks produced directly (c $\rightarrow$ e). This is very similar to the first source (b $\rightarrow$ e) considered above. The smaller masses involved here ($\approx$ 1.9 GeV) result in a different p_t distribution for electrons from this decay. This difference in the p_t distribution makes it possible to separate (in a statistical sense) the

electrons from the decay of the two heavy hadrons.

- Pions which are misidentified as electrons. These are caused by pions which share a Čerenkov counter cell with an electron from a gamma conversion (or possibly from a heavy quark decay, a Dalitz decay, or an energetic δ-ray). Since the momentum spectrum of pions in hadronic events peaks at low momentum, this background will also peak at low momentum.
- Electrons from gamma conversions or from π^o and η Dalitz decays. Since most of the gammas come from π^o decay and since most pions in hadronic events are quite soft, the gamma conversion part of this background is strongly peaked at low momentum.
- Electrons from the decays of τ's which were produced by the decay of B-hadrons. Because of the similar decay chain and because the τ mass is similar to that of the charmed hadrons, the distribution in p and p_t of electrons from this source is very similar to that from b $\rightarrow$ c $\rightarrow$ e. Because the b $\rightarrow \tau$ branching ratio is expected to be small compared to b $\rightarrow$ c, this source of electrons makes a small contribution relative to b $\rightarrow$ c $\rightarrow$ e.

3.4.1 The method

The electron spectrum in p and p_t obtained above is fit to obtain parameters which will be used in the lifetime analysis. The quantities determined by the fit are:

- z_{ob}, which describes the average momentum of the hadrons containing bottom quarks.
- z_{oc}, which describes the average momentum of the hadrons containing charmed quarks.
- BR($b \rightarrow e$), the average semileptonic branching ratio for particles containing bottom quarks.
- BR($c \rightarrow e$), the average semileptonic branching ratio for particles containing charmed quarks.

- s_π, which scales the pion background. This parameter is introduced to account for the uncertainty in the normalization of this background. It is constrained to its nominal value by a Gaussian with a width of 10% ($\sigma_\pi = 0.10$).
- s_γ, which scales the gamma conversion background. This parameter is introduced to account for the uncertainty in the normalization of this background. It is constrained to its nominal value by a Gaussian with a width of 10% ($\sigma_\gamma = 0.10$).

The likelihood function for the fit is

$$L = \prod_i \left(\prod_j P(x_{ij}, n_{ij}) \right) \cdot \frac{1}{\sqrt{2\pi}\sigma_\pi} \exp\left(-\frac{(1-s_\pi)^2}{2\sigma_\pi^2} \right) \cdot \frac{1}{\sqrt{2\pi}\sigma_\gamma} \exp\left(-\frac{(1-s_\gamma)^2}{2\sigma_\gamma^2} \right), \tag{3.2}$$

where the first product runs over the 4 run blocks ('82, '83 isobutane; '83 nitrogen; '84 nitrogen; '84 isobutane) and the second product runs over the various bins in p and p_t. The $P(x_{ij}, n_{ij})$ are just Poisson distributions:

$$P(x, n) = \frac{e^{-x} x^n}{n!}, \tag{3.3}$$

where the n_{ij} are the number of events measured in a particular bin for a particular run block, and x_{ij} is the number expected. The x_{ij} are calculated as follows:

$$\begin{aligned} x_{ij} = 2 \cdot \epsilon_{ij} \cdot \Bigg[& N_j^{b\bar{b}} \cdot BR(b \to e) \cdot \sum_{k=1}^{4} \alpha_k(z_{ob}) \cdot P_{ijk}^{b} \\ & + 1.167 \cdot N_j^{b\bar{b}} \cdot BR(c \to e) \cdot \sum_{k=1}^{4} \alpha_k(z_{ob}) \cdot P_{ijk}^{bc} \\ & + N_j^{c\bar{c}} \cdot BR(c \to e) \cdot \sum_{k=1}^{4} \beta_k(z_{oc}) \cdot P_{ijk}^{c} \Bigg] \\ & + s_\pi \cdot N_{ij}^{\pi} + s_\gamma \cdot N_{ij}^{\gamma} + N_{ij}^{\tau}. \end{aligned} \tag{3.4}$$

In the above $N_j^{b\bar{b}}$ is the number of $b\bar{b}$ events expected in the j'th run block and $N_j^{c\bar{c}}$ is the number of $c\bar{c}$ events. The factor of 2 accounts for the fact that two B-hadrons are produced in each $b\bar{b}$ event, etc. The factor of 1.167 is an estimate of the average number of charmed hadrons produced in the decay of B-hadrons. It is slightly greater than one because a $c\bar{s}$ quark pair can be produced in the decay in addition to the c-quark from the $b \rightarrow c$ transition.

The ϵ_{ij} term is a correction which accounts for deficiencies of the full detector simulation Monte Carlo. The corrections are calculated in the following manner. The cuts in the electron filter which depend on the Čerenkov counter response or on the barrel shower counter response are turned off. The efficiency of the remaining cuts is measured versus p and p_t. The ratio of the efficiency for the data to the efficiency for the Monte Carlo is ϵ_{ij}. These numbers are of the order of 0.8 and are tabulated in Appendix E. The final b-lifetime is insensitive to this correction.[27]

The backgrounds for the i'th bin in the j'th run block are N_{ij}^{π} , N_{ij}^{γ} and N_{ij}^{τ} for pions identified as electrons, electrons from gamma conversions and Dalitz decays, and electrons from ($e^+e^- \rightarrow b\bar{b}$, $b \rightarrow \tau X$, $\tau \rightarrow eX$) respectively. The backgrounds have been calculated by two different methods. The gamma conversion background is obtained from a full detector simulation Monte Carlo calculation as is the (entirely negligible) tau background. The background due to misidentified pions is obtained directly from the data by a "track flipping" algorithm. Because a pion below threshold never turns on a Čerenkov counter,[28] the pion background can be understood as a sort of "convolution" of the distribution of pions in an event and the distribution of turned on Čerenkov cells. This "convolution" can be determined from the data in the following manner. Each track in each hadronic event is flipped (one track at a time) across the sphericity axis for that event. The flipping process consists of adding new drift chamber information to the event record for a track with the same momentum but the opposite direction. The event record is also modified to include a simulated response in the barrel shower counter. This new event is then analyzed, and if the flipped track is identified as an "electron," it is

Table 3.1– Intervals used to calculate α_k and β_k (see equations 3.5 and 3.4). The intervals used do not extend all the way to zero because the fragmentation function makes a negligible contribution in those regions.

interval number - k	range - α_k	range - β_k
1	0.35 - 0.50	0.10 - 0.30
2	0.50 - 0.65	0.30 - 0.55
3	0.65 - 0.80	0.55 - 0.80
4	0.80 - 1.00	0.80 - 1.00

counted as one background event.

The terms in equation 3.4 involving summations account for the dependence of the electron spectrum on the fragmentation parameters z_{ob} and z_{oc}. The term $\alpha_k(z_{ob})$ is the probability that a B-hadron will have a momentum in the k'th momentum interval given a particular value of z_{ob}, and $\beta_k(z_{ob})$ is the analogous probability for C-hadrons. The α_k's depend on the shape of the fragmentation function used to fit the data. The shape used here is that suggested by Peterson *et. al.*[29] and has the form:

$$D_q(z) = \frac{N}{z_q(1 - \frac{1}{z_q} - \frac{\epsilon_q}{(1-z_q)})^2}, \tag{3.5}$$

where q = b or c and N is a normalization constant. The α_k's and β_k's are the integral of this function over the intervals given in Table 3.1. The fit is done in terms of the parameter z_{oq} which is related to ϵ_q by

$$\epsilon_q = z_{oq} + \frac{1}{z_{oq}} - 2. \tag{3.6}$$

This results in more symmetric error bars. This parameter can, in turn, be related to $\bar{z}_q = \frac{E_{hadron}}{E_{beam}}$ by integrating $D_q(z)$ over the appropriate interval, *i.e.*

$$\bar{z}_q = \int z \cdot D_q(z). \tag{3.7}$$

P^b_{ijk} is the probability that a B-hadron in the j'th run block, produced in the k'th momentum interval, will produce an electron which is detected in the i'th p, p_t bin. P^{bc}_{ijk} is the analogous probability for the process ($e^+e^- \rightarrow b\bar{b}$, $b \rightarrow c$, $c \rightarrow e$) and P^c_{ijk} for the process ($e^+e^- \rightarrow c\bar{c}$, $c \rightarrow e$). These probability tables are calculated using a full detector simulation Monte Carlo.

3.4.2 The results of the fit

Fig. 3.2 and Fig. 3.3 show the results of projecting the fit onto the momentum and the transverse momentum axes. The first figure is for the isobutane data and the second is for the nitrogen. (Both data sets are fit simultaneously. The projections are separated because the 2.5 GeV upper limit on p produced by the pion threshold in the Čerenkov counters for the isobutane data produces as artificial "step" in the momentum distribution.) From the figures it is clear that the electrons from the b $\rightarrow$ e process make the dominant contribution at $p_t > 1$ GeV. The backgrounds are heavily peaked at low p and low p_t. The agreement between the fit and the data for the lowest two bins in p for the nitrogen data set is poor. Whether this is a small error in the analysis or a statistical fluctuation is not known. If tracks with $p < 1$ GeV are not used, the fit yields similar values for all the parameters.[30] The results of the fit are tabulated in Appendix E along with the probability that a track in a given p and p_t bin came from any of the various sources. These probabilities are used in the maximum likelihood fit to obtain the b-lifetime. From this appendix it is clear that there are almost no electrons from gamma conversions and very few misidentified pions with $p_t > 1$ GeV. The parameters from the fit are summarized in Table 3.2 and in Table 3.3. The parameters which describe the momentum spectrum of the parent hadron (z_{oc} and z_{ob}) are also used in the lifetime analysis. As will be demonstrated later, the momentum distribution of the parent hadrons affects the distribution of the impact parameters of the hadrons' decay products.

The statistical errors from the electron analysis introduce an uncertainty in the

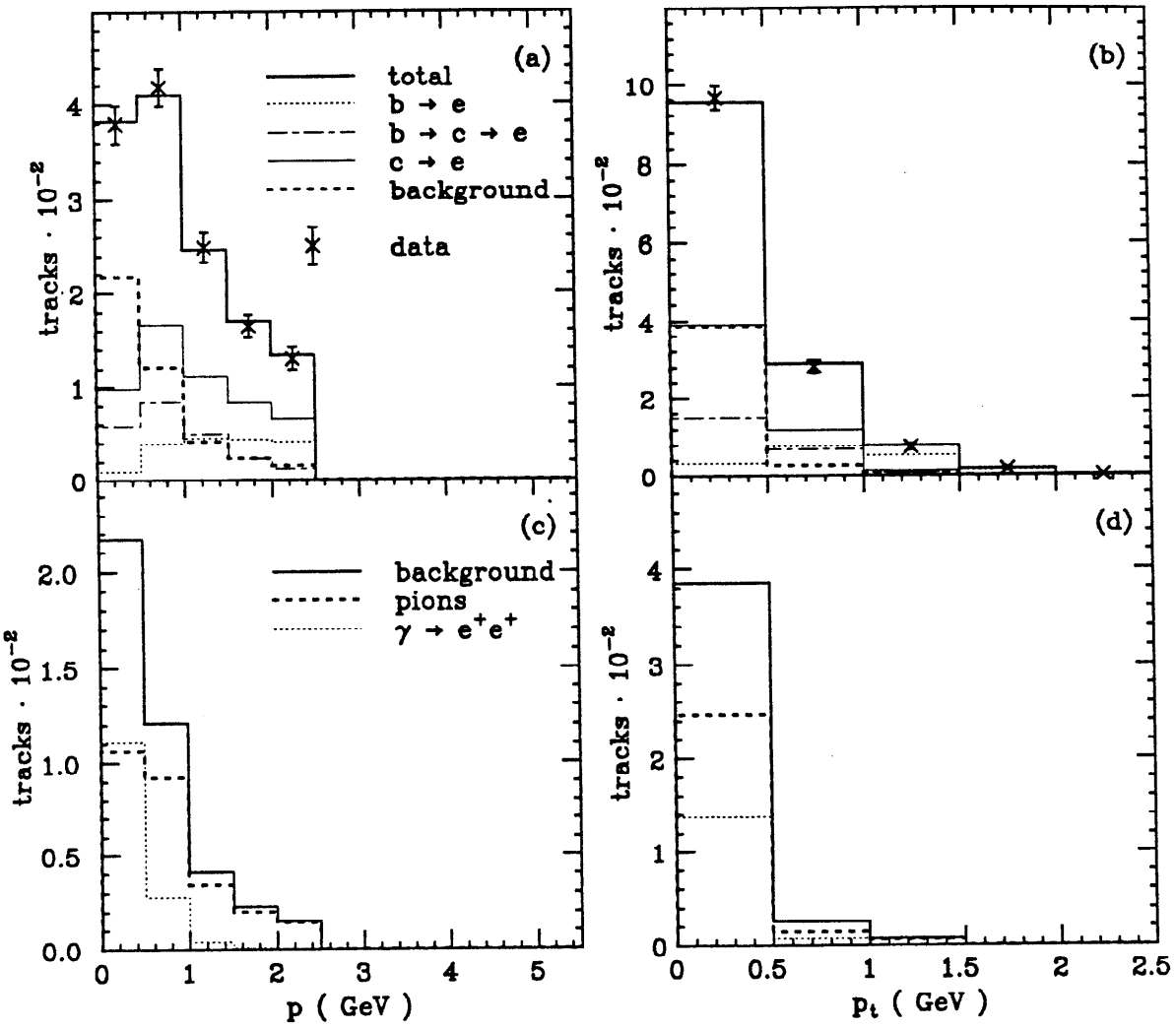

Figure 3.2. Projections of the fit to the isobutane data. Part (a) shows the result of projecting the fit to the electron spectrum onto the p-axis. The contributions to the fit are labelled on the figure. Part (c) shows the contributions to the background in part (a). Part (b) shows the result of projecting the fit onto the p_t-axis and the points and lines in this figure have the same meaning as in part (a). Part (d) shows the contribution to the background in part (b).

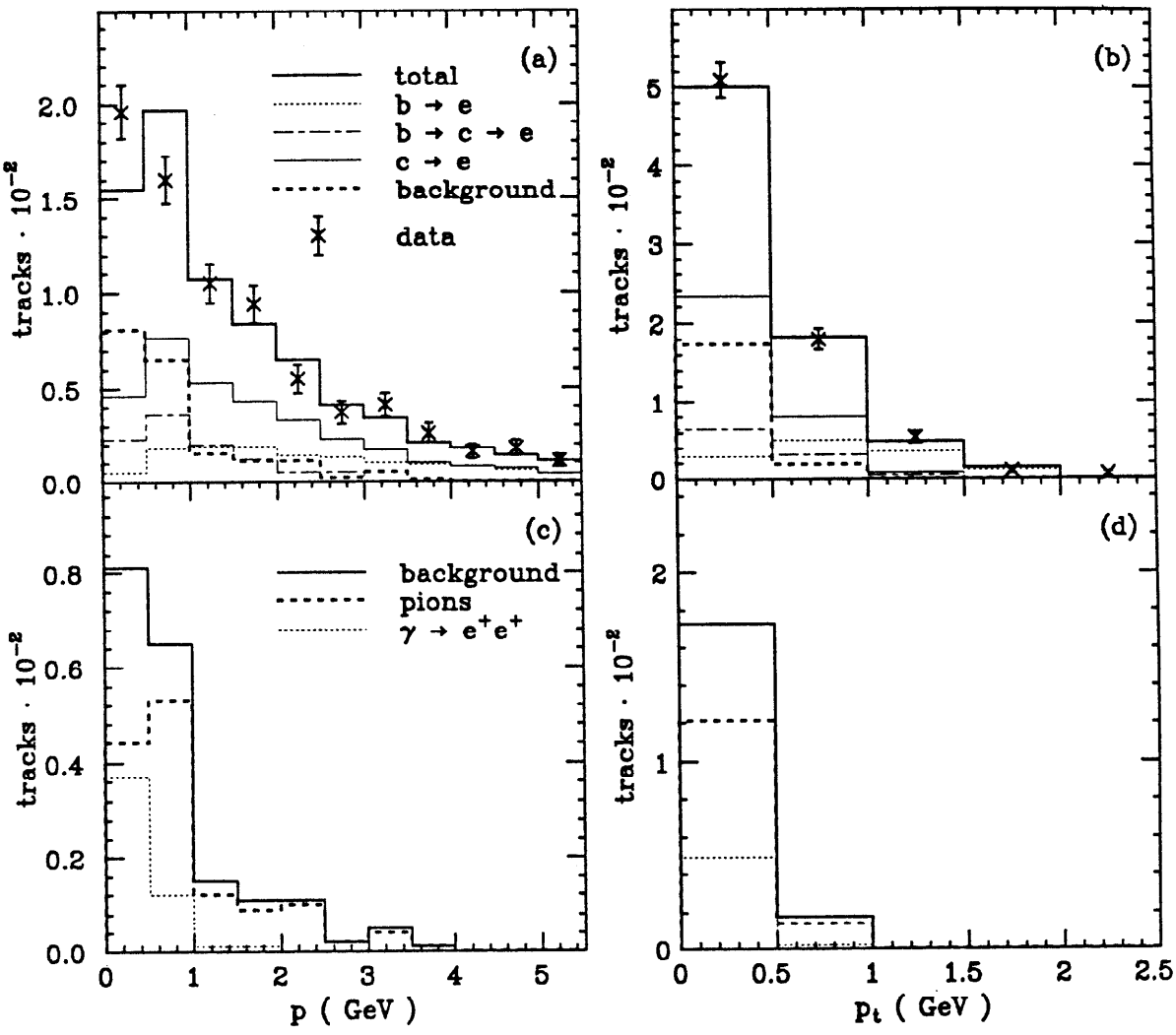

Figure 3.3. Projections of the fit to the nitrogen data. Part (a) shows the result of projecting the fit to the electron spectrum onto the p-axis. The contributions to the fit are labelled on the figure. Part (c) shows the contributions to the background in part (a). Part (b) shows the result of projecting the fit onto the p_t-axis and the points and lines in this figure have the same meaning as in part (a). Part (d) shows the contribution to the background in part (b).

Table 3.2. Parameters estimated from the electron spectrum. This table gives the estimated values of the fit parameters and the statistical errors.

parameter	fitted value	errors	
z_{ob}	0.83	+0.048	-0.060
z_{oc}	0.68	+0.050	-0.054
BR(b → e)	0.15	+0.019	-0.018
BR(c → e)	0.12	+0.0066	-0.0065
s_π	0.97	+0.090	-0.090
s_γ	1.07	+0.090	-0.090

Table 3.3. Correlation coefficients from the fit to the electron spectrum.

	z_{ob}	z_{oc}	BR(b → e)	BR(c → e)	s_π
z_{oc}	-0.52				
BR(b → e)	0.49	-0.11			
BR(c → e)	0.26	0.19	-0.53		
s_π	0.05	0.09	0.21	-0.54	
s_γ	0.01	0.15	0.08	-0.13	-0.13

measurement of the b-lifetime. Because of the significant correlations between the various parameters in the fit, it is not entirely straightforward to propagate these errors through to the end of the lifetime analysis. The procedure used here is to find another set of uncorrelated fitting variables which are linearly related to the "physical" ones given above. Having done this, it is possible to propagate the errors simply by changing each of the new variables by ± 1 sigma and observing the change in τ_b. The resulting changes can then be added in quadrature. (This last step is not justified in the presence of correlations.) The uncorrelated variables are linear combinations of the parameters given above. The coefficients are the elements of the eigenvectors obtained by diagonalizing the inverse error matrix from the fit. The errors on the new parameters are given by the square roots of the reciprocals

Table 3.4. Uncorrelated parameters from the fit. The old parameters are linear combinations of the new parameters. The coefficients are given in this table (I.e., $z_{ob} = 0.02 \cdot p_1 + ...$). The errors indicated are the statistical errors on the new parameters.

parameter	error	z_{ob}	z_{oc}	BR(b $\rightarrow$ e)	BR(c $\rightarrow$ e)	s_π	s_γ
p_1	$\pm$0.0043	0.02	0.04	-0.17	-0.98	-0.04	-0.01
p_2	$\pm$0.0152	-0.21	-0.07	0.96	-0.17	-0.04	-0.02
p_3	$\pm$0.0362	0.63	0.74	0.19	0.01	-0.09	-0.10
p_4	$\pm$0.0652	-0.74	0.65	-0.12	0.03	-0.04	-0.11
p_5	$\pm$0.0957	-0.03	0.04	-0.02	0.02	-0.69	0.73
p_6	$\pm$0.0850	0.00	-0.17	-0.05	0.04	-0.72	-0.67

of the eigenvalues. The results of this procedure are shown in Table 3.4.

4. THE IMPACT PARAMETER TECHNIQUE

The b-lifetime measurement reported on here is based on the impact parameter technique. This method has been used previously by several different groups[31,32,33] to measure the average lifetime of hadrons containing bottom quarks. The impact parameter (δ) is the distance of closest approach in the x,y plane of a track to the nominal beam center. This is shown in Fig. 4.1. The sign of the impact parameter is determined by the direction of the track relative to the assumed direction of the parent hadron. This is done in a manner so that a positive δ corresponds to the parent hadron traveling a positive distance along its assumed direction before decaying. The parent hadron direction is approximated by the

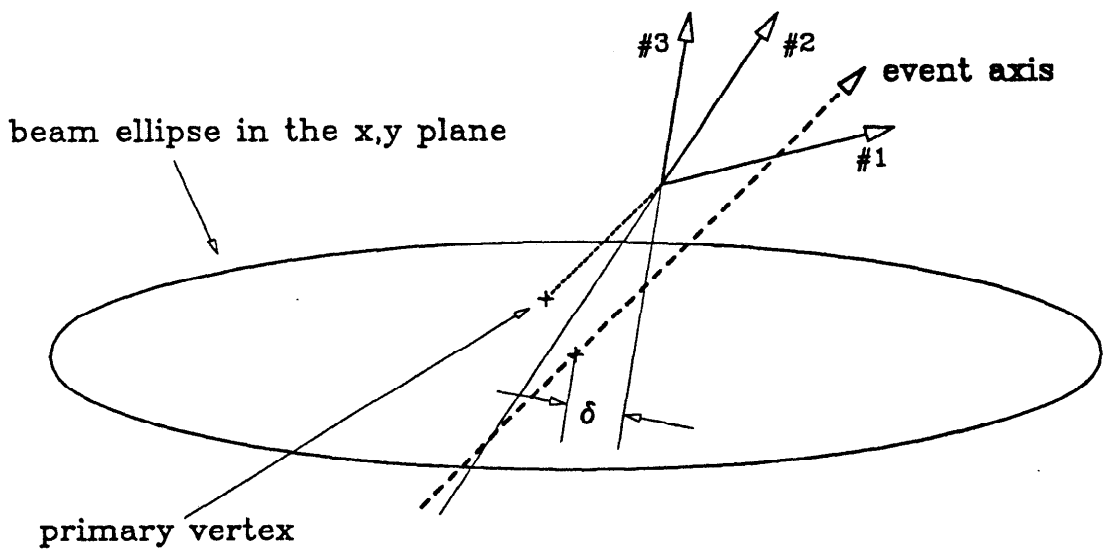

Figure 4.1. Definition of the impact parameter. A B-hadron is produced at the point marked primary vertex. In this figure the B-hadron is shown decaying into 3 charged tracks. Tracks 1 and 3 intersect the event axis at spots which correspond to the B-hadron having traveled a positive distance from the center of the beam ellipse before decaying, and they therefore have $\delta > 0$. Track 2 has $\delta < 0$. In this figure this arises because the primary vertex is not coincident with the center of the beam ellipse. Impact parameters less than zero are also produced by tracking resolution errors, and by errors in finding the events axis. In this analysis the sphericity axis, as determined from all charged tracks, is used as the event axis.

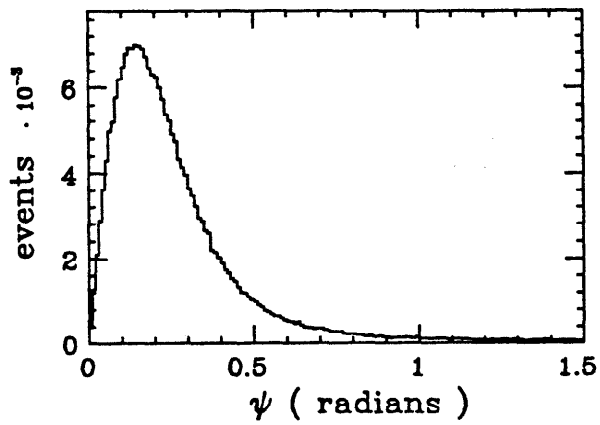

Figure 4.2. A Monte Carlo calculation of ψ (the angle between the sphericity axis and the B-hadron direction).

sphericity axis for events in this analysis. Fig. 4.2 shows a Monte Carlo calculation of the angle between the sphericity axis and the parent hadron. Typical errors in the direction are about 15°. These errors are caused by the presence of charged particles from the fragmentation process, by neutral particles produced in the decay of the bottom hadrons, and by gluon radiation. As can be appreciated from Fig. 4.1, for events in which the angle between the parent hadron direction and the decay particle direction is not $\approx 0°$ or $\approx 90°$, a small error on the parent direction has no effect on δ. The systematic error associated with this will be discussed in the next chapter.

This method of putting the sign on the impact parameter has important implications. Since the sources of error in the measurement of δ generally are unrelated to the sphericity axis, this method will flip the sign on δ in a random manner. Therefore, in the absence of particles with finite lifetimes, the average value of δ ($\bar{\delta}$) will be zero. Because of this, any deviation of $\bar{\delta}$ from zero is evidence for a non-zero lifetime. The contribution to δ made by the finite lifetime of the parent particle depends both on the parent's path length and on the geometry of the decay. From Fig. 4.1 it is clear that the decay products which make a small angle with the parent direction produce small impact parameters and vice versa.

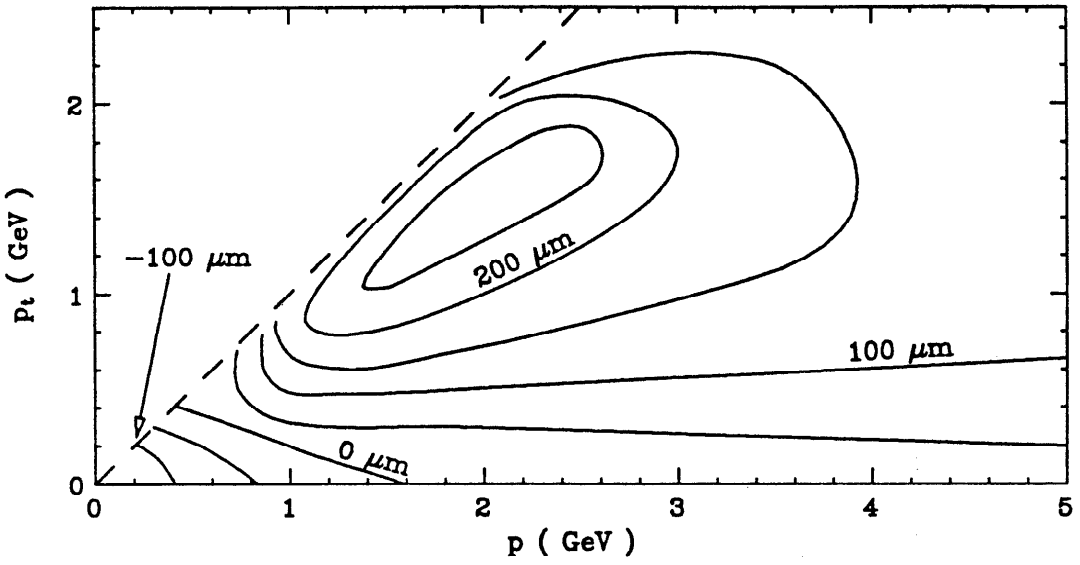

Figure 4.3. Average impact parameter as a function of p and p_t for electrons from the decay of B-hadrons. This figure is the result of a Monte Carlo calculation with $\tau_b = 1.0$ psec. The dashed line shows the $p = p_t$ limit.

This gives rise to substantial acceptance effects. Fig. 4.3 is a contour plot of a Monte Carlo calculation of the average impact parameter ($\bar{\delta}$) for electrons from the decay of B-hadrons. It shows a large variation of $\bar{\delta}$ over the range of interest. The DELCO detector's ability to identify low momentum electrons gives it a substantial advantage over other experiments because of these acceptance effects. While this advantage is partially offset by the detector's modest resolution, the measurement remains competitive.

4.1 The Track Quality Cuts for the Lifetime Analysis

Stringent track quality cuts are placed on the tracks from the electron analysis to ensure that the impact parameters are well measured and to try to eliminate any possibility of confusion due to the presence of nearby or overlapping tracks. The cuts which are applied to the tracks are:

- There must be at least 4 wires in the IDC associated with the track.
- There must be at least 7 wires in the CDC associated with the track.
- There must be at least 4 wires in the PDC associated with the track.

Table 4.1. The fractions of tracks from various sources for the b-region and the c-region defined in the text. These numbers are obtained as part of the fit to the electron spectrum which is described in Chapter 3.

region	b → e	b → c → e	c → e	bckg
b	0.70	0.09	0.17	0.04
c	0.15	0.15	0.56	0.14

- There must be at least 17 wires in the sum of the IDC, CDC, and PDC associated with the track.
- The χ^2 of the track after fitting must be less than 40. (χ^2 = the sum of the squares of the normalized residuals.)
- The greatest residual in the IDC must be less than 800 μm.
- The greatest residual in the CDC must be less than 900 μm.
- The RMS residual in the IDC must be less than 400 μm.
- The RMS residual in the CDC must be less than 450 μm.
- The distance between the z-coordinate of the track origin (z_0) and the z-coordinate of the event vertex must be less than 2.5 times the error on z_0 calculated during fitting. The z-coordinate of the event is calculated using all the tracks in the event.
- There must be no other tracks in the event within 50 mr in ϕ (where ϕ is the azimuthal angle).

4.2 The Electron Data

In order to exhibit the signal, it is useful to divide the data into two subsets. The p, p_t plane can be divided into a b-region ($p_t > 1$ GeV) and a c-region ($p > 1$ GeV, $p_t < 1$ GeV), such that most tracks in the b-region will be electrons from B-hadron decay and most tracks in the c-region will be electrons from charmed hadron decay. Table 4.1 shows the result of breaking the plane up in this manner. The fractions of tracks from various sources are calculated from the results of the fit to the electron spectrum in p and p_t.

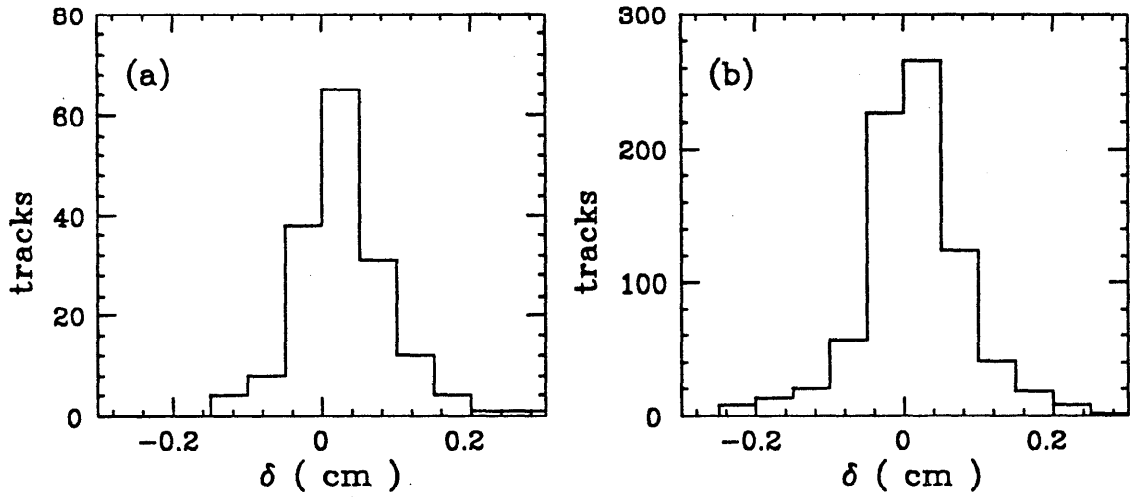

Figure 4.4. Impact parameter distributions before track quality cuts. Part (a) is for the b-region and part (b) is for the c-region.

Fig. 4.4a shows the distribution of impact parameters for tracks in the b-region and Fig.4.4b shows the same distribution for tracks in the c-region. Both of these distributions were made before the track quality cuts. The result of these cuts is to reduce the number of tracks in the b-region from 164 to 113 and in the c-region from 783 to 449. The impact parameter distributions for the two regions after these cuts are shown in Fig. 4.5. Applying the track quality cuts results in a substantial narrowing of these distributions. The widths of these distributions before the cuts were 619 ± 34 (stat.) μm and 727 ± 18 (stat.) μm for the b-region and the c-region respectively. After the cuts the widths are 529 ± 35 (stat.) μm and 594 ± 20 (stat.) μm. From the figures it is clear that a substantial portion of the tracks eliminated by the cuts were in the tails of the distributions. The mean impact parameters after the track quality cuts are $\bar{\delta} = 259 \pm 49$ (stat.) μm for the b-region and $\bar{\delta} = 146 \pm 28$ (stat.) μm for the c-region. In both cases these numbers are significantly greater than zero and suggest the existence of long lived particles. As was stated previously, tracks with impact parameters greater than 0.3 cm are not used. It is reasonably clear from the distributions of δ that this produces only a small bias. This cut will be explicitly accounted for in the fit.

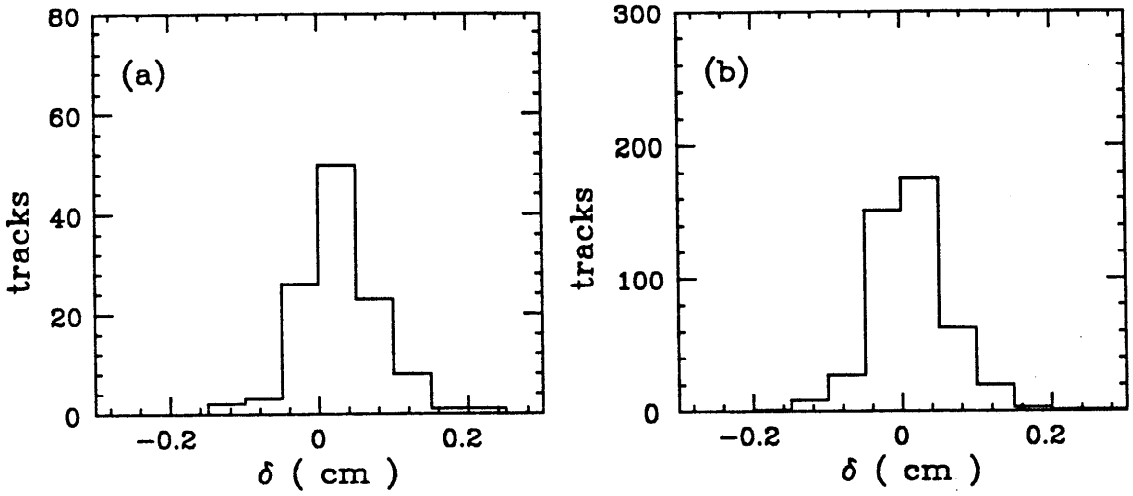

Figure 4.5. Impact parameter distributions after track quality cuts. Part (a) is for the b-region and part (b) is for the c-region.

4.3 The Errors Affecting the Measurement of δ

There are three obvious contributions to the error on δ (σ_δ). The largest comes from the finite beam size. The beam is expected to be Gaussian in x and y with the height quite small (less than 100 μm) and the width somewhat larger (several hundreds of μm's). This ϕ dependence in σ_δ is clearly present in the distribution of δ for tracks from Bhabha events. Fig. 4.6 shows the distribution of δ for tracks which are nearly vertical (a) and for tracks which are nearly horizontal (b). The difference in the widths of these distributions is clear. For tracks which are nearly horizontal, the beam size makes a small contribution. For these tracks σ_δ is dominated by the drift chamber resolution ($\sigma_{D.C.}$) which typically contributes about 230 μm. In addition to the beam size and the drift chamber resolution, multiple Coulomb scattering in the beam pipe and the inner wall of the IDC contributes to the resolution obtained in measuring δ.

4.3.1 The errors due to the beam size and the drift chambers

The errors from the finite beam size and the drift chamber resolution are assumed to be Gaussianly distributed with a width that can be written as

$$\sigma_\delta^2 = \sigma_x^2 \cdot \sin^2\phi + \sigma_y^2 \cdot \cos^2\phi, \tag{4.1}$$

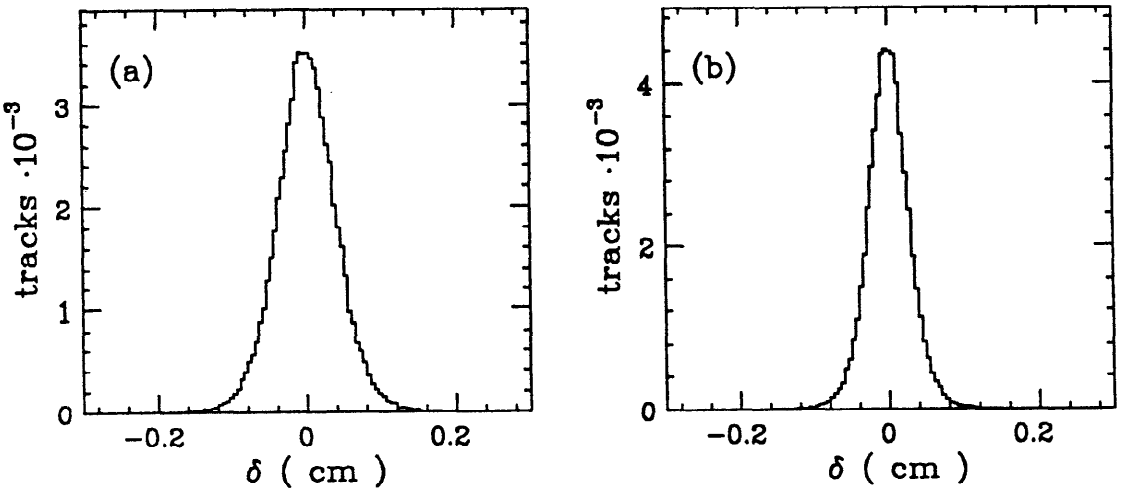

Figure 4.6. Impact parameters for vertical and horizontal tracks from Bhabha events. In part (a) the tracks are within ±45° of the vertical and in part (b) they are within ±45° of the horizontal. Both distributions have means consistent with zero. The width of the first is $393 \pm 3\mu m$ (stat.) and the width of the second is $273 \pm 1\mu m$ (stat.).

where $\phi = 0$ corresponds to a track pointing along the x-axis. The constants σ_x and σ_y describe the sum in quadrature of the drift chamber resolution and the horizontal and vertical beam size respectively. These numbers are measured using tracks from Bhabha events. Because of their large momenta, these tracks should not be affected by multiple scattering. A maximum likelihood fit is done to get σ_x and σ_y. The probability density function used is

$$P(\delta) = \frac{1}{\sqrt{2\pi}\sigma_\delta} \exp\left(-\frac{\delta^2}{2\sigma_\delta^2}\right). \tag{4.2}$$

Tracks with impact parameters greater than 2 σ_δ are not used in this fit so that the tails of the distribution will not pull the fit.[34] This causes a bias on the fitted values of σ_x and σ_y of order 14 %. A correction is made for this bias.[35] Table 4.2 summarizes the results of these fits for various run blocks.

Although it is not essential to the analysis, it is interesting to determine how much of the error on δ comes from the beam size and how much comes from the drift chamber resolution. It is possible to measure the error due to the drift chamber

Table 4.2. A summary of the resolutions obtained in measuring δ for various data sets. The exact definitions of σ_x, σ_y, $\sigma_{D.C.}$, and A are given in the text. Briefly, σ_x and σ_y are the sum in quadrature of the drift chamber resolution and the horizontal or vertical beam sizes respectively, $\sigma_{D.C.}$ is the drift chamber resolution, and A describes the contribution of the multiple scattering to the resolution.

data	σ_x (μm)	σ_y (μm)	$\sigma_{D.C.}$ (μm)	A (μm · GeV)
'82	506	212	212	246
'83	439	242	241	263
'84	388	227	220	198

resolution by using the two nearly parallel tracks produced in Bhabha events. Since these two tracks are produced at the same point, their separation near the beam center (δ_{2tr}) is just the sum of their respective drift chamber errors. More specifically, if $\hat{d}_i$ is a unit vector in the direction of track i, and if $\vec{x}_i$ is the point of closest approach of track i to the beam center, then $\delta_{2tr} = |(\vec{x}_1 - \vec{x}_2) \times \hat{d}|$ where $\hat{d}$ is a unit vector in the direction of $\hat{d}_1 - \hat{d}_2$. This procedure is necessary because the two tracks are generally not exactly parallel. The drift chamber resolution is given by $\frac{1}{\sqrt{2}}$ times the standard deviation of the δ_{2tr}'s. Events with $\delta_{2tr} > 2\sqrt{2}\sigma_{D.C.}$ are not used. This causes a bias similar to that mentioned above and is corrected in the same manner. The results are shown in Table 4.2.

This prescription for calculating σ_δ can be tested by making a histogram of the quantity $\frac{\delta}{\sigma_\delta}$. This distribution will be referred to as the resolution function. If the calculation of σ_δ is correct, and if the assumption that δ is Gaussianly distributed is correct, then the resolution function will be a Gaussian centered on zero with unit width. The result of this check for tracks from Bhabha events is shown in Fig. 4.7. The two curves agree well inside of $\pm 2.5\,\sigma$, but there is a substantial excess of events in the data outside this region. The effect of this deviation from a Gaussian shape will be investigated in the next chapter.

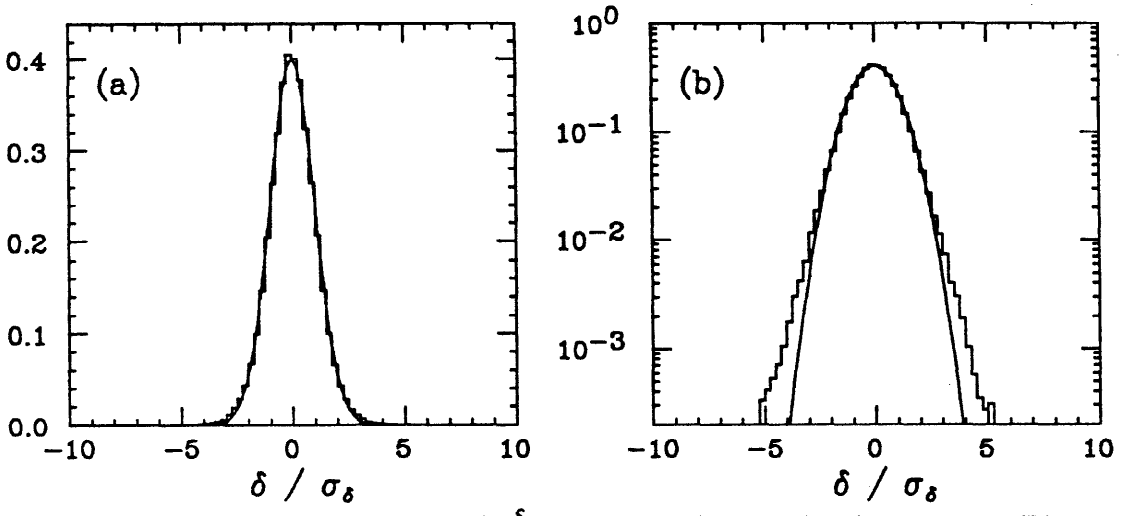

Figure 4.7. The distribution of $\frac{\delta}{\sigma_\delta}$ for tracks from Bhabha events. The histogram is the data and the smooth curve is a Gaussian centered on zero with unit width. Part (a) is plotted with a linear scale and part (b) is plotted with a logarithmic scale. The distributions are normalized to unity.

4.3.2 The errors due to multiple scattering

Multiple scattering in the beam pipe and the inner wall of the IDC contributes to the errors on δ. This contribution can be calculated according to the Gaussian approximation from the Particle Properties Data Booklet [36] as follows:

$$\sigma_{m.s.} = \frac{R}{\sin\theta}\frac{0.0141}{p\beta}\sqrt{\frac{X_r}{\sin\theta}}\left(1+\frac{1}{9}\log_{10}\left(\frac{X_r}{\sin\theta}\right)\right), \tag{4.3}$$

where θ is the polar angle, p is the momentum of the particle in GeV, β is the velocity in units of the speed of light, and X_r is the thickness of the material in radiation lengths. Table 4.3 summarizes the amount of material and its location for the various run blocks. This expression only provides a description of the Gaussian core of the multiple scattering distribution. It is well known[36] that the tails of the multiple scattering distribution are much larger than those of a Gaussian. (In the projected angle distribution they fall only as ϕ^{-3}.) In order to check the accuracy of this calculation, as well as the size of the tails on the resolution function, a source of low momentum tracks is needed. These tracks are obtained from the two-photon

Table 4.3. The material between the beam and the drift chambers at normal incidence. Numbers separated by a slash indicate a change in the detector. The original thick beam pipe was replaced with a thinner one between '83 and '84.

What	radius (cm)	# radiation lengths
beam pipe	8.79 / 7.65	0.0225 / 0.0059
IDC entrance	10.0	0.0070

process $e^+e^- \rightarrow e^+e^-e^+e^-$. Events are required to pass the following cuts:

- One and only one of the luminosity monitors must have a large pulse height.
- Each event must have exactly two "good" tracks after fitting. (See the description of the hadron filter in Chapter 3 for the definition of a "good" track.)
- Each track must be associated with a latched shower counter. A shower counter should latch in response to a minimum ionizing particle.
- Each track must have produced either eight (isobutane) or one (nitrogen) corrected photo-electrons in the Čerenkov counter.

For this data set the "sphericity axis" is taken to point in the direction of the vector sum of the two particles' momenta. The impact parameter distribution for tracks which pass the track quality cuts and which have $p > 1$ GeV is shown in Fig. 4.8. The mean of this distribution, $\bar{\delta}= -0.8 \pm 6.7$ (stat.) μm, is consistent with zero as expected. This provides some confidence that there are no subtle instrumental effects which can produce an average impact parameter greater than zero. The accuracy of the calculation of σ_δ described above is checked by making a histogram of $\frac{\delta}{\sigma_\delta}$ for this data. The histogram is shown in Fig. 4.9. The non-Gaussian tails are clearly larger than those in the Bhabha events. The core of the distribution is also wider than expected. It is clear that equation 4.3 does not provide an adequate description of the degradation of the impact parameter resolution for low momentum tracks. Because of this it was necessary to measure this degradation. For these tracks the

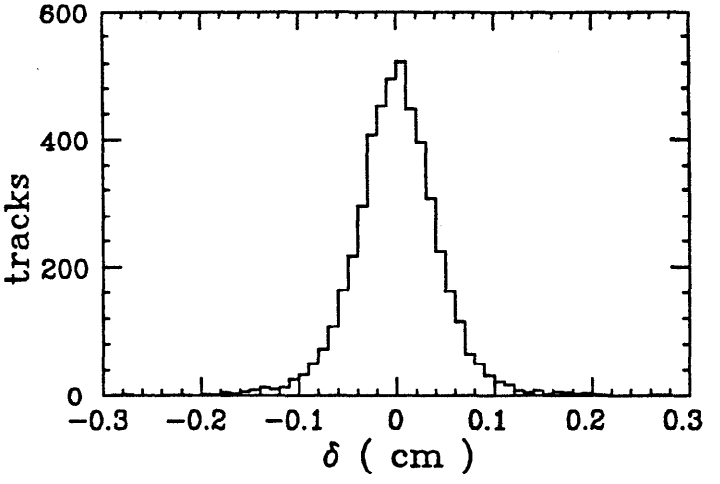

Figure 4.8. The distribution of δ for electrons from $e^+e^- \rightarrow e^+e^-e^+e^-$. This distribution serves as a check that there are no spurious sources of average impact parameters greater than zero.

error on δ can be written as

$$\sigma_\delta^2 = \sigma_x^2 \cdot \sin^2\phi + \sigma_y^2 \cdot \cos^2\phi + \left(\frac{A}{p \sin^{\frac{3}{2}}\theta}\right)^2 . \qquad (4.4)$$

The constant A is determined from a maximum likelihood fit similar to the fit used to obtain σ_x and σ_y. The factor of $\frac{1}{p}$ arises from the $\frac{1}{p}$ dependence of multiple scattering. The factor of $\sin^{-\frac{3}{2}}\theta$ is produced by the dependence of the path length and the material thickness on θ. Since the material in question has a cylindrical geometry, the path length produces a factor of $\sin^{-1}\theta$ and the material thickness a factor of $\sin^{-\frac{1}{2}}\theta$ (by way of the $\sqrt{X_r}$ term in equation 4.3). In this fit σ_x and σ_y were held constant at the values determined from the fit to the Bhabhas. The results of these fits are also shown in Table 4.2 for the various run blocks. The value expected, based on the known material between the interaction point and the first layer of the IDC, is 176 μm · Gev for '82 and '83 and 108 μm · Gev for '84. This degradation may be due to the material in the drift chambers which is not accounted for in the simple analysis given above. This material (the outer wall of the IDC, the inner wall of the CDC, and the gas and wires of both chambers) amounts to 0.0128 of a radiation length and is therefore comparable to the material

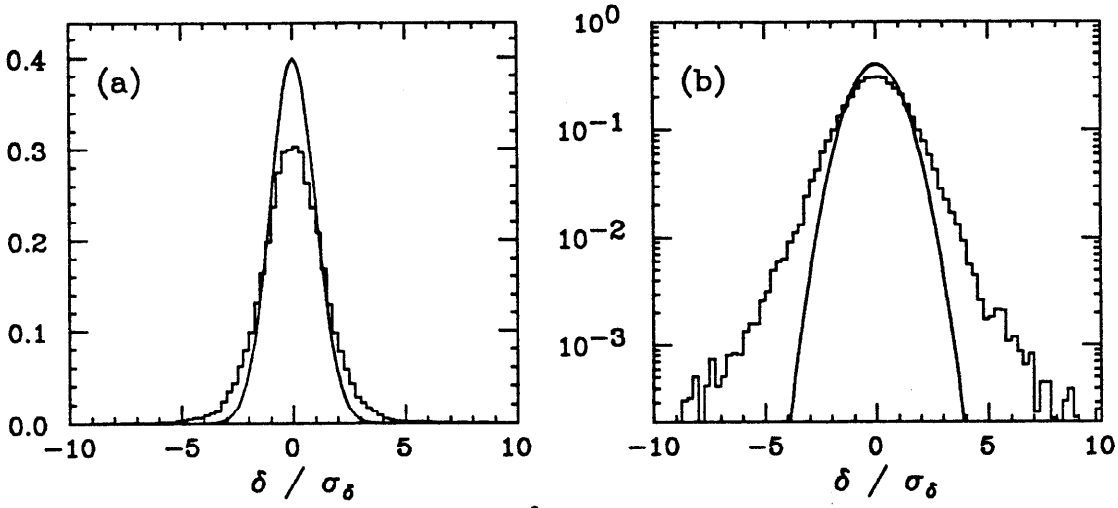

Figure 4.9. The distribution of $\frac{\delta}{\sigma_\delta}$ for tracks from two-gamma events. In this case the multiple scattering contribution to σ_δ is calculated using equation 4.3. The histogram is the data and the smooth curve is a Gaussian centered on zero with unit width. Part (a) is plotted with a linear scale and part (b) is plotted with a logarithmic scale. The distributions are normalized to unity.

between the interaction point and the first layer of the IDC. The resolution function obtained from tracks in the two-gamma data set, when σ_δ is calculated using equation 4.4, is shown in Fig. 4.10. As was the case with the tracks from Bhabha events, the distribution of $\frac{\delta}{\sigma_\delta}$ appears Gaussian in the central region, but there are substantial non-Gaussian tails outside of about $\pm 2.5\ \sigma$. A similar study has been carried out using a mixture of pions and muons from the two-gamma processes $e^+e^- \rightarrow e^+e^-\pi^+\pi^-$ and $e^+e^- \rightarrow e^+e^-\mu^+\mu^-$. The results obtained are very similar and suggest that the resolution is independent of the particle type.[37]

4.3.3 Additional errors in hadronic events

A third data set which can be used to determine the resolution consists of all the tracks in hadronic events. Impact parameter distributions from tracks in hadronic events have been examined to verify that there are not any sources of error which give rise to positive average impact parameters which are particular to hadronic events. An example of such a source would be confusion between tracks during track reconstruction. Errors from this source would clearly depend on the

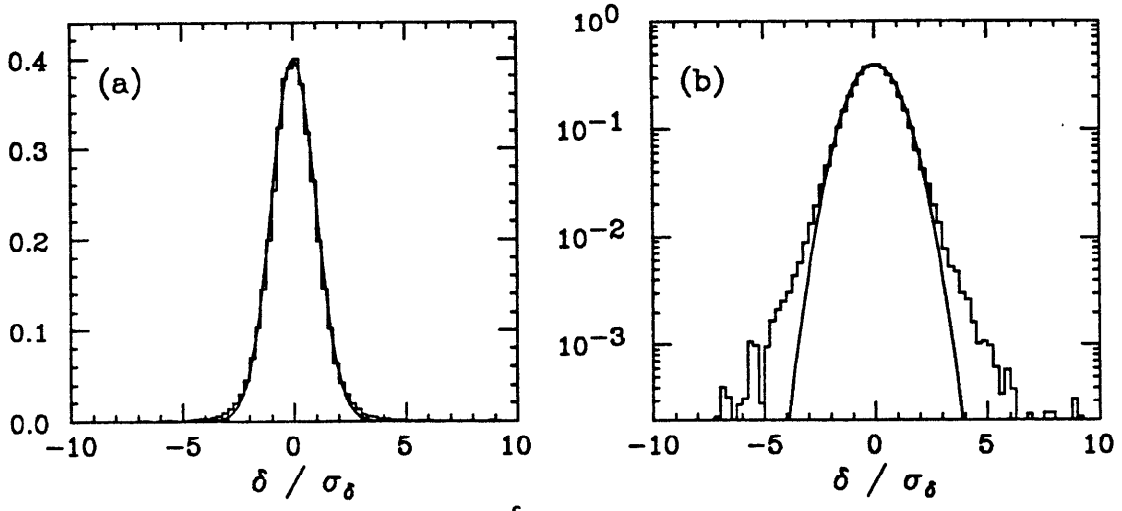

Figure 4.10. The distribution of $\frac{\delta}{\sigma_\delta}$ for tracks from two-gamma events. In this case σ_δ is calculated using the fitted value of A. The histogram is the data and the smooth curve is a Gaussian centered on zero with unit width. Part (a) is plotted with a linear scale and part (b) is plotted with a logarithmic scale. The distributions are normalized to unity.

number and distribution of tracks in the event and could, therefore, be very different for different types of events.

The cuts used to select these tracks were identical to those used to select the electron tracks for the lifetime analysis, except that no Čerenkov counter was required. The data was divided into a b-region and a c-region in the same manner as was done for the electrons. In both cases the average impact parameter is expected to be small and positive because a fraction of the tracks will be from the decay of hadrons containing heavy quarks. The distribution for the b-region is shown in Fig. 4.11a and the distribution for the c-region is shown in Fig. 4.11b. The means of these distributions are $\bar{\delta}= 46 \pm 5$ (stat.) μm for the b-region and $\bar{\delta}= 42 \pm 2$ (stat.) μm for the c-region. These means are calculated using only tracks with $|\delta| < 0.3$ cm to prevent them from being pulled by the tails of the distribution. (Pions from the decays of K_s's, for instance, can have enormous impact parameters.) This is the same maximum impact parameter used in the lifetime analysis. A full detector simulation Monte Carlo calculation of these quantities gives $\bar{\delta}= 38 \pm 11$ (stat.) μm for the b-region and $\bar{\delta}= 43 \pm 4$ (stat.) μm for the c-region. In both

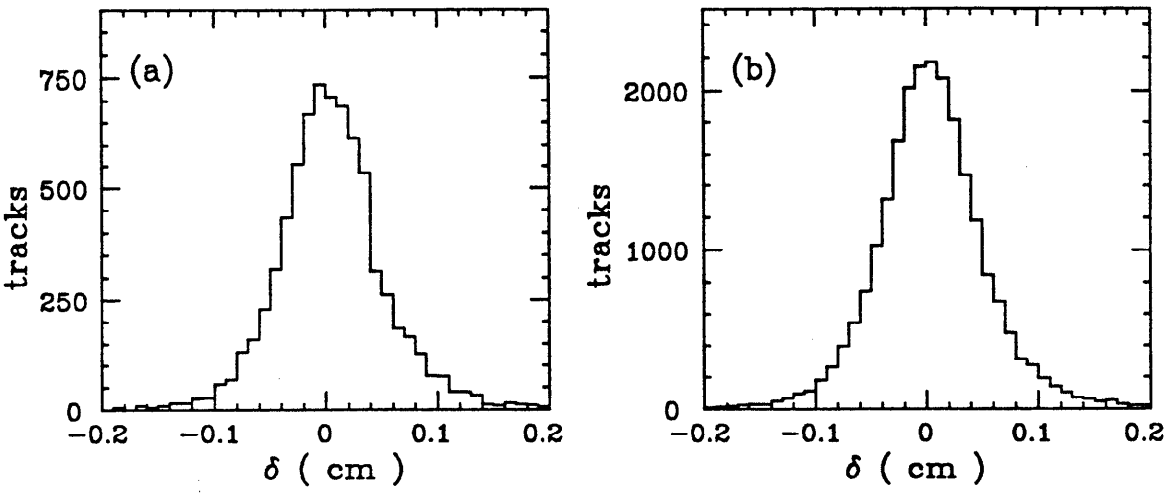

Figure 4.11. Impact parameter distribution for all tracks in hadronic events. Part (a) is for tracks in the b-region defined in the text and part (b) is for tracks in the c-region.

cases these numbers are consistent with the data. A histogram of $\frac{\delta}{\sigma_\delta}$ for the tracks from hadronic events is shown in Fig. 4.12. This resolution function is skewed in the positive direction and contains large tails. Both of these effects are due to the presence of long-lived particles in this data. The tails are due to the inclusion of pions and protons from the decay of K_s's and Λ's, and the shift of the central portion of the distribution is due to the inclusion of particles from the decay of bottom and charmed hadrons. Because of the contamination by long-lived particles, this distribution can not be directly compared with a Gaussian.

An involved "unfolding" process has been used to obtain the resolution function from this data.[38] The distribution of $\frac{\delta}{\sigma_\delta}$ obtained from the hadronic events is assumed to result from the convolution of a known lifetime distribution with an unknown resolution function. If the distribution of $\frac{\delta}{\sigma_\delta}$ in the data is given by $P^m(\frac{\delta}{\sigma_\delta})$ and the resolution function is given by $P^{rf}(\frac{\delta}{\sigma_\delta})$ then one expects

$$P^m(x) = \int_{-\infty}^{\infty} P^{rf}(y)C(y,x)dy, \tag{4.5}$$

where $C(y,x)$ is a known function which describes the smearing due to particles

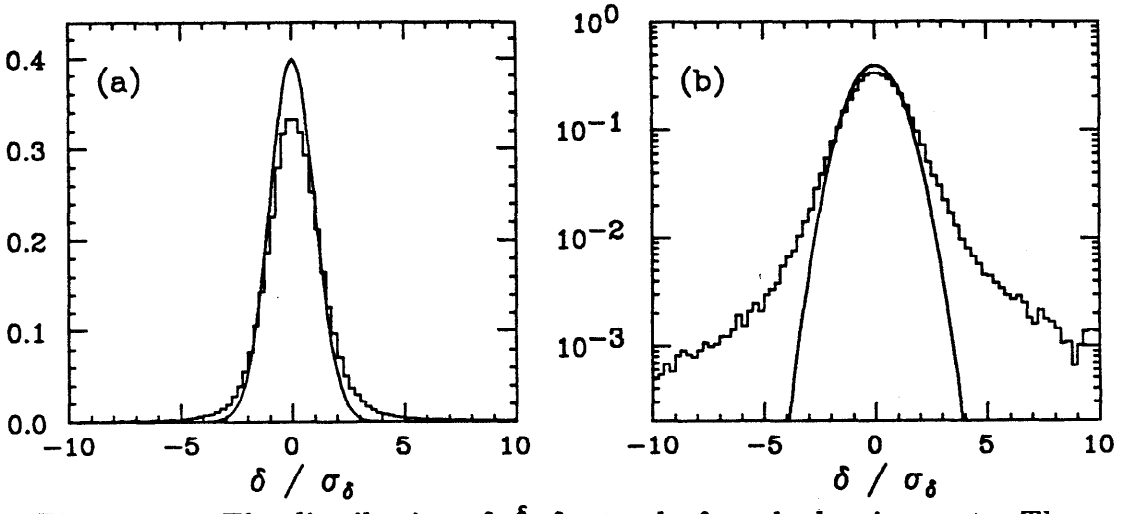

Figure 4.12. The distribution of $\frac{\delta}{\sigma_\delta}$ for tracks from hadronic events. The histogram is the data and the smooth curve is a Gaussian centered on zero with unit width. Part (a) is plotted with a linear scale and part (b) is plotted with a logarithmic scale. The distributions are normalized to unity.

with finite lifetimes. Breaking this up into a discrete form gives

$$P_i^m = \int_{-\infty}^{\infty} P^{rf}(y) C_i(y) dy, \tag{4.6}$$

where P_i^m is now the expected contents of the i'th (i=1,n) bin of the histogram of $\frac{\delta}{\sigma_\delta}$; i.e.,

$$P_i^m = \int_{i'th\ bin} P^m(x) dx. \tag{4.7}$$

If the resolution function is written as a linear combination of m other functions, then

$$P^{rf}(y) = \sum_{j=1}^{m} a_j \cdot p_j(y). \tag{4.8}$$

Plugging this into equation 4.6 gives

$$P_i^m = \int_{-\infty}^{\infty} \sum_{j=1}^{m} a_j \cdot p_j(y) \cdot C_i(y) dy, \tag{4.9}$$

and interchanging the order of summation and integration gives

$$P_i^m = \sum_{j=1}^{m} a_j \cdot \int_{-\infty}^{\infty} p_j(y) \cdot C_i(y) dy. \tag{4.10}$$

Since the $p_j(y)$'s as well as the $C_i(y)$'s are known functions, it is convenient to write the integral in the above equation as

$$C_{ij} = \int_{-\infty}^{\infty} p_j(y) \cdot C_i(y) dy. \tag{4.11}$$

Therefore, C_{ij} represents the contribution of the function $p_j(y)$ to the i'th bin of the distribution of $\frac{\delta}{\sigma_\delta}$ obtained from tracks in hadronic events. Plugging this back into equation 4.10 gives

$$P_i^m = \sum_{j=1}^{m} C_{ij} \cdot a_j. \tag{4.12}$$

If the real content of the i'th bin of the data is D_i, then the likelihood of having observed the D_i's is

$$L(a_1 ... a_m) = \prod_{i=1}^{n} \frac{e^{-P_i^m} \cdot (P_i^m)^{D_i}}{D_i!}, \tag{4.13}$$

where the product is over bins. It is then straightforward to estimate the values of the a_j by maximizing the above expression.

The functions $p_j(y)$ were chosen to be cubic b-splines. These functions are defined and graphed in Appendix B. The values of the C_{ij}'s are obtained by a Monte Carlo calculation. Each event consists of generating a value of δ_n uniformly distributed on the range [-10,10] and then smearing it by an amount $\frac{\delta_l}{\sigma_\delta}$. In this expression δ_l is the contribution to the impact parameter from a particle with finite lifetime, and σ_δ is the calculated error on the impact parameter for that particle. For each event the values of the C_{ij}'s are incremented according to

$$C_{ij} = C_{ij} + p_j(\delta_n), \tag{4.14}$$

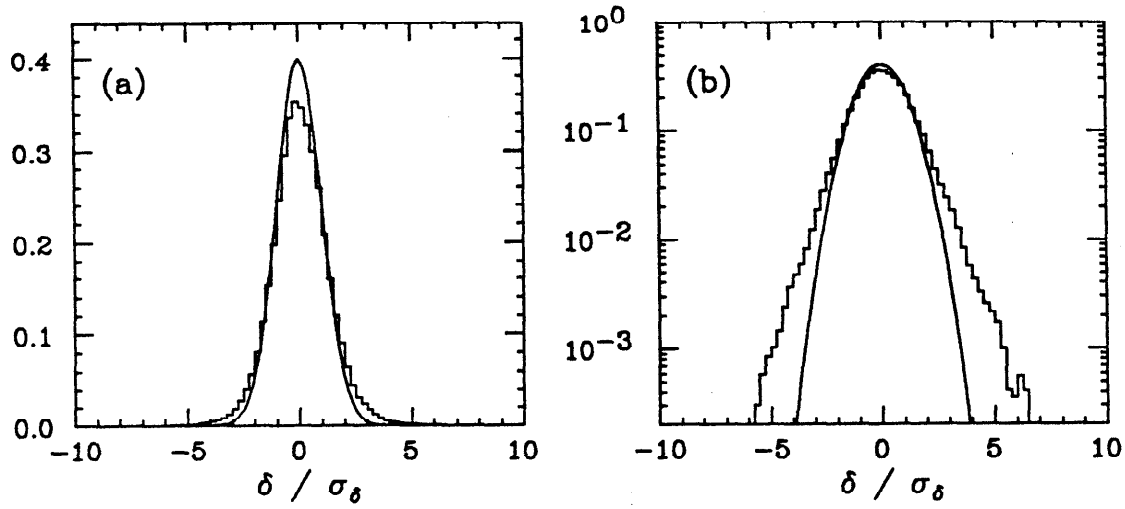

Figure 4.13. The resolution function from hadronic events. The histogram is the unfolded data and the smooth curve is a Gaussian centered on zero with unit width. Part (a) is plotted with a linear scale and part (b) is plotted with a logarithmic scale. The distributions are normalized to unity.

where j runs from 1 to m and i labels the appropriate bin for $\delta_n + \frac{\delta_l}{\sigma_n}$. The result of this unfolding is shown in Fig. 4.13. This distribution has non-Gaussian tails which are comparable to the tails in the resolution function for the tracks from $e^+e^- \rightarrow e^+e^-e^+e^-$. Unfortunately it is also somewhat wider than the resolution function obtained from the electron tracks from the two-gamma process and it is still somewhat asymmetric. Both of these characteristics lead to systematic errors in the b-lifetime. Since there is no obvious mechanism which can produce the asymmetry observed in the tails of the resolution function and which would not be associated with long-lived particles, the resolution function has been symmetrized " by hand ." This is shown in Fig. 4.14. The difference in the b-lifetime obtained with the two resolution functions will be included as a systematic error.[39]

4.4 The Tau Data Set

As a final test of the impact parameter method, a measurement of the lifetime of the tau lepton has been made. The tau lifetime has been measured with high precision by other experiments[40,41,42,43,44] and is found to have a value of

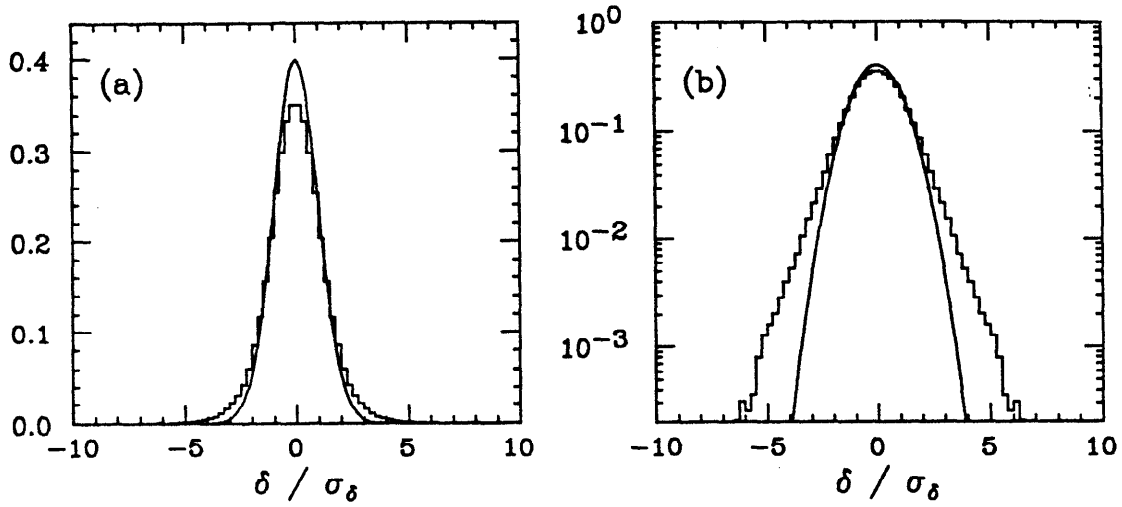

Figure 4.14. The resolution function from hadronic events after symmetrization. The histogram is the unfolded data and the smooth curve is a Gaussian centered on zero with unit width. Part (a) is plotted with a linear scale and part (b) is plotted with a logarithmic scale. The distributions are normalized to unity.

$\tau_\tau = 0.286 \pm 0.016$ (stat.) $\pm$ 0.025 (sys.) psec.[45] Comparing this "known" value of τ_τ with a measurement made using the impact parameter technique provides confidence that the b-lifetime is measured correctly. A measurement of the tau lifetime is particularly useful as a check since the three track side of the 1:3 track tau decays † used in this measurement will suffer some of the same tracking confusion problems that the electron tracks in the b-lifetime analysis suffer. The 1:3 track tau decays were picked for this analysis because they are easily identified by topological cuts only, without the need for particle identification. The large velocity of the tau before decay ($\gamma \approx 8$) results in its decay products typically all being thrown forward to produce the characteristic signature of a single high momentum track back-to-back with three other high momentum tracks. The cuts used to select the tau data set were:

- The thrust and the thrust axis are calculated for each event. Each event

---

† That is, of the two initially produced taus, one decays to produce one charged track and the other decays to produce three charged tracks.

must have a thrust greater than 0.97.

- The event is divided into hemispheres using the thrust axis. The event must have exactly one good track on one side and three good tracks on the opposite side.
- The total charged energy of the event must be at least 6.0 GeV and no greater than 24.0 GeV.
- The z-coordinate of the origin of each track must be within $\pm$ 3.5 cm of the nominal beam center.
- The momentum of each track in the event must be greater than 0.2 GeV.
- Each track in the event must have at least one hit each in the IDC, the CDC, and the PDC.
- The invariant mass of the three track system must be greater than 0.1 GeV and less than 1.8 GeV, assuming the particles have electron masses.
- The invariant mass of the three track system must be greater than 0.5 GeV and less than 2.0 GeV, assuming the particles have pion masses.
- The energy of the three track system must be greater than 3.0 GeV, assuming the particles have pion masses.
- The total charge of the event must be zero.

The result of these cuts is a data set of 1357 events. Monte Carlo calculations estimate that there are backgrounds of 31 hadronic events and 12 Bhabha events. This last background comes from radiative Bhabha events in which the photon converts in the beam pipe or the inner wall of the IDC. Both of these backgrounds will produce only very small errors in the lifetime and are neglected in the following. The tau lifetime can be estimated from the mean of the impact parameter distribution. After applying the track quality cuts listed earlier in this chapter and requiring each track to have $p > 1$ GeV, there are 2177 tracks left with impact parameters less than 0.3 cm. This is the same maximum δ cut used in the b-lifetime analysis. In this case it keeps the lifetime measurement from being pulled by tracks from K_s decay. The tracks in this data set have a mean impact parameter of

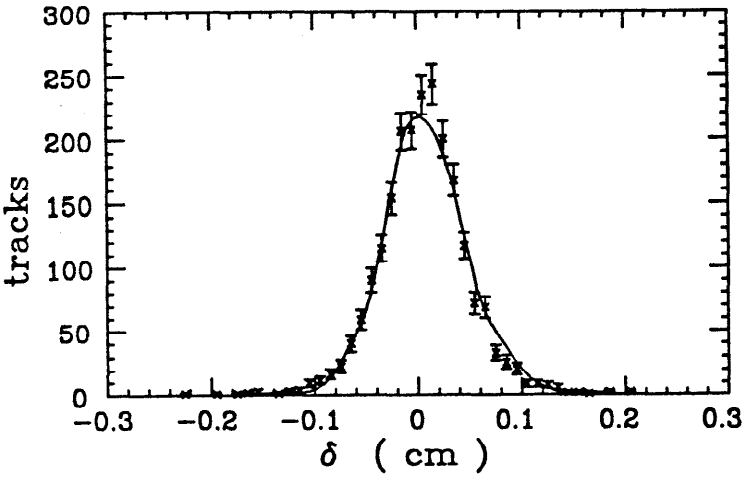

Figure 4.15. Impact parameters from tracks from tau decays. The points are the data and the smooth curve is a Monte Carlo calculation of the expected distribution based on a tau lifetime of 0.3 psec.

$\bar{\delta} = 56.8 \pm 9.3$ (stat.)μm. The distribution of these impact parameters is shown in Fig. 4.15.

The tau lifetime is obtained by a Monte Carlo calculation of $\bar{\delta}$ for various values of τ_τ. The result of this calculation is shown in Fig. 4.16. As one would expect, there is a simple linear relationship between the lifetime and the average impact parameter. The lifetime inferred from these figures is $\tau_\tau = 0.263 \pm 0.046$ (stat.) psec which is consistent with previous measurements.

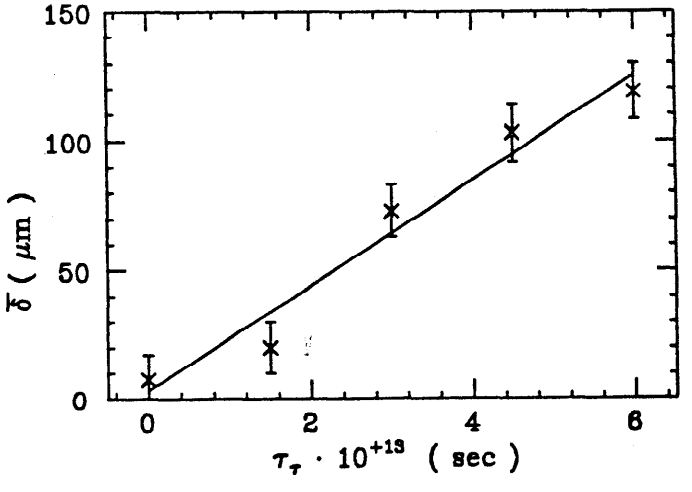

Figure 4.16. Average impact parameter as a function of τ_τ. This figure is the result of a full detector simulation Monte Carlo calculation.

5. THE FIT TO THE IMPACT PARAMETERS

A maximum likelihood (M.L.) fit has been done to estimate the B-hadron lifetime from the impact parameters in a manner similar to previous analyses.[32] This method was picked because it makes it possible to account for the variation in resolution and in the distribution of δ which one expects for tracks with different p, p_t, directions, etc. M.L. fits are also desirable because in some sense they make the best use of the data.[46] They also do not depend heavily on the data in calculating the error on the lifetime. This is in contrast, for instance, to comparing the mean impact parameter, $\bar{\delta}$, with that expected from a M.C. calculation.[33] In this case the error on $\bar{\delta}$ (which is calculated from the width of the data) is used to determine the error on τ_b. Given the limited statistics of this experiment, the uncertainty of the error on $\bar{\delta}$ could be large, making it difficult to determine the significance of the final result. A M.L. fit also makes it possible to test for certain systematic errors in a simple way. For example, it is easy to change the ratio of b $\rightarrow$ e and c $\rightarrow$ e in the fit and observe the effect this has on the measured value of τ_b.

5.1 THE PROBABILITY DENSITY FUNCTION

In order to perform a M.L. fit, it is necessary to calculate the probability of observing the i'th event (P^i). This probability is a function of the parameters we wish to estimate; i.e. $P^i = P^i(\tau_b, \tau_c)$. It is also a function of the variables which describe each event; i.e. the impact parameter (δ), the error on the impact parameter (σ_δ), the momentum of the track (p), the momentum transverse to the sphericity axis (p_t), the sphericity of the event, etc. This fit explicitly accounts for those variables which are most directly affected by the lifetimes (clearly this means δ), and also for some of the other event characteristics which affect δ. The most important of these is σ_δ, while p and p_t are of secondary importance.

The probability of observing the i'th event can be expressed as

$$P^i = f_b^i P_b^i + f_{bc}^i P_{bc}^i + f_c^i P_c^i + f_{bkg}^i P_{bkg}^i, \tag{5.1}$$

where the sum over four terms accounts for the four sources of "electrons" in the analysis. These are: the decay of a hadron containing a b-quark to produce an electron (b $\rightarrow$ e) , the decay of a hadron containing a b-quark to a hadron containing a c-quark followed by the decay of that hadron to produce an electron (b $\rightarrow$ c $\rightarrow$ e) , the decay of a hadron containing a c-quark to produce an electron (c $\rightarrow$ e) , and the various backgrounds. The f_x^i's ($x = b, bc, c, bkg$) are functions of p and p_t only and are the probabilities that an "electron" with a given p and p_t came from the indicated source. They are obtained from the electron analysis described previously. The P_x^i's are functions of δ, σ_δ, p, and p_t. They are the probabilities that an "electron" from a given source, with given p, p_t, and σ_δ, would have an impact parameter δ.

5.1.1 The fractions

The f_x^i's, which are found as part of the electron analysis, are tabulated in Appendix E. These numbers are calculated in 0.5 GeV square bins in p and p_t. They have systematic uncertainties as a result of the limited statistics of the electron analysis. It is important to note that not all of the errors in the published electron analysis apply in this case.[47,48] For instance the uncertainty in the luminosity produces an uncertainty in the branching ratios, but this error exactly cancels in the f_x^i's and so is not considered here.

5.1.2 The impact parameter distributions

The P_x^i's are calculated on the assumption that the distribution of δ can be understood as the convolution of two simpler distributions, one due to the finite lifetimes and the other due to the limited resolution in the measurement of δ. The first of these is referred to as $P_x^{i,exact}$ and the second as $P_x^{i,meas}$. P_x^i then has the form:

$$P_x^i(\delta) = \int_{-\infty}^{\infty} P_x^{i,exact}(\delta') P^{i,meas}(\delta - \delta') d\delta'. \qquad (5.2)$$

The measurement errors are described by the resolution function $P^{rf}(\delta)$ discussed in the previous chapter and are assumed to be independent of the source of the "electron." In terms of this function:

$$P^{i,meas}(\delta) = \frac{1}{\sigma_\delta^i} P^{rf}\left(\frac{\delta}{\sigma_\delta^i}\right), \tag{5.3}$$

where σ_δ^i is the error on δ for the i'th event. This definition of $P^{i,meas}(\delta)$ is just the inverse of the procedure used in the previous chapter to obtain $P^{rf}(\delta)$. The factor of $\frac{1}{\sigma_\delta}$ in front of $P^{rf}(\delta)$ is needed to maintain the normalization. Because $P^{rf}(\delta)$ is in effect scaled by σ_δ^i on an event-by-event basis, the differences in resolution from one track to the next, due to the beam size and the multiple scattering, are accounted for in the fit. Plugging the resolution function into the previous expression for $P_x^i(\delta)$ makes it possible to display explicitly the σ_δ dependence and gives

$$P_x^i(\delta) = \frac{1}{\sigma_\delta^i} \int_{-\infty}^{\infty} P_x^{i,exact}(\delta') P^{rf}\left(\frac{\delta - \delta'}{\sigma_\delta^i}\right) d\delta'. \tag{5.4}$$

The exact impact parameter distributions $P_x^{exact}(\delta; p, p_t)$ are determined by a Monte Carlo calculation. This calculation requires the generation of a large number of Monte Carlo events ($\approx 10^6$). To generate this many events using a full detector simulation Monte Carlo would require a prohibitively large amount of computer time. Because of this it was necessary to develop a simple "non-simulation" Monte Carlo which would reproduce the full simulation Monte Carlo in its gross features and which would use a minimal amount of computer time. The non-simulation Monte Carlo consists of applying the following cuts to the events generated by the Lund Monte Carlo code which is described in Appendix C:

- Only stable charged tracks inside of $|\cos\theta| \leq 0.8$ are considered (θ is the polar angle).
- Tracks with $p \leq 0.20$ GeV are kept or dropped with an efficiency of 16 %.

Table 5.1. Tracking efficiency in ϕ. This table is used in the non-simulation Monte Carlo to simulate the tracking confusion which occurs in jets.

ϕ interval (radians)	efficiency
0.00 - 0.05	0.47
0.05 - 0.10	0.64
0.10 - 0.15	0.68
0.15 - 0.20	0.76
0.20 - 0.25	0.84
0.25 - 0.30	0.86
0.30 - 0.35	0.88
0.35 - 0.40	0.90
0.40 - 0.45	0.92
0.45 - 0.50	0.94
0.50 - 0.55	0.96
0.55 - 0.60	0.98
0.60 - 3.14	1.00

- The momenta of tracks which pass the above cuts are smeared according to $p \rightarrow p/(1+\Delta)$ where Δ is drawn from a Gaussian distribution with width equal to the known detector resolution for a track with momentum p.
- Tracks are kept or dropped at random depending on how close they are to other tracks in ϕ (ϕ is the azimuthal angle). The probability of keeping a track is given in Table 5.1. This procedure is applied twice.

At this point two "event cuts" are applied. Events which fail either of these cuts are dropped:

- The total number of charged tracks left must be at least 5.
- The total energy of all of the charged tracks (assuming pion masses) must be at least 6 GeV.

If the event passes these cuts and if it still has an electron in it, then the following cuts are applied:

- The electron must be inside of $|\cos\theta| \leq 0.6$.

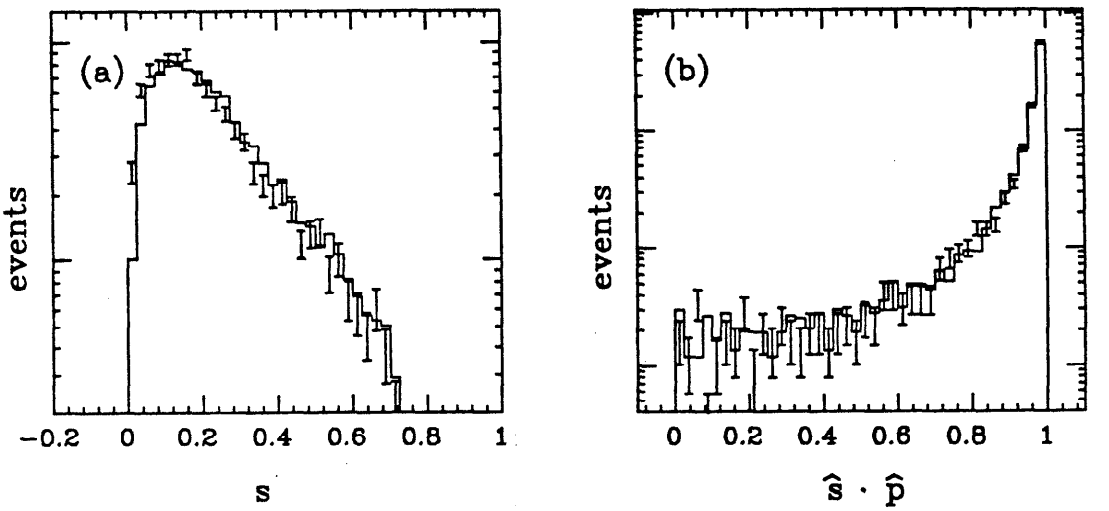

Figure 5.1. Comparison of the non-sim. and full sim. M.C. The histogram is the result of the non-detector simulation Monte Carlo and the points are the result of the full detector simulation Monte Carlo. Part (a) shows a comparison of the sphericity (s) and part (b) shows a comparison of the sphericity axis ($\hat{s}$) dotted into the direction of the B-hadron ($\hat{p}$).

- If there is another track in the same Čerenkov cell as the electron, then the efficiency for keeping the electron is 30 %.

The p_t of the electron is calculated relative to the sphericity axis determined from all of the charged tracks remaining in the event. The following distributions demonstrate the ability of this procedure to reproduce the effects of the full detector simulation Monte Carlo. Fig. 5.1a compares the distribution of the sphericity and Fig. 5.1b compares the distribution of the dot product of the parent hadron (the hadron containing the b- or c-quark) and the sphericity axis. In both cases the agreement is good and demonstrates that the non-simulation Monte Carlo reproduces the sphericity axis properly. Fig. 5.2 is a comparison of the impact parameter distributions of electrons from the decay of heavy quarks as calculated by the two Monte Carlos. The distributions are clearly consistent with each other and show that the non-simulation Monte Carlo correctly accounts for the acceptance effects in the full detector simulation. Similar agreement is obtained for electrons

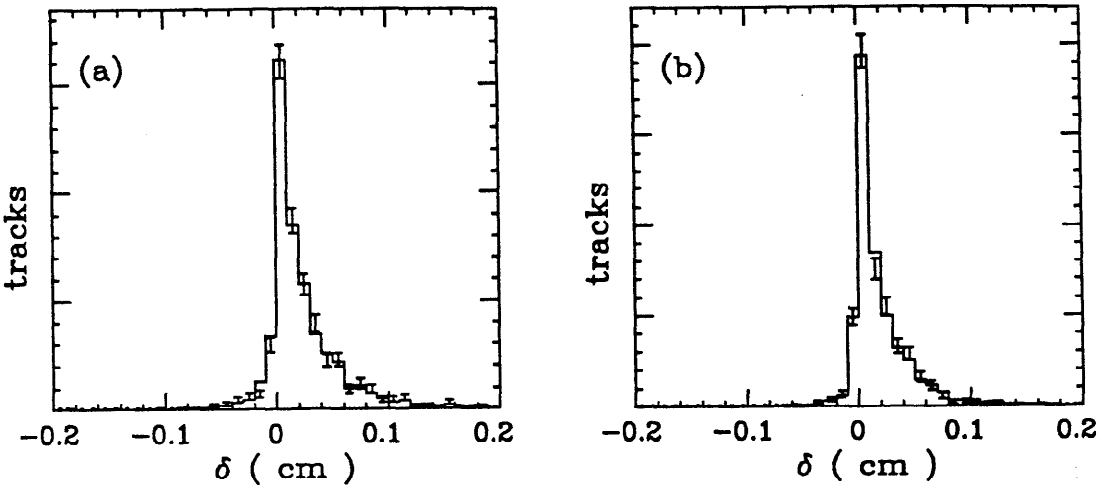

Figure 5.2. Comparison of the calculated impact parameter distributions for electrons from the decay of bottom quarks. The histograms are from the non-simulation Monte Carlo and the points are from the full detector simulation. The electrons were required to have momentum in the range $1 \leq p \leq 2.5$ GeV. Part (a) is for the b-region defined in the text and part (b) is for the c-region.

Table 5.2. Summary of the average impact parameters for electrons from the decay of b-quarks and c-quarks calculated using a full detector simulation (top number) and a non-simulation (bottom number) Monte Carlo.

	all	b-region	c-region
b-quark	$175\pm6\mu m$ $160\pm5\mu m$	$232\pm10\mu m$ $219\pm7\mu m$	$181\pm8\mu m$ $183\pm6\mu m$
c-quark	$160\pm5\mu m$ $154\pm4\mu m$	$32\pm10\mu m$ $37\pm9\mu m$	$117\pm6\mu m$ $119\pm4\mu m$

from c-quark decay. The means of these distributions are summarized in Table 5.2. The average impact parameters calculated using both the full detector simulation and the non-simulation Monte Carlos are consistent for all regions in p and p_t and for both b-quark and c-quark decay.

There exists a substantial systematic uncertainty associated with the calculation of the exact impact parameter distributions. Since the parent hadron is part of a jet produced in the fragmentation process, it does not have a unique momentum. This uncertainty in the momentum produces a corresponding

uncertainty in δ. This is not, in and of itself, a major problem. There are many other details about each event which are known only in an average sense. Because there is no clear theoretical understanding of the fragmentation process, the momentum distribution of the parent hadrons must be measured from the data. This was done in Chapter 3. The limited statistics in this measurement produce a substantial uncertainty in the final b-lifetime measurement. As has been pointed out previously,[49] it could be worse. A particle with lifetime τ will travel a distance $l = \beta\gamma c\tau$ (where β is the velocity in units of the speed of light, $\gamma = (1-\beta^2)^{\frac{1}{2}}$, and c is the speed of light) before it decays. The angle between the track and the parent direction tends to close up as $\frac{1}{\gamma}$, so that as $\beta \rightarrow 1$ the impact parameter becomes independent of the momentum of the parent hadron. In the present situation $\beta \approx 0.87$, so that the limiting case has not been reached and some sensitivity to the parent hadron momentum remains. There is also a contribution to this systematic error due to changes in the number of electrons which come from backward decays of the parent hadron. Fig. 5.3 shows the result of a Monte Carlo calculation of the average impact parameter for different values of $\bar{z}_b$. (The variable $\bar{z}_b$ describes the B-hadron momentum distribution. See Appendix C for a definition.) The details of how this systematic error is propagated through the analysis are covered later in this chapter.

For a given source of electrons, the $P_x^{i,exact}$'s depend on p and p_t. If the "electron" in the i'th event has momentum equal to p^i and transverse momentum equal to p_t^i, then

$$P_x^{i,exact}(\delta) = P_x^{exact}(\delta; p^i, p_t^i). \tag{5.5}$$

The p and p_t dependence is accounted for by binning the P_x^{exact}'s in 0.5 GeV intervals in p and p_t. Fig. 5.4 shows typical results of such a Monte Carlo calculation. Impact parameters less than zero result from backward decays in which the electron ends up in the "wrong" jet and from events in which the sphericity axis does not accurately describe the direction of the parent hadron. The lifetime contribution

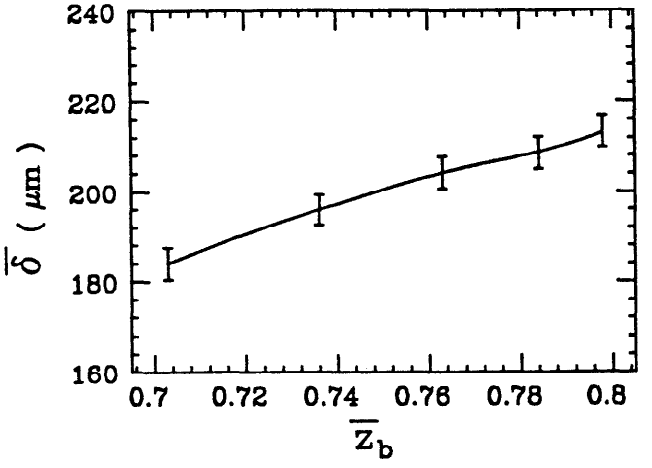

Figure 5.3. Average impact parameter as a function of $\bar{z}_b$. This figure is the result of a Monte Carlo calculation done with $\tau_b = 1.0$ psec. Only tracks with $1.0 \leq p \leq 5.5$ GeV and $p_t \geq 1.0$ GeV were used.

to the impact parameter for a given event can be thought of as being produced in a two step process: first an exponential decay characterized by a length λ, followed by a projection to give δ. This projection is necessary since the impact parameter is defined to be the distance of closest approach of the track, *as projected onto the x-y plane,* to the z-axis. The probability of observing a decay of length l is proportional to

$$P(l;\lambda) = \frac{1}{\lambda}\exp(-\frac{l}{\lambda}). \tag{5.6}$$

This distribution in l has the following property:

$$P(l;\lambda) = \frac{\lambda_0}{\lambda}P(\frac{\lambda_0}{\lambda}l;\lambda_0). \tag{5.7}$$

Since the projection is a purely geometrical operation and is independent of l, it follows that $\delta \propto l$ and therefore

$$P_x^{exact}(\delta;\tau) = \frac{\tau_0}{\tau}P_x^{exact}(\frac{\tau_0}{\tau}\delta;\tau_0), \tag{5.8}$$

so that, for the cases where the impact parameter is due to a single decay (i.e. b $\rightarrow$ e and c $\rightarrow$ e), it is possible to generate the exact distribution once for a given

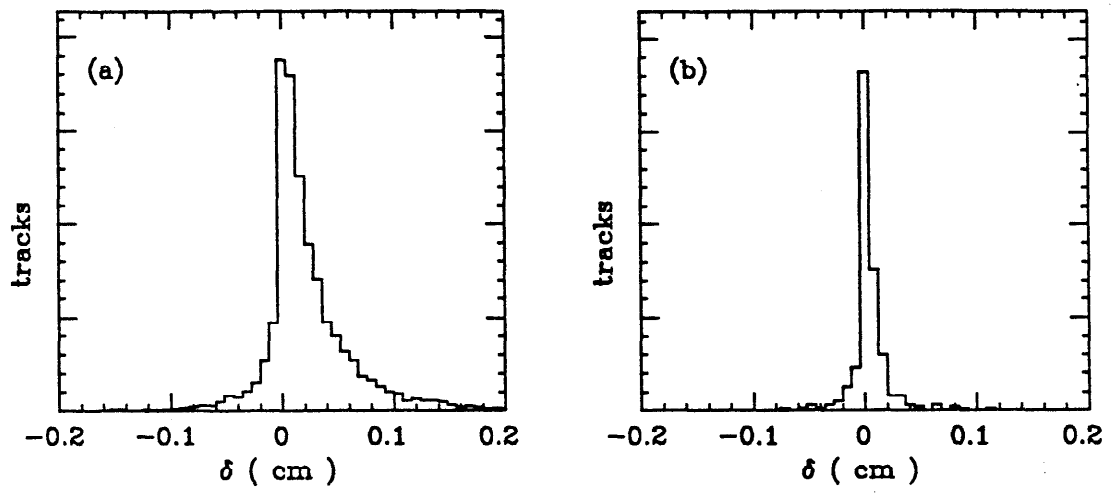

Figure 5.4. Exact impact parameter distributions. Part (a) is for the b → e process and part (b) is for the c → e process. The lifetimes used for this calculation are $\tau_b = 1.00$ psec and $\tau_c = 0.64$ psec.

lifetime, and then scale it as a function of τ_b or τ_c to do the fit. The distribution for the cascade process (b → c → e) does not possess any obvious scaling properties. It is put in as a fixed distribution, independent of τ_b and τ_c. After the fit the distribution is recalculated with the new τ_b and τ_c and the fit is repeated. Since the cascade process contributes little in the p and p_t range of interest, this procedure converges quickly.

The exact impact parameter distribution for the backgrounds does not depend on either τ_b or τ_c. It is put in as a δ-function for the part of the background which is due to misidentified pions, and as a Gaussian whose width depends on p for the part due to gamma conversions. This width arises from the apparent curvature of the electrons from $\gamma \rightarrow e^+e^-$ in the 3.3 kG magnetic field. The widths are summarized in Table 5.3. They are obtained by a full detector simulation Monte Carlo calculation in which photons are converted in the beam pipe and the resulting electrons are "swum" through the magnetic field in the detector. In this case the resolution of the drift chambers has been set to zero (no measurement error) so that only the effects of the magnetic field and the geometry will be present. Tracks are fit to the simulated drift chamber hits in the usual manner. The widths of these

Table 5.3. Widths of the distributions of δ for $\gamma \rightarrow e^+e^-$ in the beam pipe. These numbers are obtained from a full detector simulation Monte Carlo calculation in which the drift chamber resolution is set to zero. The correction to the final b-lifetime due to these effects is very small because there are very few high p_t tracks from gamma conversions.

momentum (GeV)	width (μm)
1.0 - 1.5	520
1.5 - 2.0	370
2.0 - 2.5	286
2.5 - 3.0	234
3.0 - 3.5	200
3.5 - 4.0	173
4.0 - 4.5	153
4.5 - 5.0	137
5.0 - 5.5	124

distributions have only a very small effect on the final lifetime because of the small number of gamma conversion electrons present in the b-region.

The expression above for scaling P_x^{exact} can be plugged into the convolution integral:

$$P_x^i(\delta) = \frac{1}{\sigma_\delta^i} \int_{-\infty}^{\infty} \frac{\tau_0}{\tau} P_x^{i,exact}\left(\frac{\tau_0}{\tau}\delta';\tau_0\right) P^{rf}\left(\frac{\delta-\delta'}{\sigma_\delta^i}\right) d\delta'. \qquad (5.9)$$

By defining a scaling variable s such that $\tau = s \cdot \tau_0$ and by changing the variable of integration one obtains

$$P_x^i(\delta) = \frac{1}{\sigma_\delta^i} \int_{-\infty}^{\infty} P_x^{exact}\left(\delta';p^i,p_t^i\right) P^{rf}\left(\frac{\delta-s\delta'}{\sigma_\delta^i}\right) d\delta'. \qquad (5.10)$$

(Since τ_0 is a constant, the dependence of P_x^{exact} on it is not explicitly shown.) Because the exact distributions in δ are calculated by Monte Carlo methods, it is not possible to do the convolution of P^{meas} with P^{rf} analytically. Hence, the above

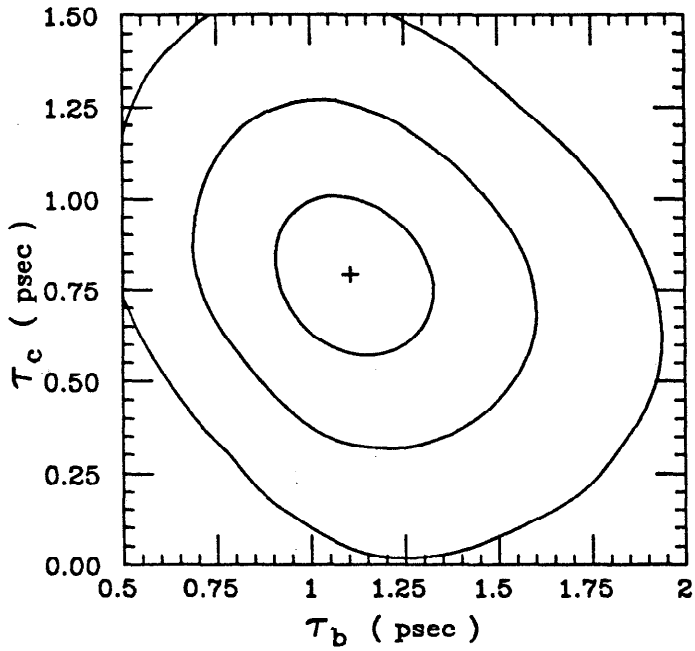

Figure 5.5. Contour plot of the likelihood function versus τ_b and τ_c for all tracks with $p > 1$ GeV. The curves shown are at the one, two, and three sigma levels.

integral becomes a summation. The P^{exact}'s are binned in δ so that the value of δ at the middle of the $j'th$ bin is

$$\delta_j = \delta_0 + j \cdot \Delta\delta, \tag{5.11}$$

where j runs from 1 to n_b and $\Delta\delta$ is the width of a bin in δ. Then for $\delta_j - \frac{1}{2}\Delta\delta < \delta < \delta_j + \frac{1}{2}\Delta\delta$:

$$P_x^{exact}(\delta; p^i, p_t^i) = P_{x,j}^{exact}(p^i, p_t^i), \tag{5.12}$$

and the previous integral becomes

$$P_x^i(\delta) = \frac{\Delta\delta}{\sigma_\delta^i} \sum_{j=1}^{n_b} P_{x,j}^{exact}\left(p^i, p_t^i\right) P^{rf}\left(\frac{s}{\sigma_\delta^i} \cdot \left(\frac{\delta}{s} - \delta_j\right)\right). \tag{5.13}$$

5.2 The Results of Fitting the Electron Data Set

Fig. 5.5 is a contour plot of the likelihood function versus τ_b and τ_c. The

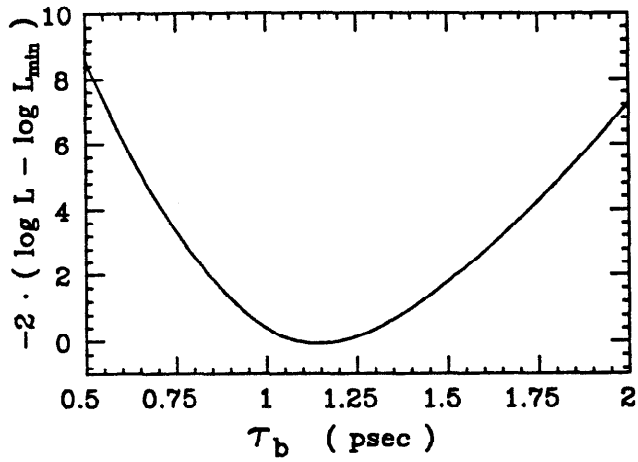

Figure 5.6. The likelihood function versus τ_b. The minimum is at τ_b = 1.15 psec and the 1 sigma error bars are +0.25 psec and −0.21 psec.

resolution function used was obtained from tracks in hadronic events by the unfolding described previously. The one, two, and three sigma contours are shown. The minimum at $\tau_b = 1.10^{+0.22}_{-0.20}$ (stat.) psec and $\tau_c = 0.79^{+0.22}_{-0.22}$ (stat.) psec is consistent with the known value of the average charmed particle lifetime of $\tau_c = 0.64^{+0.10}_{-0.08}$ psec. (See Appendix C for the origin of τ_c and its uncertainty.) This measurement of τ_b suffers from systematic uncertainties due to the uncertainty in the relative fraction of b → e and c → e in the data and due to the uncertainty in τ_c. This effect is driven by tracks in the low p_t region ($p_t < 1$ GeV) where there is a reasonable chance that the track came from the decay of either a charmed or bottom quark. The effect of this systematic error can be reduced by only using tracks with $p_t > 1$ GeV. As was stated previously, the probability that a track in this region came from the decay of a B-hadron in 70 %. The result of fitting just the tracks in the b-region (with τ_c fixed to 0.64 psec) is $\tau_b = 1.15^{+0.25}_{-0.21}$ (stat.) psec. A plot of $-2\,(\log L - \log L_{min})$ is shown in Fig. 5.6.

5.3 Goodness of Fit Tests

It is implicit in the work above that a M.L. estimate assumes an understanding of the distribution from which the data was drawn. It is desirable that some check be made that the data is consistent with the distributions to which it is fitted. This

is important because errors made in the assumed shape of the P_i's will manifest themselves as systematic errors on the lifetime. In particular if the width of the resolution function is underestimated, then the lifetime will be overestimated. This can be understood heuristically as follows. If the resolution function is too narrow, then for the correct lifetime the probability of observing an event in the tails will be underestimated leading to a small value of the likelihood function. This small value of L can be improved on in the fit by an increase in the lifetime. This is because long lifetimes produce tails in both the positive and the negative directions. The result of this will be a poor fit because the tails on the resolution function are (presumably) symmetric while the tails due to lifetimes are asymmetric. In this section several tests of the consistency of the data with the distributions are considered. The first consists of binning the data in δ and then doing a Monte Carlo calculation of the number of expected events in each bin. The second uses the value of the likelihood function at its maximum as a test of the fit, and the third considers various parameterizations of the resolution function which can be used as tests. In later sections a comparison will be made with a full detector simulation Monte Carlo calculation of the first moments of the impact parameter distribution and the effect of cutting off the events in the tails of the distribution will be considered.

5.3.1 The histogram test

It would be convenient if a full detector simulation Monte Carlo calculation could be used to obtain the expected δ distributions, however, the computer time needed to do this would be prohibitive. The calculations in this section are based on the probability tables and exact impact parameter distributions used in the M.L. fit. The procedure for generating these distributions is:

- For each real electron in the data, pick at random a type (b $\rightarrow$ e, etc.) depending on the fractions (f_x's) for an electron with that p and p_t bin.
- Using the chosen type, p, and p_t, pick an exact impact parameter using the exact impact parameter distributions $P_x^{exact}(\delta; p, p_t)$.

- Smear the exact impact parameter to account for the measurement error. This is done by generating a random number distributed according to the resolution function and multiplying it by σ_δ^i. This number is then added to δ.

Applying this procedure to each track in the data set produces a single Monte Carlo "experiment." By repeating this "experiment" many times, it is possible to obtain the desired distributions. The result of this exercise is shown for the b-region in Fig. 5.7a and for the c-region in Fig. 5.7b. These distributions are calculated with $\tau_c = 0.64$ psec and $\tau_b = 1.17$ psec. For the b-region $\bar{\delta}_{M.C.} = 222 \pm 6$ (stat.) μm, $\bar{\delta}_{data} = 257 \pm 49$ (stat.) μm, and for the c-region $\bar{\delta}_{M.C.} = 101 \pm 3$ (stat.) μm, $\bar{\delta}_{data} = 133 \pm 25$ (stat.) μm. A quantitative estimate of the agreement between the data and the Monte Carlo calculation can be had by calculating the χ^2 of the fit. The contribution of one bin to the χ^2 is

$$\frac{(N_{data} - N_{M.C.})^2}{N_{M.C.}}, \tag{5.14}$$

where N_{data} is the number of tracks in that bin and $N_{M.C.}$ is the number of tracks expected based on the Monte Carlo calculation. The sum is taken only over bins occupied by data, and the number of degrees of freedom is equal to the number of bins summed (c-region) or the number of bins summed minus one (b-region). The results of this are $\chi^2 = 7.1$ for 7 D.F. for the b-region and $\chi^2 = 6.6$ for 10 D.F. for the c-region. These numbers correspond to confidence levels of approximately 40 % and 90 % respectively.[50] In both the b-region and the c-region, the number of events in the tails of the data is consistent with the number expected from the Monte Carlo calculation.

5.3.2 The likelihood test

Appendix A contains the motivation for the statistic which is used as a goodness of fit test in this section. For the case of the Gaussian distributions considered in the appendix, the distribution of χ^2 can be calculated analytically and is well known. For the probability density function used in the lifetime fit, this is hardly the case.

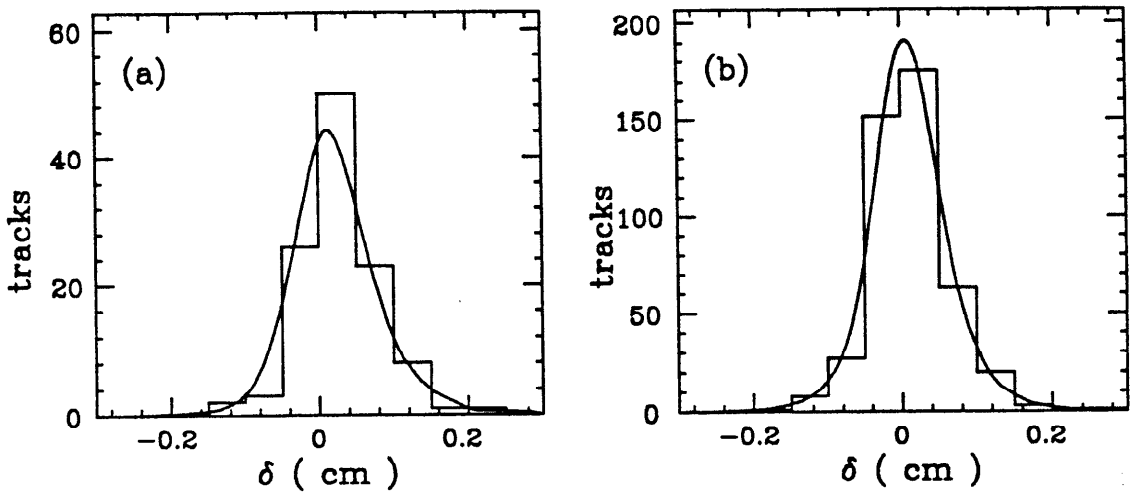

Figure 5.7. A comparison of the measured and the expected impact parameters. Part (a) is for the b-region and part (b) is for the c-region. The smooth curve is the Monte Carlo calculation. The lifetimes used in this calculation were $\tau_c = 0.64$ psec and $\tau_b = 1.17$ psec. (See the next section.)

In fact, since the exact impact parameter distributions are obtained from a Monte Carlo calculation, no analytic calculation of the distribution of " χ^2 " is possible. It is possible, however, to obtain this distribution by another Monte Carlo calculation. The procedure for generating one value of " χ^2 " is:

- Generate a fake experiment as outlined in the previous section.
- Fit the data set and save the value of " χ^2 ":

$$\text{"}\chi^2\text{"} = -2 \log L - \sum_{i=1}^{N} \log(2\pi\sigma_i^2). \tag{5.15}$$

This procedure is then repeated many times in order to obtain the distribution of " χ^2 ". The results are shown in Fig. 5.8a for the entire data set (2-d fit), and in Fig. 5.8b for just the b-region (1-d fit). The confidence levels given in the figures are the probabilities that the " χ^2 " will exceed the " χ^2 " obtained in this experiment. In all cases the data is consistent with the distribution to which it was fitted. As a by-product of this test, one can check for bias in the fitting procedure (see Appendix A). The result of such a test is that the bias is less than 5%.

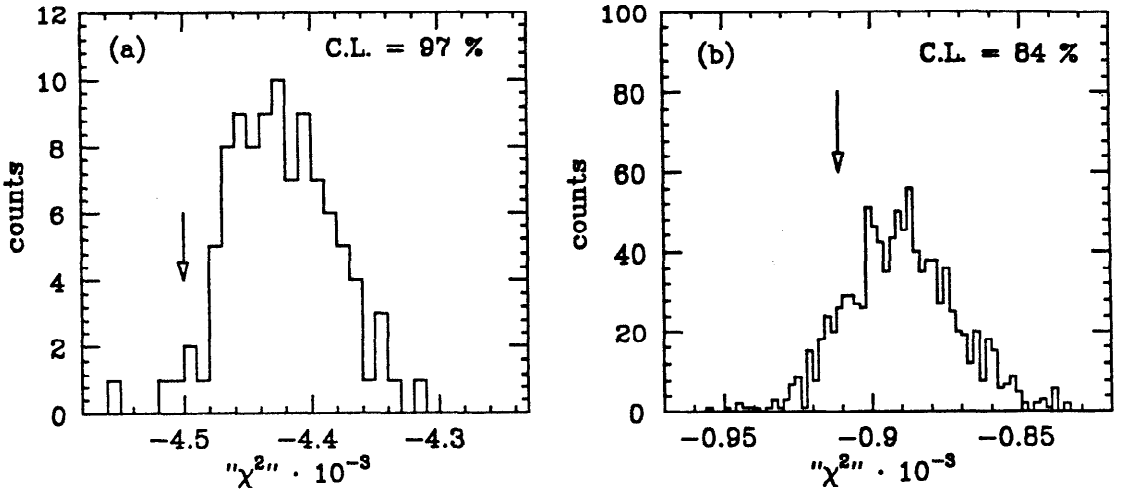

Figure 5.8. Distribution of " χ^2 " expected for the data. Part (a) is for all tracks with $p > 1$ GeV and part (b) is for just the b-region. The small arrows mark the value of " χ^2 " for the data.

5.3.3 *Changes in the shape of the resolution function*

It is possible to use the data being fitted to test the assumptions that were made about the distributions from which the data was drawn. The general form for doing this is as follows. If the original P.D.F. was $P(\tau)$, then an additional parameter (ϵ), which affects the shape of the distributions, is introduced so that $P(\tau) \rightarrow P(\tau, \epsilon)$. For some nominal value of ϵ the two distributions coincide; i.e.

$$P(\tau) = P(\tau, \epsilon_0). \tag{5.16}$$

Then the data being fit can be used to estimate the value of ϵ. If the estimated value of ϵ is not consistent with ϵ_0, then it is clear that the fit is not being done correctly. The converse does not hold, however. Since changing ϵ only sweeps out a particular family of distributions, it is not possible to know whether there is a more correct one which has not been considered. In what follows two different parameterizations will be considered. By showing that it is possible to rule out a couple of obvious deviations from the assumed resolution, some confidence is gained that the data agrees with the distribution to which it was fitted. The first parameter (ϵ_1) scales the calculated errors; i.e., $\sigma_\delta \rightarrow \epsilon_1 \cdot \sigma_\delta$. This provides a measure of the accuracy

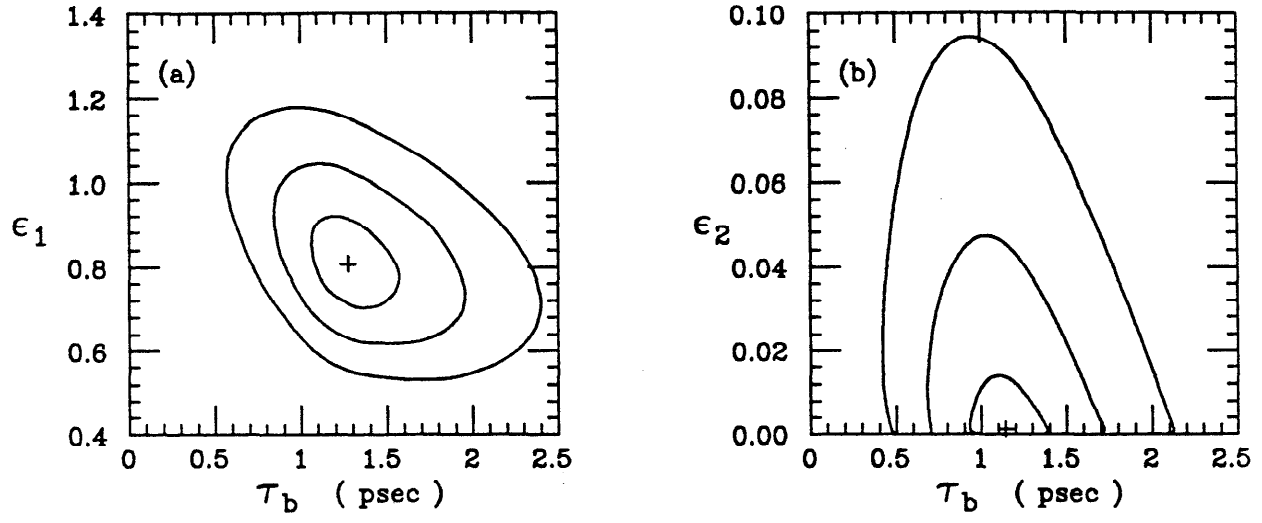

Figure 5.9. Contour plots of L in the (τ_b, ϵ_1) and (τ_b, ϵ_2) planes. The contours are drawn at the one, two, and three sigma levels. These plots use only the data in the b-region.

with which the width of the central part of the distribution is calculated. A contour plot of the likelihood function in the (τ_b, ϵ_1) plane for the b-region is shown in Fig. 5.9. The values from the fit ($\tau_b = 1.27$ psec and $\epsilon_1 = 0.81$) are consistent with the measured value of the b-lifetime and with a correct calculation of the detector resolution.

The second additional parameter (ϵ_2) allows a flat background in the fit (flat in the sense that it does not depend on the impact parameter). In this case if P_i is the probability of observing the i'th event, then $P_i \rightarrow \epsilon_2 + (1 - \epsilon_2) \cdot P_i$. A contour plot of the likelihood function in the (τ_b, ϵ_2) plane for the b-region is shown in Fig. 5.9b. The values from the fit ($\tau_b = 1.14$ psec and $\epsilon_2 = 0.001$) are consistent with the measured value of the b-lifetime and consistent with a correct calculation of the detector resolution.

5.4 A First Moment Comparison with a Full Simulation Monte Carlo

As an additional check on the maximum likelihood fit, a comparison has been made between the first moments of the data and the first moments as calculated by a full detector simulation Monte Carlo using the measured value of τ_b. The

Table 5.4. A first moment comparison of the average impact parameters in the data and the Monte Carlo. The Monte Carlo calculation uses a full detector simulation with $\tau_c = 0.64$ and $\tau_b = 1.17$ (see the next section for the reason for using this value of τ_b).

	Data	Monte Carlo
b-region	259 ± 49 (stat.) μm	192 ± 14 (stat.) μm
c-region	146 ± 28 (stat.) μm	116 ± 8 (stat.) μm

results of this comparison are shown in Table 5.4. The errors on the Monte Carlo calculations are statistical only. The data and the Monte Carlo agree within the statistics.

5.5 The Effect of Truncation on the Fit

It was stated above that tracks with impact parameters greater than 0.3 cm have not been used in this analysis. The impact parameter distributions calculated in the previous section suggest that this should have a negligible effect on the fit since the tails outside of $\pm$ 0.3 cm are very small. It is possible to account explicitly for this "truncation" in the course of the maximum likelihood fit. The details of this procedure are described below. The general idea is as follows. If the fit is to be done only over a certain window, then events outside this window are (obviously) dropped from the fit. The shape of the P.D.F. inside this window is the same as before, but because the tails have been cut off, the normalization is no longer correct. Fixing this requires integrating the tails of the distribution and multiplying the P.D.F. by the appropriate correction factor. Specifically, if δ_{max} is the greatest impact parameter allowed in the analysis, then the P.D.F. is modified to:

$$P^i(new) \propto \begin{cases} P^i(old), & |\delta| < \delta_{max} \\ 0, & |\delta| > \delta_{max}, \end{cases} \tag{5.17}$$

so that the shape of the P^i is unchanged for $|\delta| < \delta_{max}$, but the normalization is

different. Thus for $|\delta| < \delta_{max}$

$$P^i(new) = \frac{1}{1 - t_1 - t_2} \cdot P^i(old), \tag{5.18}$$

where

$$t_1 = \int_{\delta_{max}}^{\infty} P^i(\delta) d\delta, \tag{5.19}$$

and

$$t_2 = \int_{-\infty}^{-\delta_{max}} P^i(\delta) d\delta. \tag{5.20}$$

If this holds for the complete P.D.F., then clearly it also holds for the $P_x^i(\delta)$'s. Therefore they can be written as

$$P_x^i(\delta) = \frac{1}{1 - t_1^i - t_2^i} \cdot \frac{\Delta\delta}{\sigma_\delta^i} \sum_{j=1}^{n_b} P_{x,j}^{exact}\left(p^i, p_t^i\right) P^{rf}\left(\frac{s}{\sigma_\delta^i} \cdot \left(\frac{\delta}{s} - \delta_j\right)\right), \tag{5.21}$$

where

$$t_1^i = \int_{\delta_{max}}^{\infty} \frac{\Delta\delta}{\sigma_\delta^i} \sum_{j=1}^{n_b} P_{x,j}^{exact}\left(p^i, p_t^i\right) P^{rf}\left(\frac{s}{\sigma_\delta^i} \cdot \left(\frac{\delta}{s} - \delta_j\right)\right) d\delta, \tag{5.22}$$

and similarly for t_2^i. Moving the integration inside the summation gives

$$t_1^i = \frac{\Delta\delta}{\sigma_\delta^i} \sum_{j=1}^{n_b} P_{x,j}^{exact}\left(p^i, p_t^i\right) \int_{\delta_{max}}^{\infty} P^{rf}\left(\frac{s}{\sigma_\delta^i} \cdot \left(\frac{\delta}{s} - \delta_j\right)\right) d\delta. \tag{5.23}$$

A change of variable gives

$$t_1^i = \Delta\delta \sum_{j=1}^{n_b} P_{x,j}^{exact}\left(p^i, p_t^i\right) \int_{\frac{1}{\sigma_\delta^i}(\delta_{max} - s \cdot \delta_j)}^{\infty} P^{rf}(x) dx. \tag{5.24}$$

This integral can be performed numerically and the result expressed as a cubic spline. By defining the new function:

$$C^{rf}(x) = \int_x^{\infty} P^{rf}(x) dx, \tag{5.25}$$

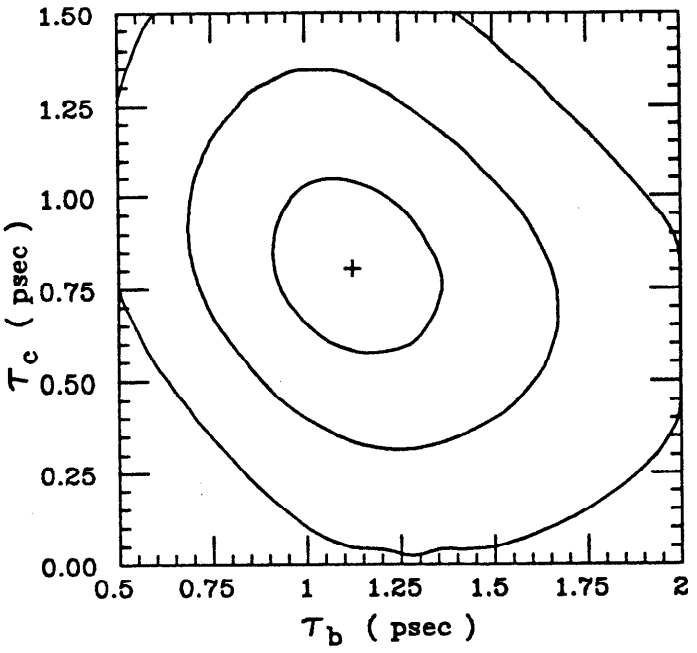

Figure 5.10. Contour plot of the likelihood function versus τ_b and τ_c for the full data set, this time accounting for the ± 0.3 cm maximum impact parameter cut.

t_1^i can be expressed as

$$t_1^i = \Delta\delta \sum_{j=1}^{n_b} P_{x,j}^{exact}\left(p^i, p_t^i\right) C^{rf}\left(\frac{1}{\sigma_\delta^i}\left(\delta_{max} - s\cdot\delta_j\right)\right). \tag{5.26}$$

Similarly for t_2:

$$t_2^i = \Delta\delta \sum_{j=1}^{n_b} P_{x,j}^{exact}\left(p^i, p_t^i\right) C^{rf}\left(\frac{1}{\sigma_\delta^i}\left(s\cdot\delta_j - \delta_{max}\right)\right). \tag{5.27}$$

The result of this modification for the 2-D fit is $\tau_b = 1.12^{+0.24}_{-0.21}$ (stat.) psec and $\tau_c = 0.81^{+0.24}_{-0.24}$ (stat.) psec, and for the 1-D fit is $\tau_b = 1.17^{+0.27}_{-0.22}$ (stat.) psec. These changes are small as expected. Fig. 5.10 shows the contour plot for the 2-D fit including truncation effects.

This procedure can also be used to check that the fit is not being pulled by the tails of the data. If the data contains more events in the tails of the distribution

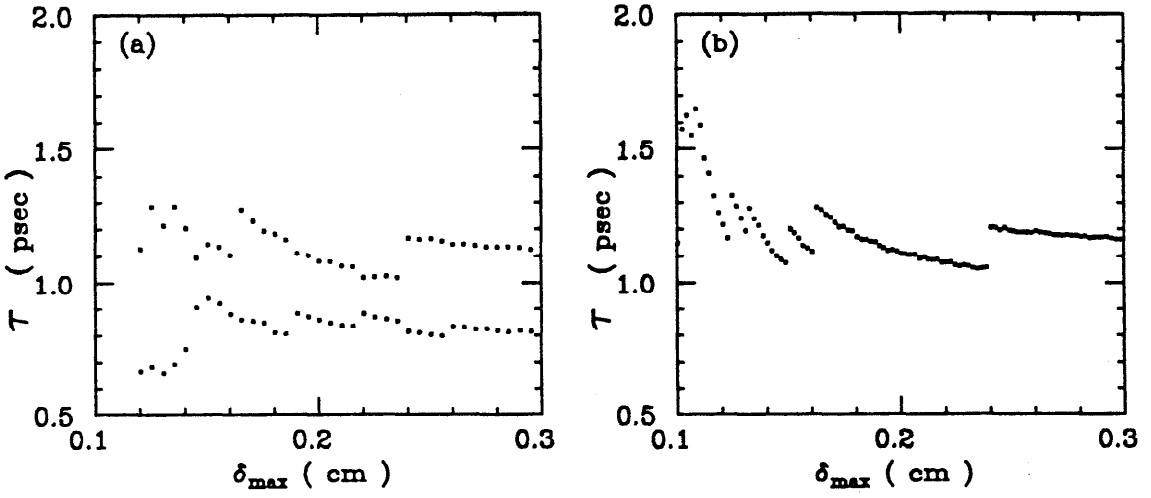

Figure 5.11. Lifetimes as a function of the largest impact parameter ($\delta_{\max}$) used in the fit. Part (a) shows the values of τ_b (top) and τ_c (bottom) obtained using all the data with a 2-D fit, and part (b) shows the value of τ_b obtained from a 1-D fit to just the b-region.

than is expected based on the events in the core of the distribution, then there could be a systematic shift in the measured lifetime as the tails are dropped from the fit. This check consists of plotting the lifetimes as a function of the cut and looking for any net drift as the cut is changed. Fig. 5.11a shows the result for the 2-D fit and Fig. 5.11b shows the result for the 1-D fit. While the sensitivity of this test is clearly limited by the available statistics, the values of τ_b and τ_c for all values of the cut are consistent with the lifetime obtained from the ± 0.3 cm cut used for the final analysis. The "sawtooth" shape can be understood as follows. As $\delta_{\max}$ is made smaller, the size of the correction to the lifetime becomes larger. This gives rise to the slope of the curves. At distinct values of $\delta_{\max}$ individual tracks are dropped from the fit. This gives rise to discontinuous jumps in the lifetime. From the figure it is clear that the gradual changes offset the jumps so that the lifetime remains constant within the statistics for different values of $\delta_{\max}$. As $\delta_{\max}$ is made very small (≈ 0.1 cm), the statistical uncertainty becomes comparatively large. For the case of Fig. 5.11b, the error bars on τ_b are $^{+0.70}_{-0.43}$ cm when $\delta_{\max} = 0.1$ cm

and $^{+0.32}_{-0.27}$ when $\delta_{max} = 0.2$ cm. A similar increase in the error bars occurs for the two parameter fit.

5.6 The Systematic Errors

Most of the systematic errors affecting δ have been discussed in previous sections as each one arose. In addition to these there is clearly a dependence of τ_b on the average charmed particle lifetime. Since τ_c is a parameter in the fit, it is trivial to display this error. The particular charmed particles, their lifetimes, and relative production ratios are listed in Appendix C. The overall systematic uncertainty on τ_c is taken to be $^{+0.10}_{-0.08}$ psec. This gives rise to an uncertainty on τ_b of less than 0.01 psec and is neglected. The remaining systematic errors can be broken into three groups. The first group occurs as a result of the uncertainty in the experimental resolution; the second group occurs as a result of the limited statistics in the electron analysis, and the third comes from the uncertainty in the modeling of the sphericity axis.

The uncertainty in the modeling of the sphericity axis is parameterized in the non-simulation Monte Carlo in the following way. If $\hat{s}$ is a unit vector in the direction of the sphericity axis and $\hat{p}$ is a unit vector in the direction of the parent hadron, then one can define a new vector: [51]

$$\vec{e} = (1 - \rho) \cdot \hat{s} + \rho \cdot \hat{p}. \tag{5.28}$$

The new "sphericity axis" is taken to point in the direction of $\vec{e}$. Thus for $\rho = 0$ there is no change; for $\rho = 1$ the parent direction is used, and for $\rho = -1$ the error is overestimated by 100 %. The effect of these changes on the b-lifetime is determined by generating new sets of $P^{exact}(x)$'s for different values of ρ. Letting ρ vary over the range of 0.5 to -0.5 changes the fitted lifetime by $^{+0.03}_{-0.00}$ psec.This range of ρ was picked rather arbitrarily. It corresponds to a ± 50 % error on the determination of the error introduced by using the sphericity axis to approximate the parent direction, and is hopefully a conservative guess.

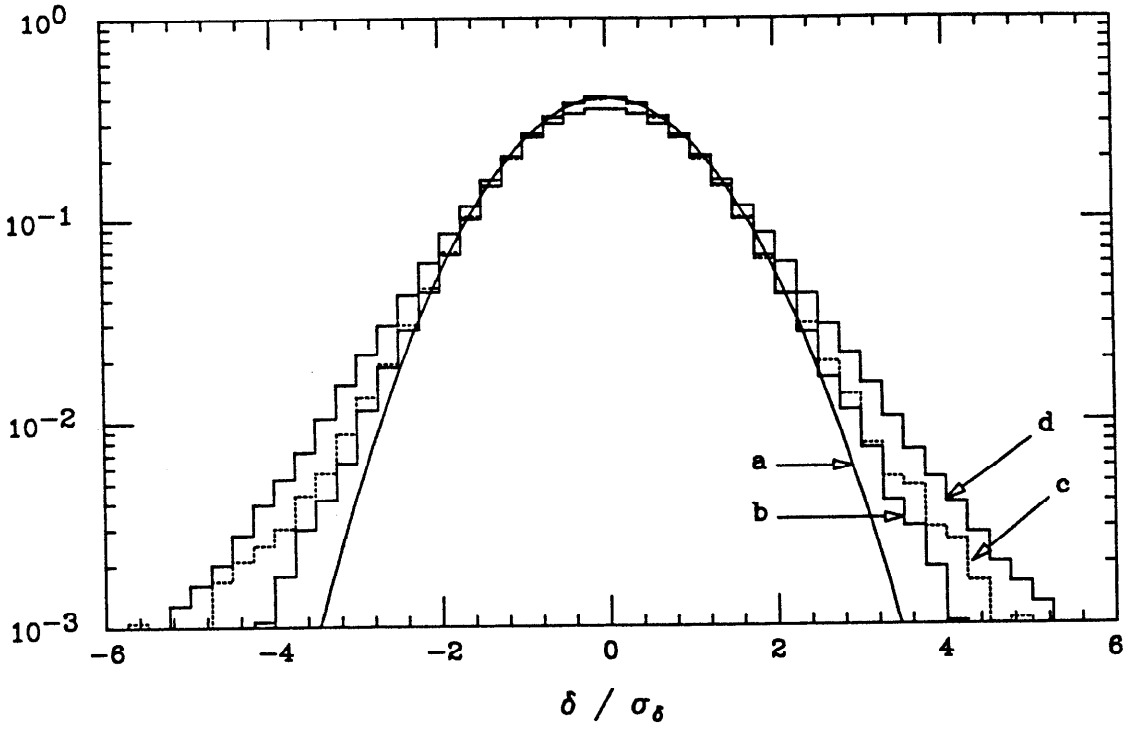

Figure 5.12. Various resolution functions. Curve (a) shows a Gaussian with unit width. Histogram (b) shows the resolution function for tracks from Bhabha events; (c) shows the resolution function for tracks from two-gamma events, and (d) shows the resolution function obtained from the unfolding procedure (after symmetrizing). The curve and the histograms are normalized to unity.

The various resolution functions obtained from different data sets were shown individually in the previous chapter. Here they are overplotted for purposes of comparison in Fig. 5.12. The symmetrized resolution function obtained from the unfolding procedure has been used in the b-lifetime analysis. It is possible to test the others using some of the procedures outlined previously. A sensitive test can be made by doing a 2-D fit to the tracks in both the b-region and the c-region. The result of this for the four resolution functions is shown in Table 5.5. From this table it is clear that the Gaussian and Bhabha resolution functions can be excluded based on the values of τ_c measured. The two remaining resolution functions are both consistent with the data. The one obtained by the unfolding method has been used

Table 5.5. Tests of the resolution functions. Results of 2-D fits to all tracks with $p > 1$ GeV using various resolution functions. The "known" value of the charmed particle lifetime ($\tau_c = 0.64^{+0.10}_{-0.08}$ psec) can be used to exclude certain resolution functions. In the table "unfolded hadrons" refers to the resolution function obtained from the unfolding procedure after symmetrizing.

resolution function	τ_b (psec)	τ_c (psec)
Gaussian	$1.24^{+0.24}_{-0.19}$	$1.40^{+0.28}_{-0.27}$
Bhabha	$1.23^{+0.24}_{-0.20}$	$1.19^{+0.32}_{-0.26}$
two-gamma	$1.21^{+0.24}_{-0.20}$	$1.07^{+0.28}_{-0.25}$
unfolded hadrons	$1.12^{+0.24}_{-0.21}$	$0.81^{+0.24}_{-0.24}$

in this analysis for the obvious reason that the electrons come from hadronic events. The small possibility that the degradation in resolution observed for tracks in hadronic events might not affect electrons is discounted because (as was stated previously) the resolution obtained from pions and muons produced in two-gamma events is very similar to that obtained from electrons, and because the resolution function from the hadronic events gives a reasonable fit to the tau data (see below). This suggests that the degradation observed in the hadrons is independent of the particle type. The cause of this degradation is not known. The systematic uncertainty associated with this problem is taken to be the difference in τ_b obtained using the two consistent resolution functions. Using the two-gamma resolution function to fit the tracks in the b-region gives a lifetime of $\tau_b = 1.24$ psec, which is 0.07 psec greater than that obtained using the unfolded symmetrized resolution function. Fitting the impact parameters with the unsymmetrized resolution function obtained from the unfolding process gives $\tau_b = 1.13$ psec, which is 0.04 psec lower than the value obtained from the symmetric resolution function. This difference is also included as a systematic error.

The problem of propagating the errors from the electron analysis has been discussed in Chapter 3. At that time it was pointed out that the correlations

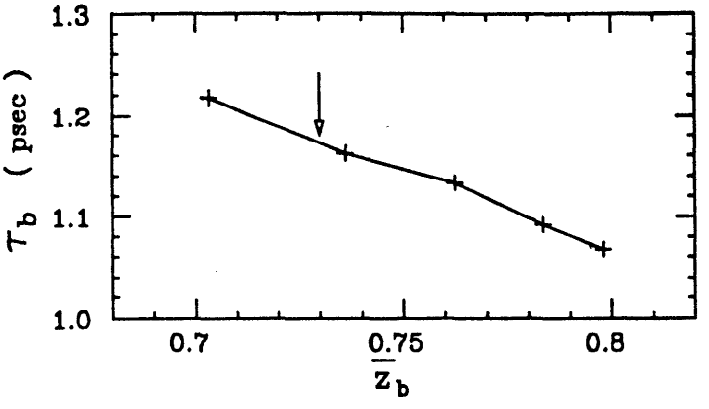

Figure 5.13. The b-lifetime versus $\bar{z}$ for b-quark fragmentation. This figure is made by generating new $P^{exact}(x)$'s and redoing the 1-D fit. The arrow marks the nominal value.

between the "physical" variables make them unsuited for propagating the errors, and another set of uncorrelated variables was introduced. At this point it is necessary to calculate τ_b as a function of each of the new variables. This is complicated by the fact that each of these new variables affects both the fractions (f_x's) and the exact impact parameter distributions ($P^{exact}(x)$'s). The later are affected by way of the momentum spectrum of the parent hadron as was discussed previously. The first is easily accounted for by generating a new set of f_x's. The second is somewhat more difficult because the $P^{exact}(x)$'s are produced by a Monte Carlo calculation. The dependence of τ_b on $\bar{z}_b$ is shown in Fig. 5.13. The points are produced by varying the value of $\bar{z}_b$, recalculating the $P^{exact}(x)$'s, and refitting the lifetime. The dependence of τ_b on $\bar{z}_c$ is extremely small. The final result of propagating the electron analysis errors is shown in Table 5.6. The sum in quadrature of the entries in the last column is $^{+0.068}_{-0.120}$ psec. From the table it is clear that the uncertainty on the f_x's makes a negligible contribution to the systematic error on τ_b. Most of the uncertainty comes from the $P^{exact}(x)$'s which are influenced by the fragmentation parameter. The most probable value of $\bar{z}_b$ is 0.73. The statistical uncertainty from the electron analysis lets $\bar{z}_b$ vary between 0.70 and 0.81. This is consistent with many recent measurements and a recent world average.[52] Table 5.7 summarizes the systematic errors affecting the b-lifetime. The

Table 5.6. The systematic errors due to the electron analysis. The column labeled "total" is the linear sum of the column labeled "f^x's" and the column labeled "$P^{exact}(x)$'s." The sum in quadrature of the entries in the last column is $^{+0.068}_{-0.120}$.

parameter	f^x's	$P^{exact}(x)$'s	total
p_1	-0.0027 $+0.0022$	≈ 0	-0.0027 $+0.0022$
p_2	-0.0095 $+0.0109$	≈ 0	-0.0095 $+0.0109$
p_3	-0.0077 $+0.0076$	-0.0200 $+0.0300$	-0.0277 $+0.0376$
p_4	-0.0050 $+0.0039$	$+0.0600$ -0.1200	$+0.0550$ -0.1161
p_5	≈ 0	≈ 0	≈ 0
p_6	-0.0060 $+0.0062$	≈ 0	-0.0060 $+0.0062$

Table 5.7. A summary of the systematic errors affecting the b-lifetime. The result of adding these errors linearly is $^{+0.17}_{-0.16}$ psec.

source	+ error (psec)	- error (psec)
electron analysis	+ 0.07	- 0.12
resolution functions	+ 0.07	- 0.04
sphericity axis	+ 0.03	- 0.00

largest error is due to the statistics in the electron analysis and results primarily from the uncertainty in the fragmentation function. The total systematic error on τ_b is obtained by adding the errors linearly and is $^{+0.17}_{-0.16}$ psec.

5.7 The Result of Fitting the Tau Data Set

One additional check can be had by fitting the tracks from the tau data set described in the previous section. This data set provides an additional opportunity to check the understanding of the resolution function since it combines high statistics with the possibility of tracking confusion as in the hadronic events. In this case many of the previous details of the fit can be ignored. The unique 1-3 topology of the tau decays makes it possible to skim a very high purity sample. The backgrounds are of

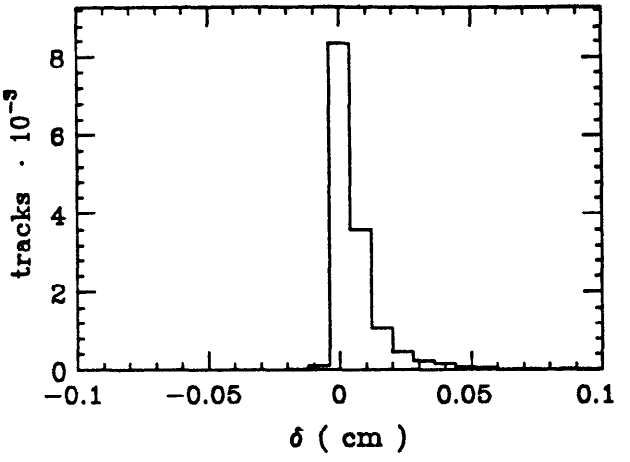

Figure 5.14. Exact impact parameter distribution for tracks from tau decay as determined by a full detector simulation Monte Carlo calculation with $\tau_\tau = 0.30$ psec.

the order of a couple of percent and are neglected in this fit. This means that there is only one source of tracks ($x = tau$) and $f^x = 1$ independent of p and p_t. The exact impact parameter distributions remain somewhat problematic. The non-simulation Monte Carlo described above was "tuned" to produce agreement on hadronic events run through the electron analysis and would not necessarily work on taus. In order to simplify this check, the following compromise was made. Only one $P^{exact}(x)$, which averaged over all of p and p_t, was used. Since this greatly reduces the number of events needed, it is possible to find $P^{exact}(x)$ by a full simulation Monte Carlo calculation. The resulting distribution is shown in Fig. 5.14. It has a mean of $\bar{\delta} = 66.7 \pm 0.6$ μm and is consistent with what one would expect from Fig. 4.16.

The maximum likelihood fit has been done as a function of the tau lifetime (τ_τ) and ϵ_1 (which expands the errors on δ). The results of this fit are shown in Fig. 5.15 for two different resolution functions. It is clear from this figure that neither resolution function provides an entirely adequate description of the data. The resolution function obtained from the two-gamma data set results in best fit values of $\tau_\tau = 0.298$ psec and $\epsilon_1 = 1.09$. From the contour plot in Fig. 5.15b it is clear that this resolution function can be excluded with high probability. The

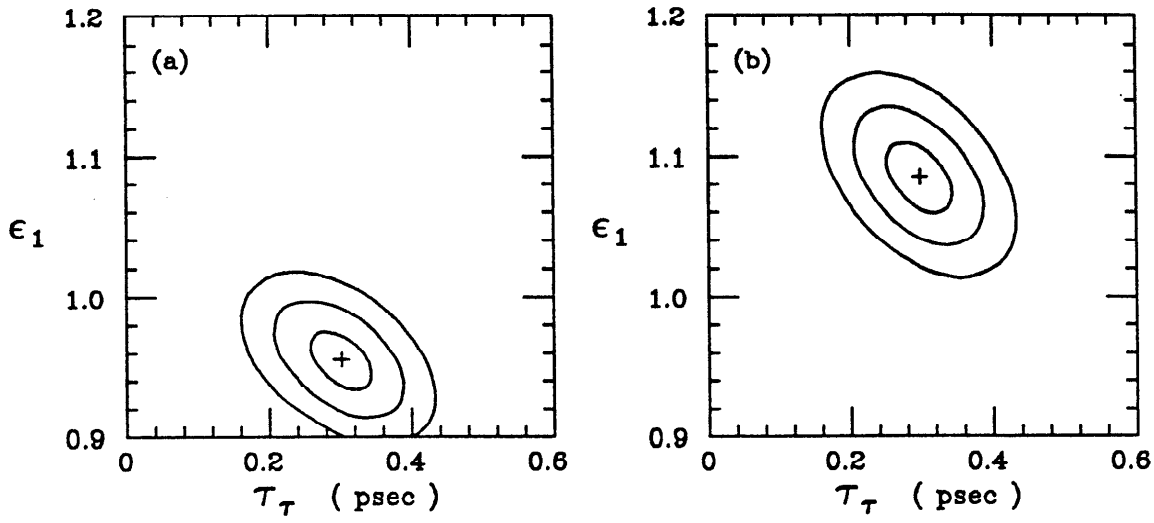

Figure 5.15. Contour plots from fits to taus. Part (a) shows the result of the fit when the resolution function unfolded from hadronic tracks is used, and part (b) shows the result when the resolution function from the two-gamma data set is used. Contours are drawn at the one, two, and three sigma levels.

resolution function obtained from the unfolding process described previously results in best fit values of $\tau_\tau = 0.301$ psec and $\epsilon_1 = 0.96$. The contour plot in Fig. 5.15a is obtained using this resolution function. The nominal value of ϵ_1 lies just outside of the two sigma contour. The probability of ϵ_1 being this small if the detector resolution is described correctly is only a couple of percent. It is not possible to reject definitively this resolution function, but it is also difficult to accept it. For this reason ϵ_1 is left as a free parameter in this fit. This provides a certain amount of robustness and makes the fit much less sensitive to the details of the resolution function. (The two resolution functions tried here produce the same tau lifetime to within 0.003 psec if ϵ_1 is left to float.) The cost of this procedure is an increase in the statistical error on τ_τ. The result of this fit is $\tau_\tau = 0.30^{+0.05}_{-0.04}$ (stat.) psec. If ϵ_1 is fixed to 1 the result is $\tau_\tau = 0.25^{+0.04}_{-0.04}$ (stat.) psec. In either case the measured value is consistent with the value obtained in the previous chapter ($\tau_\tau = 0.263 \pm 0.046$ (stat.) psec) and with the "known value" ($\tau_\tau = 0.286 \pm 0.016$(stat.)$\pm 0.025$(sys.) psec). This situation is consistent with the degradation of the resolution observed

in hadronic events coming from the large number of tracks in a typical event. In the case of the taus, the average number of tracks is intermediate between the two-gamma events and the hadronic events and this gives rise to an intermediate degradation in the resolution.

6. CONCLUSIONS

6.1 A SUMMARY OF THE B-LIFETIME MEASUREMENT

The b-lifetime measurement reported on here is obtained from a maximum likelihood fit to the impact parameters of 113 "electron" tracks with $p_t > 1$ GeV. The result of this fit is

$$\tau_b = 1.17 \, ^{+0.27}_{-0.22} \text{ (stat.)} \, ^{+0.17}_{-0.16} \text{ (sys.) psec.} \tag{6.1}$$

This fit accounts for the various non-b-decay sources of tracks in the data sample, the non-Gaussian tails on the detector resolution, and the ± 0.3 cm maximum impact parameter cut. This measurement has been checked by (among other things) doing a two-parameter fit to τ_b and τ_c with all 562 tracks which have $p > 1$ GeV. Values are found which are consistent with the measurement of τ_b obtained using just the high p_t tracks and with the known value of τ_c. The distribution of δ for the b-region is shown in Fig. 6.1 and the distribution of δ for the c-region is shown in Fig. 6.2. The curves plotted on these figures are Monte Carlo calculations of the expected distributions based on the fitted value of τ_b and $\tau_c = 0.64$ psec.

6.2 CONSTRAINTS ON THE STANDARD MODEL

As was explained in the first chapter, τ_b can be used to constrain the elements of the K-M mixing matrix. In that chapter it was shown that τ_b is related to $|V_{cb}|$ and $|V_{ub}|$ by

$$\frac{1}{\tau_b} = \Gamma = \frac{1}{BR(b \to eX)} \cdot \left[0.58 \cdot |V_{cb}|^2 + 1.18 \cdot |V_{ub}|^2 \right] \cdot 10^{14} \text{sec}^{-1}. \tag{6.2}$$

The semileptonic branching ratio for B-mesons has been measured by many collaborations.[52] The most precise single measurement comes from CLEO and is $BR(b \to eX) = 0.12 \pm 0.007$ (stat.) ± 0.005 (sys.).[53] This gives

$$\tau_b = \left[4.8 \cdot |V_{cb}|^2 + 9.8 \cdot |V_{ub}|^2 \right]^{-1} \cdot 10^{-14} \text{sec}. \tag{6.3}$$

B-REGION ($p_t > 1$ GeV)
of tracks = 113
$\bar{\delta} = 259 \pm 49$ (stat.) μm
$\tau_b = 1.17^{+0.27}_{-0.22}$ (stat.) $^{+0.17}_{-0.16}$ (sys.) psec

Sources of Tracks in the B-Region	
b → e	0.70
b → c → e	0.09
c → e	0.17
background	0.04

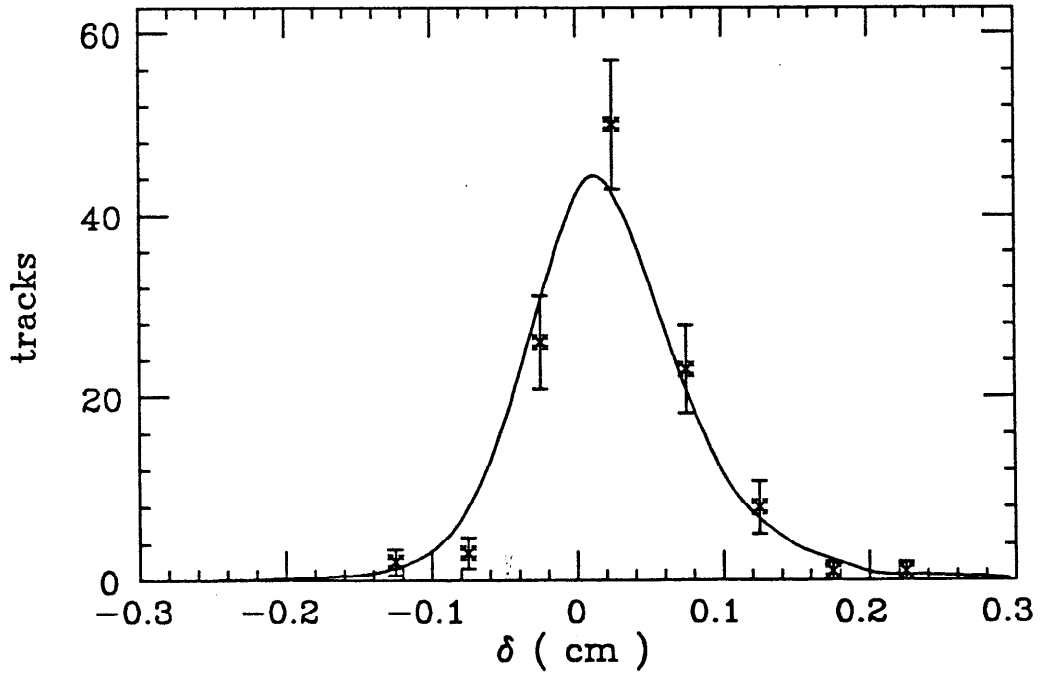

Figure 6.1. A summary of the b-region. The top box shows the number of tracks in this region, the average impact parameter, and the b-lifetime obtained from the maximum likelihood fit. The second box summarizes the sources of the tracks in the b-region. The figure shows the distribution of impact parameters in this region. The points are the data (the error bars are statistical only). The smooth curve is a Monte Carlo calculation of the expected distribution based on $\tau_b = 1.17$ psec and $\tau_c = 0.64$ psec.

C-REGION
(p > 1 GeV, p_t < 1 GeV)
of tracks = 449
$\bar{\delta} = 146 \pm 28$ (stat.) μm

Sources of Tracks in the C-Region	
b → e	0.15
b → c → e	0.15
c → e	0.56
background	0.14

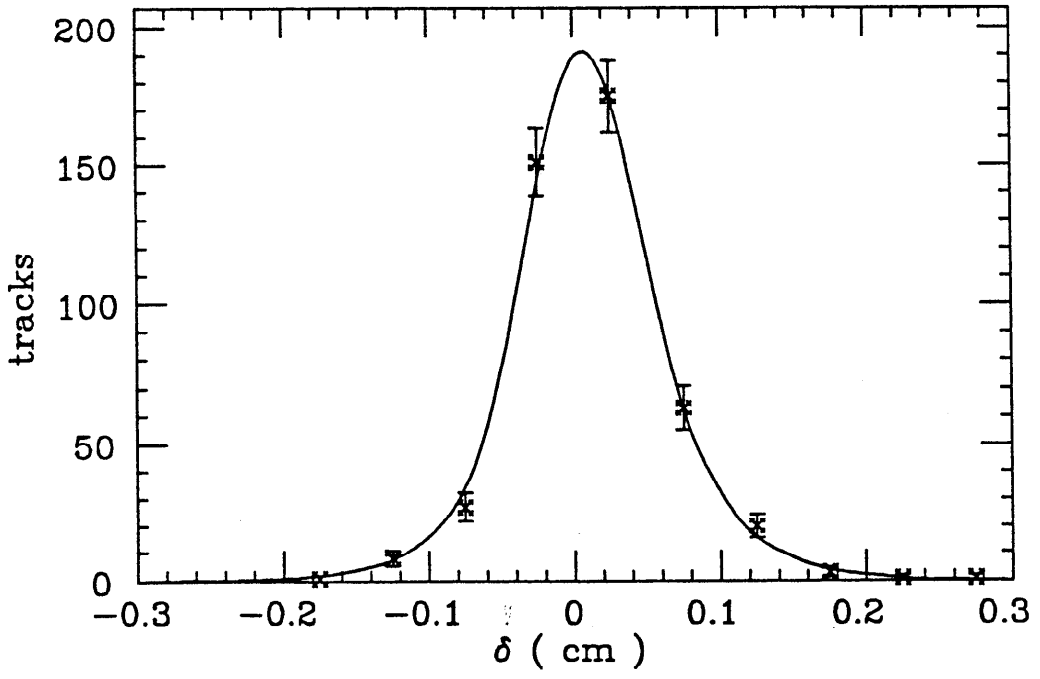

Figure 6.2. A summary of the c-region. The top box shows the number of tracks in this region and the average impact parameter. The second box summarizes the sources of the tracks in the c-region. The figure shows the distribution of impact parameters in this region. The points are the data (the error bars are statistical only). The smooth curve is a Monte Carlo calculation of the expected distribution based on $\tau_b = 1.17$ psec and $\tau_c = 0.64$ psec.

Because the mass of the charmed quark shifts the endpoint of the lepton spectrum for the decay $b \rightarrow ce\bar{\nu}_e$ relative to the endpoint for $b \rightarrow ue\bar{\nu}_e$, it is possible to determine the relative strengths of these two transitions. Fits to this spectrum were discussed in the first chapter in the context of determining the quark masses. CLEO[14] has reported $\frac{\Gamma(b\rightarrow ue\bar{\nu}_e)}{\Gamma(b\rightarrow ce\bar{\nu}_e)} < 4\%$ and CUSB[15] has reported $\frac{\Gamma(b\rightarrow ue\bar{\nu}_e)}{\Gamma(b\rightarrow ce\bar{\nu}_e)} < 5.5\%$, both of which are at the 90% confidence level. Since that time E. Thorndike[52] has reported that when certain models are used for the decay $b \rightarrow ue\bar{\nu}_e$, the limit obtained from the CLEO data deteriorates to 9%. In any case the contribution to the total decay rate from $b \rightarrow ue\bar{\nu}_e$ is small compared to the errors on the lifetime. The constraint from $\frac{\Gamma(b\rightarrow ue\bar{\nu}_e)}{\Gamma(b\rightarrow ce\bar{\nu}_e)} < 9\%$ along with the constraint from the lifetime are shown in Fig. 6.3. If the $b \rightarrow ue\bar{\nu}_e$ transition is ignored, then

$$|V_{cb}|^2 = \frac{1}{\tau_b} \cdot 0.21 \cdot 10^{-14}\text{sec.} \tag{6.4}$$

Using the value of τ_b from equation 6.1 produces

$$|V_{cb}| = 0.042 \, ^{+0.005}_{-0.004} \text{ (stat.)} \, ^{+0.004}_{-0.002} \text{ (sys.)},^{54} \tag{6.5}$$

where the systematic error reflects only the systematic uncertainty associated with τ_b and not the uncertainty associated with equation 6.4.

6.3 A Comparison with Other Results

Since the first null result on the lifetime of bottom hadrons by the JADE collaboration[31] in 1982, there has been a succession of improving measurements. The first non-zero result was by the MAC collaboration[33] in the summer of 1983, followed closely by the MARKII collaboration. Fig. 6.4 is a (not necessarily complete) chronology of bottom lifetime measurements. The entries in this figure are not all independent. Some later measurements contain the data from earlier measurements. Table 6.1 contains a summary of the latest bottom lifetime measurements from most groups.[52] The first MARKII measurement uses

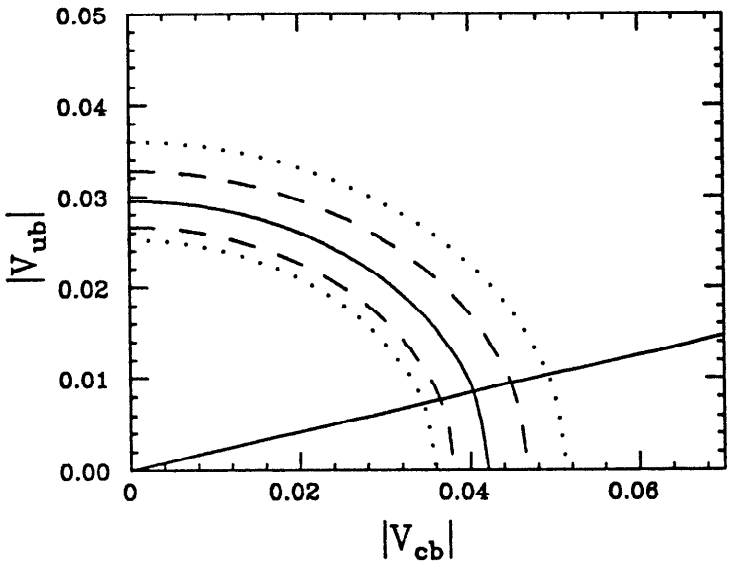

Figure 6.3. Constraints on $|V_{ub}|$ and $|V_{cb}|$. The solid curved line comes from $\tau_b = 1.17$ psec. The dashed lines near it are the limits due to the statistical errors. The dotted lines are the limits due to adding the statistical and systematic errors linearly. The solid straight line is the 90% confidence limit from the ratio $\frac{\Gamma(b\to ue\bar{\nu}_e)}{\Gamma(b\to ce\bar{\nu}_e)} < 9\%$.

a maximum likelihood fit to the impact parameters of leptons from B-decay which is very similar to the fit used in this analysis. The MAC analysis also uses high p_t leptons from B-decay; however, they estimate the bottom lifetime by comparing the average impact parameter with a Monte Carlo calculation. The JADE measurement is an average over two methods of analysis. They obtain a set of events tagged as B-decay by the presence of high p_t leptons. In the first method they relate the average impact parameter to the lifetime using a Monte Carlo calculation. In the second method they make additional use of the aplanarity of the event to provide more information on whether the event is really due to $b\bar{b}$ production. The TASSO result is obtained by a comparison of a measured impact parameter with Monte Carlo calculations. The tracks used in this analysis are not leptons however. TASSO obtains their b-enriched data by making cuts on event shape and then uses all tracks in the events with $p > 1$ GeV. The second MARKII measurement is made by reconstructing the vertices in events which have been

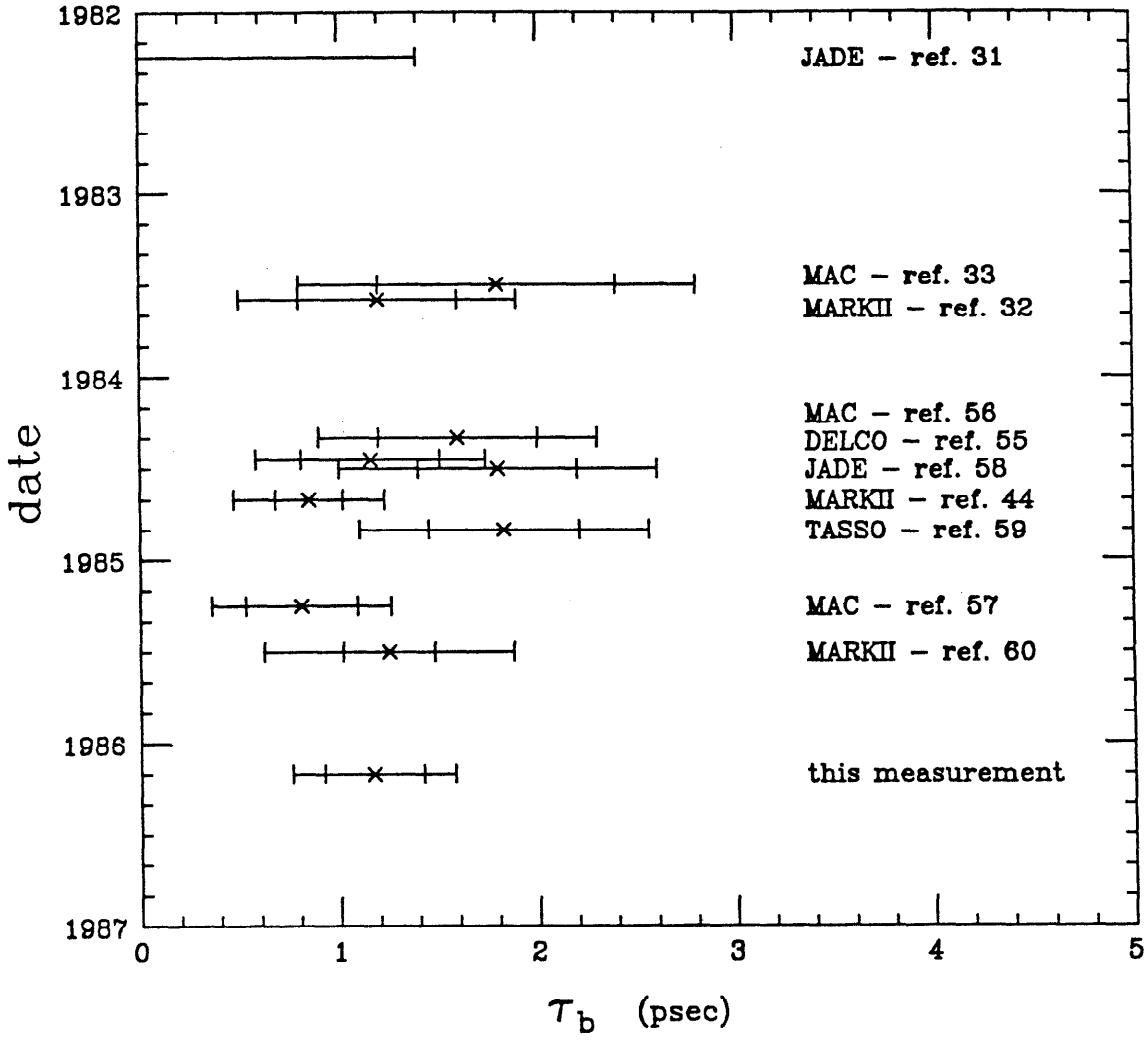

Figure 6.4. A chronology of bottom lifetime measurements. Most of the b-lifetime measurements which have been reported in the literature appear here. The inner error bar is the statistical error only and the outer error is the linear sum of the statistical and the systematic errors.

identified as B-decay by the presence of high p_t leptons. The average value of these measurements (obtained by adding the statistical and the systematic errors linearly and then weighting them by the reciprocal squared error) is

$$\tau_b^{\text{world average}} = 1.10 \pm 0.21 \text{ psec.}$$

Table 6.1. A summary of bottom lifetime measurements to date. This table contains the latest numbers from various collaborations.

τ_b (psec)	Source
$1.17^{+0.27}_{-0.22}$ (stat.) $^{+0.17}_{-0.16}$ (sys.)	this measurement
$0.85^{+0.17}_{-0.17}$ (stat.) $^{+0.21}_{-0.21}$ (sys.)	MARKII - ref. 44
$0.81^{+0.28}_{-0.28}$ (stat.) $^{+0.17}_{-0.17}$ (sys.)	MAC - ref. 57
$1.80^{+0.50}_{-0.30}$ (stat.) $^{+0.40}_{-0.40}$ (sys.)	JADE - ref. 58
$1.83^{+0.38}_{-0.37}$ (stat.) $^{+0.37}_{-0.34}$ (sys.)	TASSO - ref. 59
$1.25^{+0.26}_{-0.40}$ (stat.) $^{+0.35}_{-0.40}$ (sys.)	MARKII - ref. 60

Since some of the above measurements are made using very similar methods, the systematic errors are probably not all independent and the error on the above value of τ_b probably understates the real uncertainty.

Appendix A. The Maximum Likelihood Method

This appendix is a brief review of the maximum likelihood (M.L.) method. For a thorough discussion of the subject, see the literature.[46,61] Given:

- a collection of N events, each of which is described by n parameters (for the i'th event one has $(r_{i1}, r_{i2}, ...r_{in})$) and,
- a known probability density function (P.D.F.), from which the events were drawn, which is a function of m parameters $(x_1, x_2, ...x_m)$; i.e.,

$$P(r_1, r_2, ...r_n; x_1, x_2, ...x_m), \tag{A.1}$$

then the "likelihood" of observing the i'th event is defined to be

$$P_i = P(r_{i1}, r_{i2}, ...r_{in}; x_1, x_2, ...x_m). \tag{A.2}$$

The likelihood of observing all N events is the product of the individual likelihoods:

$$L(x_1, x_2, ...x_m) = \prod_{i=1}^{N} P_i. \tag{A.3}$$

The M.L. estimates of the parameters $(x_1, x_2, ...x_m)$ are the values of these parameters which maximize L. Alternately, one can minimize the quantity

$$-2 \log L(x_1, x_2, ...x_m). \tag{A.4}$$

The reason for choosing this particular function will became clear latter on. As a concrete example, consider the case of N events drawn from a Gaussian distribution with mean μ and width σ. Then the P.D.F. is

$$P(r; \mu, \sigma) = \frac{1}{\sqrt{2\pi}\sigma} \exp\left[-\frac{1}{2}\left(\frac{r-\mu}{\sigma}\right)^2\right], \tag{A.5}$$

and the log of the likelihood function is

$$-2\log L(\mu) = \sum_{i=1}^{N}\left[\left(\frac{x_i-\mu}{\sigma}\right)^2 + \log\left(2\pi\sigma^2\right)\right], \tag{A.6}$$

so that the motivation for choosing $-2\log L$ is clear. For the case where sigma is known, the second term is constant and it is sufficient to minimize

$$\sum_{i=1}^{N}\left(\frac{x_i-\mu}{\sigma}\right)^2, \tag{A.7}$$

which is exactly chi-squared. This of course yields

$$\mu = \frac{1}{N}\sum_{i=1}^{N} x_i. \tag{A.8}$$

If μ is known then an estimate of the width of the distribution is

$$\sigma^2 = \frac{1}{N}\sum_{i=1}^{N}(x_i-\mu)^2. \tag{A.9}$$

If μ and σ are unknown, then both can be estimated by minimizing $-2\log L$. This produces the same equations as obtained above, except that in the equation for σ, the value of μ used is the estimated value. This illustrates an important point. Since it is well known[36] that an unbiased estimate of the width of a Gaussian distribution with an unknown mean is

$$\sigma^2 = \frac{1}{N-1}\sum_{i=1}^{N}(x_i-\mu)^2, \tag{A.10}$$

it is clear that the M.L. estimate has a bias of order $\frac{1}{N}$. It is generally known[46] that M.L. estimators are only asymptotically ($N \to \infty$) unbiased.

A goodness of fit test can be motivated by the following example. If N data points $(x_i; i = 1, N)$ are drawn from Gaussian distributions with a common mean (μ) and independent widths $(\sigma_i; i = 1, N)$, then the log of the likelihood function is

$$\log L(\mu) = -\frac{1}{2}\sum_{i=1}^{N}\left[\left(\frac{x_i - \mu}{\sigma_i}\right)^2 + \log\left(2\pi\sigma_i^2\right)\right]. \qquad (A.11)$$

The chi-square term in this expression is clear, so if we define

$$\chi^2 = \sum_{i=1}^{N}\left(\frac{x_i - \mu}{\sigma_i}\right)^2, \qquad (A.12)$$

then

$$\chi^2 = -2\log L - \sum_{i=1}^{N}\log\left(2\pi\sigma_i^2\right). \qquad (A.13)$$

This suggests a statistic to use as a goodness of fit test. For the lack of a better name, this quantity is called " χ^2 " in this work.

This example also suggests the method of determining the confidence intervals from the fit. If the likelihood function has a minimum at $(x_1^m, x_2^m, ...x_m^m)$, then there should exist a (not necessarily linear) transformation such that $-2\log L$ will be quadratic in terms of a new set of parameters $(y_1, y_2, ...y_m)$. In that case the confidence intervals are just given by the surface in m-space such that

$$-2\log L(y_1, y_2, ...y_m) = -2\log L_{min} + \chi^2_{step}, \qquad (A.14)$$

where

$$-2\log L_{min} = -2\log L(y_1^m, y_2^m, ...y_m^m), \qquad (A.15)$$

and $\chi^2_{step} = 1$, 4 and 9 for the 1, 2 and 3 sigma error ellipses. It follows immediately that the confidence interval for the x_i's is given by

$$-2\log L(x_1, x_2, ...x_m) = -2\log L_{min} + \chi^2_{step}, \qquad (A.16)$$

where

$$-2\log L_{min} = -2\log L(x_1^m, x_2^m, ...x_m^m) \qquad (A.17)$$

also, and that it is not actually necessary to find the transformation between the x_i's and the y_i's.

Appendix B. Cubic B-Splines

The functions described in this appendix are a type of cubic spline function.[62] A cubic spline is defined by a set of cubic polynomials with one polynomial for each of a finite number of intervals. The points separating intervals are called knots. The polynomials are required to be continuous and to have continuous first and second derivatives at the knots. The particular splines (B-splines) used in this analysis are shown in Fig. B.1 and defined by

$$
\begin{array}{rcll}
 & = & \frac{1}{6}z^3 & z=(x-t_j)/d \qquad t_j \le x \le t_{j+1} \\
 & = & \frac{1}{6}(1+3(1+z(1-z))z) & z=(x-t_{j+1})/d \qquad t_{j+1} \le x \le t_{j+2} \\
b_j(x) & = & \frac{1}{6}(1+3(1+z(1-z))(1-z)) & z=(x-t_{j+2})/d \qquad t_{j+2} \le x \le t_{j+3} \\
 & = & \frac{1}{6}(1-z)^3 & z=(x-t_{j+3})/d \qquad t_{j+3} \le x \le t_{j+4} \\
 & = & 0 & \text{otherwise,}
\end{array}
\tag{B.1}
$$

where j goes from 1 to 24. The knots are given by $t_j = \frac{20}{17}(j-4) - 10$. There are a total of 20 B-splines. Each spline has the form of a bump extending over four intervals. The B-splines have the property that for $-10 \le x \le 10$: $\sum_{j=1}^{20} b_j(x) = 1$.

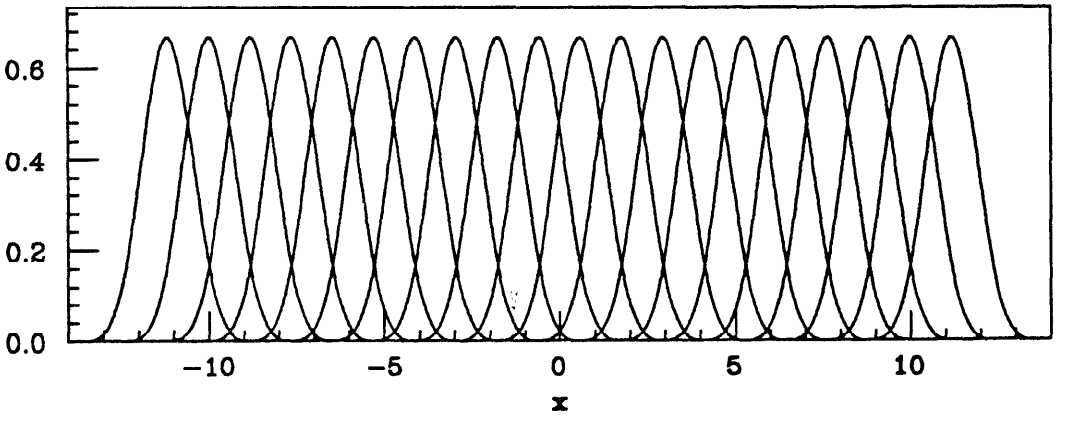

Figure B.1. The B-splines used to fit the resolution function. The twenty splines shown in this figure are defined by equation B.1.

Appendix C. The Lund Monte Carlo

The Monte Carlo generator used in this analysis (JETSET 4.3E) was developed at the University of Lund in Sweden.[63,64] It provides a phenomenological description of the hadronization process. It is motivated by the idea of a color flux tube connecting the original $q\bar{q}$ pair. The energy density in the tube is constant, which gives rise to a linear potential between the $q\bar{q}$ pair. This is consistent with what is expected from, for instance, charmonium spectroscopy. Transverse momentum is introduced by way of a tunneling approximation and gluons appear as "kinks" in the color flux tube.

The Monte Carlo has also been modified to use a different decay scheme for B-hadrons. In the case of the semileptonic decays, the existing code is satisfactory. The momenta of the D, l, and $\bar{\nu}_l$ (l = lepton) are determined by the standard V-A matrix element. The "D" is a charmed hadron made from the c-quark produced in the decay of the b-quark and from the spectator quark (or quarks) in the original B-hadron. The momentum distribution obtained is shown in Fig. C.1. The distribution in this figure agrees with the stiff distributions measured by CLEO[14] and CUSB.[15] In the case of non-leptonic decays, the existing code is not satisfactory.

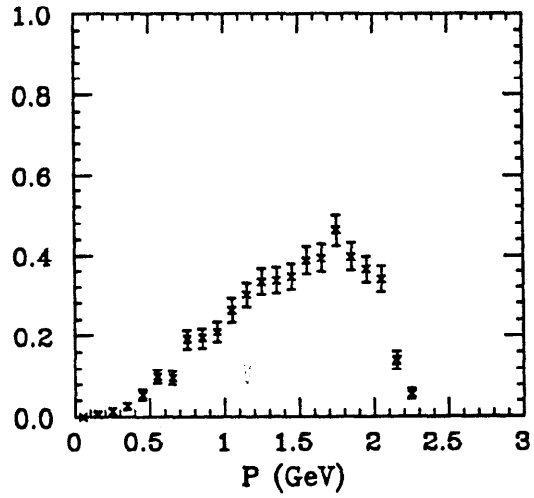

Figure C.1. The electron spectrum from the decays $B \rightarrow De\bar{\nu}_e$ and $B \rightarrow D^* e\bar{\nu}_e$ produced in the Monte Carlo. This figure shows the expected stiff momentum distribution from the V-A decay.

It uses n-body phase space to determine the momenta of the decay products, where n is a random number whose mean and width have been picked to reproduce the observed multiplicity distributions. This results in a very soft spectrum for the D^*'s and D^o's produced in the decay. Such a spectrum is not consistent with the observations of the CLEO collaboration.[65,66] Because of this an alternate decay scheme is used in this analysis. In this scheme the B-hadron is broken into three pieces: a "D" composed of the charmed quark and the spectator quark(s), plus two other quarks from the decay of the virtual W. These three particles are given momenta according to the standard V-A matrix element (just as was done in the leptonic decays). The two quarks are then fragmented according to the standard LUND fragmentation procedure. If the invariant mass of the two quark system is too small, then the quarks are assumed to fuse into a single meson and the momenta are adjusted accordingly. This procedure produces the momentum distribution for D^o's and D^*'s shown in Fig. C.2.

This Monte Carlo has also been modified to use a different fragmentation function for the production of heavy (bottom and charm) hadrons.[29]

$$D_q(z) = \frac{N}{z_q(1 - \frac{1}{z_q} - \frac{\epsilon_q}{(1-z_q)})^2} \qquad (C.1)$$

One must not confuse the z_q $(q = b, c)$ which appears in this expression with the $\bar{z}_q$ which appears in the fit to the electron spectrum. The present z is internal to the Lund Monte Carlo and is defined to be

$$z_q = \frac{E_{had} + p_{zhad}}{E_{quark} + p_{zquark}}, \qquad (C.2)$$

where p_z is a momentum along the quark direction. In equation C.1 N is a normalization constant and ϵ_q is a parameter which describes the momentum spectrum of the heavy hadrons. This parameter can be related to the $\bar{z}_q$ measured in the electron analysis by running the Lund Monte Carlo with various values of ϵ_q

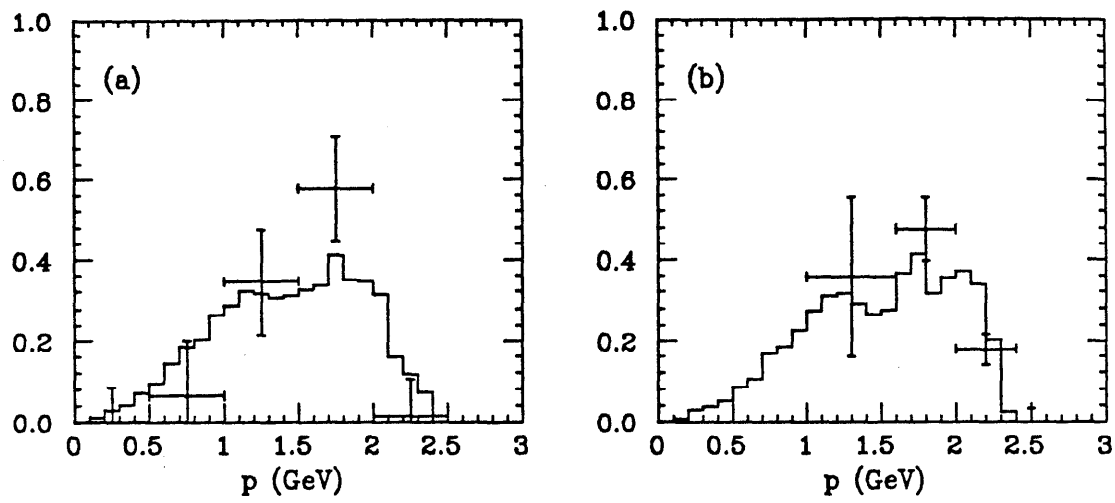

Figure C.2. The momentum distribution of D's from B-decay. Part (a) shows the momentum distribution of D^o's from the decay of B-mesons (including D^o's from D^*'s). The histogram is produced by the Monte Carlo and the data points are from CLEO.[65] Part (b) is the analogous distribution for D^*'s from the decay of B-mesons. The points in (b) are also from CLEO.[66] In both (a) and (b) structure is evident in the momentum distribution produced by the Monte Carlo. This is the result of two particle final states (i.e., $\bar{B}^o \rightarrow D^{*+}\rho^-$, etc.). Such decays have been observed.[67,68]

and finding the average value of $\bar{z}_q = \frac{E_{hadron}}{E_{beam}}$ in the events generated. The result of this exercise is shown in Fig. C.3. A similar exercise has been done for charmed particle events. In the text of this thesis when it is stated that the Monte Carlo was run with a particular value of $\bar{z}_q$, it is understood that $\bar{z}_q$ has been related to the appropriate value of ϵ_q and that this parameter is set in the Monte Carlo.

The Monte Carlo has also been modified to include the effects of the finite lifetimes of the heavy hadrons. The lifetimes of the bottom hadrons (B°, B^+, B_s, Λ_B, *etc.*) are all set equal to each other. The particular value used is given in the text where it is relevant. The charmed particle lifetimes, semileptonic branching ratios and relative fractions produced are summarized in Table C.1. This data is taken from ref. 36. A recent measurement of the D^0 lifetime[69] is somewhat larger than the value in ref. 36. In addition the data reported on in ref. 69 contains an event with a proper lifetime $\tau > 5.5$ psec. The authors

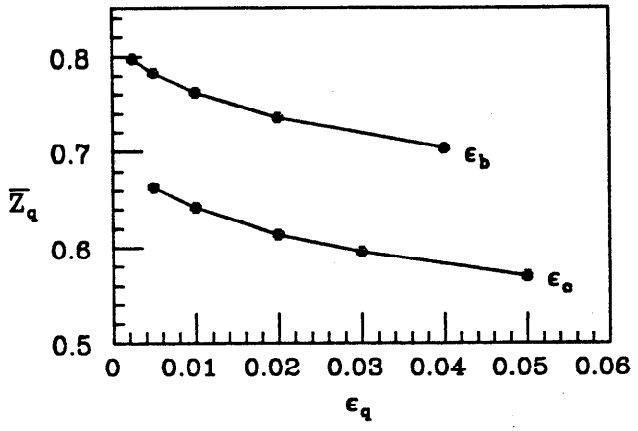

Figure C.3. Average value of $\bar{z}_b$ as a function of ϵ_b for events generated by the Lund Monte Carlo using a modified fragmentation function.

Table C.1. A list of the charmed particles in the Monte Carlo. The column labeled "BR(eX)" is the branching ratio for that particular hadron into e + anything. The column labeled "Fraction" gives the probability that a charmed quark will hadronize into the indicated particle.

Particle	Lifetime	Fraction	BR(eX)
D^0	$0.44^{+0.17}_{-0.17}$ psec	53 %	5 %
D^+	$0.92^{+0.17}_{-0.12}$ psec	27 %	16 %
F^+	$0.19^{+0.13}_{-0.07}$ psec	13 %	10 %
c - baryons	$0.23^{+0.05}_{-0.05}$ psec	7 %	5 %

estimate that the probability of observing such an event in their data sample is $6 \cdot 10^{-4}$ if the value of τ_{D0} in ref. 36 is correct. Because of this the errors on τ_{D0} have been expanded to ± 0.17 psec. The average value of the charmed particle lifetime based on this table is

$$\tau_c = 0.64^{+0.10}_{-0.08} \text{psec.}$$

Appendix D. The Bottom Quark Lifetime in the Spectator Model

In the absence of strong interaction effects, the decay of a hadron containing a bottom quark can be understood as the decay of just the bottom quark. In this picture the semileptonic part of this decay is given by the diagrams in Fig. D.1. The first diagram makes a contribution to the total rate which is proportional to $|V_{cb}|^2$ and the second makes a contribution proportional to $|V_{ub}|^2$. For the sake of definiteness only the first diagram is calculated here and the factor of $|V_{cb}|^2$ is suppressed. The relation between the two is clear. Since the mass of the intermediate vector boson $M_w = 80$ GeV is large compared to any other masses or energies appearing in the problem, the effect of the W^- can be ignored. The problem then reduces to calculating the diagram in Fig. D.2.[70,71] The matrix element for this diagram has the form:†

$$M = \frac{G}{\sqrt{2}} (\bar{c}O^\alpha b)\ (\bar{e}O_\alpha \nu_e), \tag{D.1}$$

where O_α is the standard V-A interaction:

$$O_\alpha = \gamma_\alpha(1+\gamma_5), \tag{D.2}$$

G is the Fermi coupling constant ($G = 1.166{\cdot}10^{-5}\ GeV^{-2}$) and the four component spinors $u = (b, c, e, \nu_e)$ satisfy the Dirac equation:

$$(\not{p} - m_u)u = 0 \ \text{ and} \tag{D.3}$$

$$\bar{u}(\not{p} - m_u) = 0, \qquad (\bar{u} = u^\dagger\gamma^0). \tag{D.4}$$

---

† In the following the letters generally denote 4-vectors ($p = (E_p, p_x, p_y, p_z)$); letters with arrows on top denote 3-vectors ($\vec{p} = (p_x, p_y, p_z)$); and the meaning of dot product depends on the type of vector ($p \cdot q = E_pE_q - p_xq_x - p_yq_y - p_zq_z$ or $\vec{p} \cdot \vec{q} = p_xq_x + p_yq_y + p_zq_z$). The usual Feynman dagger notation is used ($\not{p} = p_\mu\gamma^\mu$).

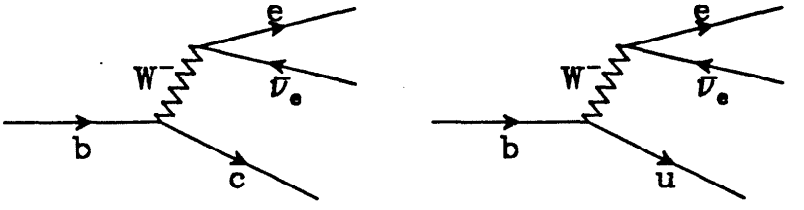

Figure D.1. Feynman diagrams for the semileptonic decay of a bottom quark.

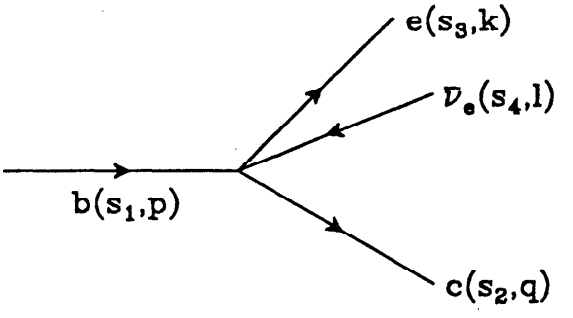

Figure D.2. Feynman diagram for the semileptonic decay of a bottom quark where the W^- has been ignored. The first variable in the parenthesis labels the spin and the second labels the 4-momenta.

The expression for M given in equation D.1 can be transformed by applying the following Fierz identities:

$$(\bar{a}\gamma^\alpha b)(\bar{c}\gamma_\alpha d) = (\bar{a}d)(\bar{c}b) - \frac{1}{2}(\bar{a}\gamma^\alpha d)(\bar{c}\gamma_\alpha b) \qquad (D.5)$$

$$-\frac{1}{2}(\bar{a}\gamma_5\gamma^\alpha d)(\bar{c}\gamma_5\gamma_\alpha b) + (\bar{a}\gamma_5 d)(\bar{c}\gamma_5 b), \text{ and}$$

$$(\bar{a}\gamma_5\gamma^\alpha b)(\bar{c}\gamma_5\gamma_\alpha d) = -(\bar{a}d)(\bar{c}b) - \frac{1}{2}(\bar{a}\gamma^\alpha d)(\bar{c}\gamma_\alpha b) \qquad (D.6)$$

$$-\frac{1}{2}(\bar{a}\gamma_5\gamma^\alpha d)(\bar{c}\gamma_5\gamma_\alpha b) - (\bar{a}\gamma_5 d)(\bar{c}\gamma_5 b).$$

Since the first and last terms in D.5 and D.6 cancel, the matrix element can be

written as

$$M = -\frac{G}{\sqrt{2}} \, (\bar{c} O^{\alpha} \nu_e) \, (\bar{e} O_{\alpha} b). \tag{D.7}$$

The complex conjugate of this is

$$M^{\dagger} = -\frac{G}{\sqrt{2}} \, (b^{\dagger} O_{\alpha}^{\dagger} \bar{e}^{\dagger}) \, (\nu_e^{\dagger} O^{\alpha \dagger} \bar{c}^{\dagger}). \tag{D.8}$$

Since $u^{\dagger} = \bar{u}\gamma^0$ and $\bar{u}^{\dagger} = \gamma^0 u$:

$$M^{\dagger} = -\frac{G}{\sqrt{2}} \, (\bar{b}\gamma^0 O_{\alpha}^{\dagger} \gamma^0 e) \, (\bar{\nu}_e \gamma^0 O^{\alpha \dagger} \gamma^0 c). \tag{D.9}$$

Since $\gamma^0 O_{\alpha}^{\dagger} \gamma^0 = O_{\alpha}$:

$$M^{\dagger} = -\frac{G}{\sqrt{2}} \, (\bar{b} O_{\alpha} e) \, (\bar{\nu}_e O^{\alpha} c). \tag{D.10}$$

Then combining equation D.10 and equation D.1 the squared magnitude of the matrix element is

$$|M|^2 = MM^{\dagger} = -\frac{G^2}{2} (\bar{c} O^{\alpha} b)(\bar{b} O_{\beta} e)(\bar{e} O_{\alpha} \nu_e)(\bar{\nu}_e O^{\beta} c). \tag{D.11}$$

This is calculated between states of known momentum and spin. Since the polarizations are not measured, one must take the appropriate sums and averages. This gives

$$\overline{|M|^2} = -\frac{G^2}{4} \sum_{\substack{s_1, s_2 \\ s_3, s_4}} \bar{c}(s_2) O^{\alpha} b(s_1) \; \bar{b}(s_1) O_{\beta} e(s_3) \; \bar{e}(s_3) O_{\alpha} \nu_e(s_4) \; \bar{\nu}_e(s_4) O^{\beta} c(s_2). \tag{D.12}$$

At this point it is useful to recall the expression for the density matrix:

$$\sum_{s} u(p,s)\bar{u}(p,s) = \not{p} + m_u, \tag{D.13}$$

so that

$$\overline{|M|^2} = -\frac{G^2}{4} \mathrm{Tr} \left\{ O^{\alpha} (\not{p} + \mathrm{m_b}) O_{\beta} (\not{k} + \mathrm{m_e}) O_{\alpha} (\not{l}) O^{\beta} (\not{q} + \mathrm{m_c}) \right\}. \tag{D.14}$$

Here the trace is over the indices on the gamma matrices. Since m_e is very small compared to typical energies in this decay it can be neglected to give:

$$\overline{|M|^2} \approx -\frac{G^2}{4}\mathrm{Tr}\left\{O^\alpha(\not{p}+m_b)O_\beta(\not{k})O_\alpha(\not{l})O^\beta(\not{q}+m_c)\right\}, \text{ or} \qquad (D.15)$$

$$\begin{aligned}\overline{|M|^2} = &-\frac{G^2}{4}\mathrm{Tr}\left\{O^\alpha \not{p} O_\beta \not{k} O_\alpha \not{l} O^\beta \not{q}\right\} \qquad (D.16)\\ &-\frac{G^2}{4}m_b\mathrm{Tr}\left\{O^\alpha O_\beta \not{k} O_\alpha \not{l} O^\beta \not{q}\right\}\\ &-\frac{G^2}{4}m_c\mathrm{Tr}\left\{O^\alpha \not{p} O_\beta \not{k} O_\alpha \not{l} O^\beta\right\}\\ &-\frac{G^2}{4}m_b m_c\mathrm{Tr}\left\{O^\alpha O_\beta \not{k} O_\alpha \not{l} O^\beta\right\}.\end{aligned}$$

The first term in this express can be written as

$$\mathrm{Tr}\left\{\gamma^\alpha(1+\gamma_5)\not{p}\gamma_\beta(1+\gamma_5)\not{k}\gamma_\alpha(1+\gamma_5)\not{l}\gamma^\beta(1+\gamma_5)\not{q}\right\}. \qquad (D.17)$$

Since $(1+\gamma_5)\gamma_\alpha = \gamma_\alpha(1-\gamma_5)$ and $(1+\gamma_5)^2 = 2(1+\gamma_5)$ this is equal to

$$8\cdot\mathrm{Tr}\left\{\gamma^\alpha(1+\gamma_5)\not{p}\gamma_\beta\not{k}\gamma_\alpha\not{l}\gamma^\beta\not{q}\right\}. \qquad (D.18)$$

Using the identities $\gamma^\alpha \not{a}\not{b}\not{c}\gamma_\alpha = -2\not{c}\not{b}\not{a}$ and then $\gamma^\alpha \not{a}\not{b}\gamma_\alpha = 4a\cdot b$ reduces this to

$$-64\ k\cdot q\ \mathrm{Tr}\left\{(1+\gamma_5)\not{p}\not{l}\right\}. \qquad (D.19)$$

The identities $\mathrm{Tr}\{\not{a}\not{b}\gamma_5\} = 0$ and $\mathrm{Tr}\{\not{a}\not{b}\} = 4\mathrm{a}\cdot\mathrm{b}$ allow this to be reduced to

$$-256\ (k\cdot q)\ (p\cdot l). \qquad (D.20)$$

The three remaining terms all contain factors of the form:

$$O^\alpha O_\beta = \gamma^\alpha(1+\gamma_5)\gamma_\beta(1+\gamma_5) \qquad (D.21)$$

$$= \gamma^\alpha \gamma_\beta (1-\gamma_5)(1+\gamma_5)$$

$$= \gamma^\alpha \gamma_\beta (1-\gamma_5^2) = 0$$

since $\gamma_5^2 = 1$. Thus

$$\overline{|M|^2} = 64G^2\ (k\cdot q)\ (p\cdot l). \qquad (D.22)$$

This is the end of the dynamical part of the calculation. The phase space and kinematical factors are accounted for by[71]

$$\Gamma_0 = \int \frac{\overline{|M|^2}}{2m_b} \frac{d^3k}{2E_k(2\pi)^3} \frac{d^3l}{2E_l(2\pi)^3} \frac{d^3q}{2E_q(2\pi)^3} (2\pi)^4 \delta^4(p-k-l-q) \qquad (D.23)$$

where E_k is the electron energy, etc. Since the neutrino is massless and the electron mass can be neglected $E_l = |\overrightarrow{l}| = l$, $E_q = |\overrightarrow{q}| = q$. For the charmed quark $E_k = (m_c^2 + |k|^2)^{\frac{1}{2}} = E$. This gives

$$\Gamma_0 = \frac{1}{16m_b(2\pi)^5} \int \overline{|M|^2} \frac{d^3k}{E} \frac{d^3l}{l} \frac{d^3q}{q} \delta^4(p-k-l-q). \qquad (D.24)$$

Plugging in $\overline{|M|^2}$ produces

$$\Gamma_0 = \frac{4G^2}{m_b(2\pi)^5} \int (p\cdot l)\ (k\cdot q)\ \frac{d^3k}{E} \frac{d^3l}{l} \frac{d^3q}{q} \delta^4(p-k-l-q). \qquad (D.25)$$

If Γ_0 is evaluated in the rest frame of the bottom quark, then $p = (m_b, 0, 0, 0)$ so that

$$\Gamma_0 = \frac{4G^2}{(2\pi)^5} \int \frac{k\cdot q}{E\ q} d^3k\ d^3l\ d^3q\ \delta^4(p-k-l-q). \qquad (D.26)$$

The $k\cdot q$ term can be written out explicitly to give

$$\Gamma_0 = \frac{4G^2}{(2\pi)^5} \int \left(1 - \frac{\overrightarrow{k}\cdot\overrightarrow{q}}{E\ q}\right) d^3k\ d^3l\ d^3q\ \delta^4(p-k-l-q). \qquad (D.27)$$

The momentum conservation part of the delta function can be used to eliminate the integration over the neutrino momentum:

$$\Gamma_0 = \frac{4G^2}{(2\pi)^5}\int\left(1-\frac{\vec{k}\cdot\vec{q}}{E\,q}\right)d^3k\;d^3q\;\delta(m_b-E-q-|\vec{k}+\vec{q}|), \qquad (D.28)$$

where $|\vec{k}+\vec{q}| = \left[k^2+q^2+2\vec{k}\cdot\vec{q}\right]^{\frac{1}{2}}$. The integral over one direction (say $\vec{k}$) and one azimuthal coordinate (say for $\vec{q}$) can both be done trivially and give factors of 4π and 2π respectively. The decay rate can then be written as

$$\Gamma_0 = \frac{8G^2}{(2\pi)^3}\int\left(1-\frac{kq\cos\theta}{E\,q}\right)k^2dk\;q^2dq\;d\cos\theta\;\delta(m_b-E-q-|\vec{k}+\vec{q}|), \quad (D.29)$$

where θ is the angle between $\vec{k}$ and $\vec{q}$. Letting $x=\cos\theta$ this can be written as

$$\Gamma_0 = \frac{8G^2}{(2\pi)^3}\int\left(1-\frac{kx}{E}\right)k^2dk\;q^2dq\;dx\;\delta(m_b-E-q-\sqrt{k^2+q^2+2kqx}). \quad (D.30)$$

The energy conservation delta function can now be used to eliminate the integration over x. Setting the argument of the delta function to zero one finds for x

$$x = \frac{2m_bE+2m_bq+2Eq-m_b^2-m_c^2}{2kq}. \qquad (D.31)$$

Recalling that

$$\int f(x)\delta\left(g(x)\right)dx = \frac{f(x_0)}{|g'(x_0)|}, \qquad (D.32)$$

where x_0 is the only solution to $g(x)=0$, one must solve for $g'(x_0)$. This produces a factor of

$$\frac{m_b-E-q}{kq.} \qquad (D.33)$$

Plugging this in gives

$$\Gamma_0 = \frac{4G^2}{(2\pi)^3}\int\left(2m_bE+2m_bq-m_b^2-m_c^2\right)(m_b-E-q)\,dEdq. \qquad (D.34)$$

This can be put into a simpler form by defining a new constant $\lambda = \frac{m_b^2+m_c^2}{2m_b}$ so that

$$\Gamma_0 = \frac{8G^2 m_b}{(2\pi)^3} \int (E+q-\lambda)\,(E+q-m_b)\,dE dq. \qquad (D.35)$$

Up to this point the limits of integration have been $\pm\infty$ for each component of the momentum. Since x is limited to being a real number on the interval $[-1,1]$, equation D.31 can not be solved for completely arbitrary values of E and q. Setting $x = \pm 1$ one can obtain (after some algebra) the following contours in the E, q plane:

$$E = \frac{2q(q-m_b)+m_b\lambda}{m_b-2q}, \qquad (D.36)$$

$$E = \lambda. \qquad (D.37)$$

They coincide at $q = 0$ and $q = \frac{m_b^2-m_c^2}{2m_b}$. The region of integration is bounded by these two contours. At this point it is straightforward to integrate with respect to E in equation D.35 and to plug in the appropriate limits. After some algebra this reduces to

$$\Gamma_0 = \frac{16G^2 m_b}{(2\pi)^3} \int_0^\delta \frac{q^2(\delta-q)^2}{(m_b-2q)^3} \left[(m_b-2q)(m_b-\delta) + \frac{4}{3}q(q-\delta)\right] dq, \qquad (D.38)$$

where $\delta = \frac{m_b^2-m_c^2}{2m_b}$. It is convenient to define a new constant $x_m = \frac{m_b^2-m_c^2}{m_b^2}$ and a new variable of integration $x = \frac{2q}{m_b}$. In terms of these [72]

$$\Gamma_0 = \frac{G^2 m_b^5}{96\pi^3} \int_0^{x_m} \frac{x^2(x_m-x)^2}{(1-x)^3} \left[(1-x_m)(3-x) + (2x-3)(x-1)\right] dx. \qquad (D.39)$$

This integral is also straightforward to evaluate. The result of this is

$$\Gamma_0 = \frac{G^2 m_b^5}{192\pi^3} \left(1 - 8z^2 + 8z^6 - z^8 - 24z^4 \ln z\right), \qquad (D.40)$$

where $z = \frac{m_c}{m_b}$. This is identical to the expression for the muon lifetime when the electron mass is taken into account.[73] This is not immediately obvious since it is

the charmed quark and not the electron which has a finite mass in this problem. From equation D.22 it is clear that the matrix element is not changed by $k \leftrightarrow q$ so that equation D.40 is as expected.

Appendix E. Results from the Electron Analysis

This appendix contains the detailed results of the fit to the electron spectrum. Each section corresponds to one run block. Each entry in each table corresponds to a single 0.5 GeV square bin in the fit. The labels on the tables indicate the lower edge of the bin. For the two isobutane run blocks, bins corresponding to $p > 2.5$ GeV are zero and left blank because of the 2.5 GeV pion threshold.

In each section the first table (labeled "Data") is just the number of tracks identified as electrons in that run block. The second table (labeled "Efficiency Corrections") contains the ratios of the efficiencies of the kinetic and the topological cuts in the electron analysis as applied to the data and the Monte Carlo (i.e., ϵ_{ij} in Equation 3.4). After this the tables come in pairs, the first for the number of tracks from a given source and the second for the fraction of the total signal in each bin which comes from this source. The tables labeled "Total background" are the sum of the backgrounds due to pions, gamma conversions, and taus.

E.1 FIRST RUN BLOCK - '82 + '83 ISOBUTANE

Data					0.00	2.0
(number of tracks)				5.00	9.00	1.5
			20.00	20.00	10.00	1.0
		52.00	51.00	28.00	26.00	0.5
	216.00	192.00	86.00	50.00	32.00	0.0 ↑ p_t
$p \rightarrow$	0.0	0.5	1.0	1.5	2.0	
Efficiency Corrections					0.91	2.0
				0.89	0.87	1.5
			0.85	0.85	0.86	1.0
		0.87	0.86	0.85	0.85	0.5
	0.88	0.83	0.82	0.79	0.77	0.0 ↑ p_t
$p \rightarrow$	0.0	0.5	1.0	1.5	2.0	
Electrons from b → e					0.69	2.0
(number of tracks)				4.58	4.57	1.5
			13.25	11.71	8.38	1.0
		19.66	12.43	8.47	8.28	0.5
	4.94	4.55	2.65	2.76	3.64	0.0 ↑ p_t
(fraction of total)					0.69	2.0
				0.72	0.73	1.5
			0.70	0.70	0.53	1.0
		0.32	0.23	0.21	0.30	0.5
	0.02	0.02	0.03	0.06	0.11	0.0 ↑ p_t
$p \rightarrow$	0.0	0.5	1.0	1.5	2.0	
Electrons from b → c → e					0.05	2.0
(number of tracks)				0.56	0.32	1.5
			1.73	1.67	0.77	1.0
		17.50	16.26	6.33	3.85	0.5
	35.54	33.16	13.36	5.96	3.00	0.0 ↑ p_t
(fraction of total)					0.05	2.0
				0.09	0.05	1.5
			0.09	0.10	0.05	1.0
		0.28	0.30	0.16	0.14	0.5
	0.15	0.16	0.15	0.14	0.09	0.0 ↑ p_t
$p \rightarrow$	0.0	0.5	1.0	1.5	2.0	
Electrons from c → e					0.17	2.0
(number of tracks)				1.20	1.39	1.5
			2.08	2.70	3.71	1.0
		15.60	24.48	22.44	13.32	0.5
	59.49	89.81	47.28	26.49	20.84	0.0 ↑ p_t
(fraction of total)					0.17	2.0
				0.19	0.22	1.5
			0.11	0.16	0.23	1.0
		0.25	0.45	0.55	0.48	0.5
	0.24	0.44	0.52	0.60	0.65	0.0 ↑ p_t
$p \rightarrow$	0.0	0.5	1.0	1.5	2.0	

Total Background				0.00	2.0
(number of tracks)			0.00	0.00	1.5
		1.81	0.75	2.99	1.0
	9.50	1.70	3.31	2.55	0.5
145.02	75.58	27.10	8.60	4.48	0.0 ↑ p_t
(fraction of total)				0.00	2.0
			0.00	0.00	1.5
		0.10	0.04	0.19	1.0
	0.15	0.03	0.08	0.09	0.5
0.59	0.37	0.30	0.20	0.14	0.0 ↑ p_t
$p \rightarrow$ 0.0	0.5	1.0	1.5	2.0	
Background Due to Pions				0.00	2.0
(number of tracks)			0.00	0.00	1.5
		1.49	0.75	2.98	1.0
	4.48	0.75	2.98	2.24	0.5
67.87	58.92	23.87	7.46	4.48	0.0 ↑ p_t
(fraction of total)				0.00	2.0
			0.00	0.00	1.5
		0.08	0.04	0.19	1.0
	0.07	0.01	0.07	0.08	0.5
0.28	0.29	0.26	0.17	0.14	0.0 ↑ p_t
$p \rightarrow$ 0.0	0.5	1.0	1.5	2.0	
Background Due to $\gamma \rightarrow e^+e^-$				0.00	2.0
(number of tracks)			0.00	0.00	1.5
		0.30	0.00	0.00	1.0
	4.98	0.92	0.30	0.30	0.5
77.12	16.63	3.23	1.13	0.00	0.0 ↑ p_t
(fraction of total)				0.00	2.0
			0.00	0.00	1.5
		0.02	0.00	0.00	1.0
	0.08	0.02	0.01	0.01	0.5
0.31	0.08	0.04	0.03	0.00	0.0 ↑ p_t
$p \rightarrow$ 0.0	0.5	1.0	1.5	2.0	
Background Due to Taus				0.00	2.0
(number of tracks)			0.00	0.00	1.5
		0.01	0.00	0.00	1.0
	0.04	0.03	0.02	0.01	0.5
0.03	0.03	0.01	0.01	0.01	0.0 ↑ p_t
(fraction of total)				0.00	2.0
			0.00	0.00	1.5
		0.00	0.00	0.00	1.0
	0.00	0.00	0.00	0.00	0.5
0.00	0.00	0.00	0.00	0.00	0.0 ↑ p_t
$p \rightarrow$ 0.0	0.5	1.0	1.5	2.0	

E.2 Second Run Block - '83 Nitrogen

Data (number of tracks)				1.00	0.00	1.00	0.00	0.00	1.00	0.00	2.0
			0.00	1.00	0.00	1.00	0.00	1.00	0.00	0.00	1.5
		8.00	4.00	4.00	0.00	1.00	3.00	0.00	1.00	0.00	1.0
	13.00	14.00	11.00	11.00	8.00	6.00	2.00	1.00	1.00	1.00	0.5
84.00	48.00	22.00	14.00	5.00	5.00	7.00	5.00	4.00	6.00	3.00	0.0 ↑ p_t
$p \rightarrow$ 0.0	0.5	1.0	1.5	2.0	2.5	3.0	3.5	4.0	4.5	5.0	
Efficiency Corrections				0.88	0.88	0.88	0.88	0.88	0.88	0.88	2.0
			0.88	0.88	0.87	0.86	0.86	0.85	0.85	0.84	1.5
		0.87	0.86	0.85	0.84	0.84	0.83	0.83	0.82	0.82	1.0
	0.87	0.84	0.84	0.83	0.81	0.80	0.79	0.79	0.79	0.79	0.5
0.86	0.82	0.79	0.77	0.76	0.77	0.79	0.79	0.79	0.78	0.78	0.0 ↑ p_t
$p \rightarrow$ 0.0	0.5	1.0	1.5	2.0	2.5	3.0	3.5	4.0	4.5	5.0	
Electrons from b → e (number of tracks)				0.19	0.31	0.14	0.08	0.04	0.13	0.00	2.0
			0.89	1.27	1.05	0.64	0.22	0.31	0.16	0.05	1.5
		2.46	2.78	2.10	1.37	1.08	0.66	0.56	0.22	0.50	1.0
	5.09	3.15	2.25	1.66	1.54	1.37	1.19	1.06	1.02	0.37	0.5
1.67	1.25	0.71	0.55	1.00	1.15	0.55	1.03	1.00	1.11	0.81	0.0 ↑ p_t
(fraction of total)				0.19	0.31	0.14	0.08	0.04	0.13	0.00	2.0
			0.71	0.80	0.75	0.56	0.22	0.31	0.16	0.05	1.5
		0.71	0.70	0.65	0.77	0.73	0.66	0.56	0.22	0.50	1.0
	0.25	0.28	0.24	0.17	0.29	0.34	0.48	0.41	0.69	0.37	0.5
0.03	0.02	0.04	0.03	0.09	0.18	0.10	0.27	0.31	0.33	0.40	0.0 ↑ p_t
$p \rightarrow$ 0.0	0.5	1.0	1.5	2.0	2.5	3.0	3.5	4.0	4.5	5.0	
Electrons from b → c → e (number of tracks)				0.00	0.00	0.02	0.00	0.00	0.00	0.00	2.0
			0.07	0.17	0.08	0.06	0.00	0.00	0.05	0.00	1.5
		0.36	0.53	0.45	0.18	0.07	0.00	0.09	0.00	0.00	1.0
	5.08	2.68	1.72	0.97	0.67	0.07	0.13	0.05	0.00	0.09	0.5
7.30	7.85	3.40	1.76	0.66	0.55	0.41	0.21	0.15	0.00	0.09	0.0 ↑ p_t
(fraction of total)				0.00	0.00	0.02	0.00	0.00	0.00	0.00	2.0
			0.05	0.11	0.06	0.05	0.00	0.00	0.05	0.00	1.5
		0.10	0.13	0.14	0.10	0.05	0.00	0.09	0.00	0.00	1.0
	0.25	0.23	0.19	0.10	0.12	0.02	0.05	0.02	0.00	0.09	0.5
0.14	0.15	0.17	0.11	0.06	0.09	0.08	0.05	0.05	0.00	0.04	0.0 ↑ p_t
$p \rightarrow$ 0.0	0.5	1.0	1.5	2.0	2.5	3.0	3.5	4.0	4.5	5.0	
Electrons from c → e (number of tracks)				0.12	0.10	0.17	0.00	0.00	0.00	0.00	2.0
			0.29	0.14	0.27	0.35	0.23	0.00	0.22	0.00	1.5
		0.55	0.64	0.70	0.14	0.32	0.21	0.22	0.16	0.10	1.0
	4.10	5.07	4.48	6.50	3.16	2.44	1.16	1.48	0.46	0.31	0.5
15.66	22.23	13.31	10.26	5.99	4.60	3.64	1.87	2.04	2.26	1.11	0.0 ↑ p_t
(fraction of total)				0.12	0.10	0.17	0.00	0.00	0.00	0.00	2.0
			0.23	0.09	0.20	0.30	0.23	0.00	0.22	0.00	1.5
		0.16	0.16	0.21	0.08	0.22	0.21	0.22	0.16	0.10	1.0
	0.21	0.45	0.49	0.65	0.59	0.61	0.47	0.57	0.31	0.31	0.5
0.29	0.42	0.66	0.64	0.53	0.72	0.68	0.49	0.64	0.67	0.55	0.0 ↑ p_t
$p \rightarrow$ 0.0	0.5	1.0	1.5	2.0	2.5	3.0	3.5	4.0	4.5	5.0	

Total Background (number of tracks)				0.00	0.00	0.00	0.00	0.00	0.00	0.00	2.0
			0.00	0.00	0.00	0.10	0.00	0.00	0.00	0.00	1.5
		0.11	0.01	0.01	0.09	0.00	0.00	0.00	0.00	0.00	1.0
	5.70	0.50	0.76	0.85	0.00	0.10	0.01	0.00	0.00	0.00	0.5
29.32	21.80	2.66	3.52	3.73	0.09	0.75	0.75	0.00	0.00	0.00	0.0 ↑ p_t
(fraction of total)				0.00	0.00	0.00	0.00	0.00	0.00	0.00	2.0
			0.00	0.00	0.00	0.09	0.00	0.00	0.00	0.00	1.5
		0.03	0.00	0.00	0.05	0.00	0.00	0.00	0.00	0.00	1.0
	0.29	0.04	0.08	0.09	0.00	0.02	0.00	0.00	0.00	0.00	0.5
0.54	0.41	0.13	0.22	0.33	0.01	0.14	0.19	0.00	0.00	0.00	0.0 ↑ p_t
$p \rightarrow$ 0.0	0.5	1.0	1.5	2.0	2.5	3.0	3.5	4.0	4.5	5.0	
Background Due to Pions (number of tracks)				0.00	0.00	0.00	0.00	0.00	0.00	0.00	2.0
			0.00	0.00	0.00	0.00	0.00	0.00	0.00	0.00	1.5
		0.00	0.00	0.00	0.00	0.00	0.00	0.00	0.00	0.00	1.0
	4.48	0.00	0.75	0.75	0.00	0.00	0.00	0.00	0.00	0.00	0.5
10.44	17.15	1.49	2.98	3.73	0.00	0.75	0.75	0.00	0.00	0.00	0.0 ↑ p_t
(fraction of total)				0.00	0.00	0.00	0.00	0.00	0.00	0.00	2.0
			0.00	0.00	0.00	0.00	0.00	0.00	0.00	0.00	1.5
		0.00	0.00	0.00	0.00	0.00	0.00	0.00	0.00	0.00	1.0
	0.22	0.00	0.08	0.07	0.00	0.00	0.00	0.00	0.00	0.00	0.5
0.19	0.32	0.07	0.19	0.33	0.00	0.14	0.19	0.00	0.00	0.00	0.0 ↑ p_t
$p \rightarrow$ 0.0	0.5	1.0	1.5	2.0	2.5	3.0	3.5	4.0	4.5	5.0	
Background Due to $\gamma \rightarrow e^+e^-$ (number of tracks)				0.00	0.00	0.00	0.00	0.00	0.00	0.00	2.0
			0.00	0.00	0.00	0.10	0.00	0.00	0.00	0.00	1.5
		0.10	0.00	0.00	0.09	0.00	0.00	0.00	0.00	0.00	1.0
	1.18	0.47	0.00	0.09	0.00	0.09	0.00	0.00	0.00	0.00	0.5
18.86	4.63	1.16	0.52	0.00	0.09	0.00	0.00	0.00	0.00	0.00	0.0 ↑ p_t
(fraction of total)				0.00	0.00	0.00	0.00	0.00	0.00	0.00	2.0
			0.00	0.00	0.00	0.08	0.00	0.00	0.00	0.00	1.5
		0.03	0.00	0.00	0.05	0.00	0.00	0.00	0.00	0.00	1.0
	0.06	0.04	0.00	0.01	0.00	0.02	0.00	0.00	0.00	0.00	0.5
0.35	0.09	0.06	0.03	0.00	0.01	0.00	0.00	0.00	0.00	0.00	0.0 ↑ p_t
$p \rightarrow$ 0.0	0.5	1.0	1.5	2.0	2.5	3.0	3.5	4.0	4.5	5.0	
Background Due to Taus (number of tracks)				0.00	0.00	0.00	0.00	0.00	0.00	0.00	2.0
			0.00	0.00	0.00	0.00	0.00	0.00	0.00	0.00	1.5
		0.01	0.01	0.01	0.00	0.00	0.00	0.00	0.00	0.00	1.0
	0.05	0.03	0.01	0.01	0.00	0.00	0.01	0.00	0.00	0.00	0.5
0.02	0.01	0.01	0.01	0.00	0.00	0.00	0.00	0.00	0.00	0.00	0.0 ↑ p_t
(fraction of total)				0.00	0.00	0.00	0.00	0.00	0.00	0.00	2.0
			0.00	0.00	0.00	0.00	0.00	0.00	0.00	0.00	1.5
		0.00	0.00	0.00	0.00	0.00	0.00	0.00	0.00	0.00	1.0
	0.00	0.00	0.00	0.00	0.00	0.00	0.00	0.00	0.00	0.00	0.5
0.00	0.00	0.00	0.00	0.00	0.00	0.00	0.00	0.00	0.00	0.00	0.0 ↑ p_t
$p \rightarrow$ 0.0	0.5	1.0	1.5	2.0							

E.3 THIRD RUN BLOCK - '84 NITROGEN

Data (number of tracks)					0.00	1.00	1.00	1.00	0.00	0.00	0.00	2.0
				3.00	1.00	1.00	0.00	1.00	1.00	0.00	0.00	1.5
			9.00	6.00	4.00	4.00	3.00	4.00	1.00	1.00	1.00	1.0
		23.00	23.00	21.00	9.00	6.00	14.00	4.00	6.00	3.00	3.00	0.5
	112.00	76.00	29.00	35.00	19.00	12.00	7.00	6.00	2.00	5.00	3.00	0.0 ↑ p_t
$p \rightarrow$	0.0	0.5	1.0	1.5	2.0	2.5	3.0	3.5	4.0	4.5	5.0	
Efficiency Corrections					0.88	0.88	0.88	0.88	0.88	0.88	0.88	2.0
				0.88	0.88	0.87	0.86	0.86	0.85	0.85	0.84	1.5
			0.87	0.86	0.85	0.84	0.84	0.83	0.83	0.82	0.82	1.0
		0.87	0.84	0.84	0.83	0.81	0.80	0.79	0.79	0.79	0.79	0.5
	0.86	0.82	0.79	0.77	0.76	0.77	0.79	0.79	0.79	0.78	0.78	0.0 ↑ p_t
$p \rightarrow$	0.0	0.5	1.0	1.5	2.0	2.5	3.0	3.5	4.0	4.5	5.0	
Electrons from b → e (number of tracks)					0.32	0.21	0.24	0.12	0.09	0.03	0.00	2.0
				1.99	2.34	0.93	0.73	0.75	0.39	0.15	0.12	1.5
			5.93	5.29	3.33	2.83	2.20	1.94	1.10	0.88	0.28	1.0
		8.90	5.60	4.24	2.10	2.44	2.17	1.86	1.66	1.65	1.42	0.5
	2.82	2.69	1.03	1.14	1.43	1.83	1.36	1.45	1.76	1.37	1.27	0.0 ↑ p_t
(fraction of total)					0.32	0.21	0.24	0.12	0.09	0.03	0.00	2.0
				0.85	0.86	0.77	0.73	0.75	0.39	0.15	0.12	1.5
			0.76	0.70	0.67	0.62	0.79	0.78	0.86	0.79	0.28	1.0
		0.32	0.23	0.23	0.16	0.24	0.31	0.37	0.44	0.63	0.56	0.5
	0.03	0.03	0.03	0.05	0.08	0.16	0.12	0.26	0.35	0.23	0.34	0.0 ↑ p_t
$p \rightarrow$	0.0	0.5	1.0	1.5	2.0	2.5	3.0	3.5	4.0	4.5	5.0	
Electrons from b → c → e (number of tracks)					0.00	0.00	0.07	0.00	0.00	0.00	0.06	2.0
				0.07	0.07	0.20	0.00	0.00	0.00	0.00	0.00	1.5
			0.68	0.73	0.56	0.54	0.44	0.06	0.00	0.06	0.00	1.0
		7.14	7.00	3.02	1.47	0.79	0.27	0.32	0.12	0.06	0.00	0.5
	16.34	16.38	6.45	3.09	1.32	0.74	0.46	0.06	0.00	0.11	0.12	0.0 ↑ p_t
(fraction of total)					0.00	0.00	0.07	0.00	0.00	0.00	0.06	2.0
				0.03	0.03	0.17	0.00	0.00	0.00	0.00	0.00	1.5
			0.09	0.10	0.11	0.12	0.16	0.03	0.00	0.06	0.00	1.0
		0.26	0.28	0.16	0.11	0.08	0.04	0.06	0.03	0.02	0.00	0.5
	0.16	0.17	0.16	0.13	0.08	0.06	0.04	0.01	0.00	0.02	0.03	0.0 ↑ p_t
$p \rightarrow$	0.0	0.5	1.0	1.5	2.0	2.5	3.0	3.5	4.0	4.5	5.0	
Electrons from c → e (number of tracks)					0.24	0.18	0.18	0.00	0.37	0.00	0.00	2.0
				0.27	0.32	0.08	0.00	0.08	0.15	0.08	0.00	1.5
			1.16	1.55	1.04	1.23	0.15	0.50	0.17	0.17	0.00	1.0
		7.42	11.20	10.46	8.94	6.20	2.93	2.84	1.96	0.89	1.14	0.5
	30.47	43.74	22.38	15.63	9.17	7.94	7.57	4.07	3.32	4.43	2.33	0.0 ↑ p_t
(fraction of total)					0.24	0.18	0.18	0.00	0.37	0.00	0.00	2.0
				0.11	0.12	0.07	0.00	0.08	0.15	0.08	0.00	1.5
			0.15	0.20	0.21	0.27	0.05	0.20	0.14	0.15	0.00	1.0
		0.27	0.45	0.56	0.70	0.60	0.42	0.57	0.52	0.34	0.44	0.5
	0.30	0.46	0.56	0.63	0.52	0.70	0.65	0.73	0.65	0.73	0.63	0.0 ↑ p_t
$p \rightarrow$	0.0	0.5	1.0	1.5	2.0	2.5	3.0	3.5	4.0	4.5	5.0	

Total Background (number of tracks)				0.00	0.00	0.00	0.00	0.00	0.00	0.00	2.0
			0.00	0.00	0.00	0.00	0.00	0.00	0.00	0.00	1.5
		0.01	0.01	0.00	0.00	0.00	0.00	0.00	0.00	0.00	1.0
	4.32	0.95	0.93	0.35	0.92	1.66	0.00	0.00	0.00	0.00	0.5
51.79	32.89	9.88	4.82	5.55	0.91	2.24	0.00	0.00	0.17	0.00	0.0 ↑ p_t
(fraction of total)				0.00	0.00	0.00	0.00	0.00	0.00	0.00	2.0
			0.00	0.00	0.00	0.00	0.00	0.00	0.00	0.00	1.5
		0.00	0.00	0.00	0.00	0.00	0.00	0.00	0.00	0.00	1.0
	0.16	0.04	0.05	0.03	0.09	0.24	0.00	0.00	0.00	0.00	0.5
0.51	0.34	0.25	0.20	0.32	0.08	0.19	0.00	0.00	0.03	0.00	0.0 ↑ p_t
$p \rightarrow$ 0.0	0.5	1.0	1.5	2.0	2.5	3.0	3.5	4.0	4.5	5.0	
Background Due to Pions (number of tracks)				0.00	0.00	0.00	0.00	0.00	0.00	0.00	2.0
			0.00	0.00	0.00	0.00	0.00	0.00	0.00	0.00	1.5
		0.00	0.00	0.00	0.00	0.00	0.00	0.00	0.00	0.00	1.0
	3.73	0.75	0.75	0.00	0.75	1.49	0.00	0.00	0.00	0.00	0.5
33.56	28.34	9.70	4.48	5.22	0.75	2.24	0.00	0.00	0.00	0.00	0.0 ↑ p_t
(fraction of total)				0.00	0.00	0.00	0.00	0.00	0.00	0.00	2.0
			0.00	0.00	0.00	0.00	0.00	0.00	0.00	0.00	1.5
		0.00	0.00	0.00	0.00	0.00	0.00	0.00	0.00	0.00	1.0
	0.13	0.03	0.04	0.00	0.07	0.21	0.00	0.00	0.00	0.00	0.5
0.33	0.30	0.24	0.18	0.30	0.07	0.19	0.00	0.00	0.00	0.00	0.0 ↑ p_t
$p \rightarrow$ 0.0	0.5	1.0	1.5	2.0	2.5	3.0	3.5	4.0	4.5	5.0	
Background Due to $\gamma \rightarrow e^+e^-$ (number of tracks)				0.00	0.00	0.00	0.00	0.00	0.00	0.00	2.0
			0.00	0.00	0.00	0.00	0.00	0.00	0.00	0.00	1.5
		0.00	0.00	0.00	0.00	0.00	0.00	0.00	0.00	0.00	1.0
	0.55	0.18	0.18	0.35	0.17	0.17	0.00	0.00	0.00	0.00	0.5
18.20	4.51	0.17	0.33	0.32	0.16	0.00	0.00	0.00	0.17	0.00	0.0 ↑ p_t
(fraction of total)				0.00	0.00	0.00	0.00	0.00	0.00	0.00	2.0
			0.00	0.00	0.00	0.00	0.00	0.00	0.00	0.00	1.5
		0.00	0.00	0.00	0.00	0.00	0.00	0.00	0.00	0.00	1.0
	0.02	0.01	0.01	0.03	0.02	0.02	0.00	0.00	0.00	0.00	0.5
0.18	0.05	0.00	0.01	0.02	0.01	0.00	0.00	0.00	0.03	0.00	0.0 ↑ p_t
$p \rightarrow$ 0.0	0.5	1.0	1.5	2.0	2.5	3.0	3.5	4.0	4.5	5.0	
Background Due to Taus (number of tracks)				0.00	0.00	0.00	0.00	0.00	0.00	0.00	2.0
			0.00	0.00	0.00	0.00	0.00	0.00	0.00	0.00	1.5
		0.01	0.01	0.00	0.00	0.00	0.00	0.00	0.00	0.00	1.0
	0.04	0.02	0.01	0.00	0.00	0.00	0.00	0.00	0.00	0.00	0.5
0.03	0.03	0.01	0.01	0.01	0.00	0.00	0.00	0.00	0.00	0.00	0.0 ↑ p_t
(fraction of total)				0.00	0.00	0.00	0.00	0.00	0.00	0.00	2.0
			0.00	0.00	0.00	0.00	0.00	0.00	0.00	0.00	1.5
		0.00	0.00	0.00	0.00	0.00	0.00	0.00	0.00	0.00	1.0
	0.00	0.00	0.00	0.00	0.00	0.00	0.00	0.00	0.00	0.00	0.5
0.00	0.00	0.00	0.00	0.00	0.00	0.00	0.00	0.00	0.00	0.00	0.0 ↑ p_t
$p \rightarrow$ 0.0	0.5	1.0	1.5	2.0	2.5	3.0	3.5	4.0	4.5	5.0	

E.4 Fourth Run Block - '84 Isobutane

Data					1.00	2.0
(number of tracks)				2.00	2.00	1.5
			7.00	11.00	7.00	1.0
		52.00	38.00	21.00	13.00	0.5
	163.00	122.00	47.00	28.00	30.00	0.0 ↑ p_t
$p \rightarrow$	0.0	0.5	1.0	1.5	2.0	
Efficiency Corrections					0.91	2.0
				0.89	0.87	1.5
			0.85	0.85	0.86	1.0
		0.87	0.86	0.85	0.85	0.5
	0.88	0.83	0.82	0.79	0.77	0.0 ↑ p_t
$p \rightarrow$	0.0	0.5	1.0	1.5	2.0	
Electrons from b → e					0.42	2.0
(number of tracks)				2.14	2.54	1.5
			8.11	5.57	5.74	1.0
		11.09	8.09	5.83	3.93	0.5
	4.48	3.11	1.31	1.77	1.81	0.0 ↑ p_t
(fraction of total)					0.42	2.0
				0.78	0.77	1.5
			0.79	0.64	0.76	1.0
		0.33	0.27	0.25	0.23	0.5
	0.03	0.03	0.03	0.06	0.08	0.0 ↑ p_t
$p \rightarrow$	0.0	0.5	1.0	1.5	2.0	
Electrons from b → c → e					0.08	2.0
(number of tracks)				0.36	0.26	1.5
			0.76	0.66	0.91	1.0
		11.12	8.68	3.66	1.36	0.5
	21.77	22.13	9.13	2.70	2.36	0.0 ↑ p_t
(fraction of total)					0.08	2.0
				0.13	0.08	1.5
			0.07	0.08	0.12	1.0
		0.33	0.29	0.16	0.08	0.5
	0.16	0.20	0.21	0.10	0.11	0.0 ↑ p_t
$p \rightarrow$	0.0	0.5	1.0	1.5	2.0	
Electrons from c → e					0.14	2.0
(number of tracks)				0.24	0.50	1.5
			1.43	1.71	0.87	1.0
		8.86	11.68	12.03	10.38	0.5
	38.59	51.64	25.29	16.82	14.37	0.0 ↑ p_t
(fraction of total)					0.14	2.0
				0.09	0.15	1.5
			0.14	0.20	0.12	1.0
		0.26	0.38	0.52	0.60	0.5
	0.28	0.47	0.58	0.59	0.65	0.0 ↑ p_t
$p \rightarrow$	0.0	0.5	1.0	1.5	2.0	

Total Background				0.00	2.0
(number of tracks)			0.00	0.00	1.5
		0.01	0.76	0.00	1.0
	2.60	1.93	1.72	1.50	0.5
72.22	32.66	7.67	7.11	3.73	0.0 ↑ p_t
(fraction of total)				0.00	2.0
			0.00	0.00	1.5
		0.00	0.09	0.00	1.0
	0.08	0.06	0.07	0.09	0.5
0.53	0.30	0.18	0.25	0.17	0.0 ↑ p_t
$p \rightarrow$ 0.0	0.5	1.0	1.5	2.0	
Background Due to Pions				0.00	2.0
(number of tracks)			0.00	0.00	1.5
		0.00	0.75	0.00	1.0
	1.49	1.49	1.49	1.49	0.5
38.04	27.60	7.46	6.71	3.73	0.0 ↑ p_t
(fraction of total)				0.00	2.0
			0.00	0.00	1.5
		0.00	0.09	0.00	1.0
	0.04	0.05	0.06	0.09	0.5
0.28	0.25	0.17	0.24	0.17	0.0 ↑ p_t
$p \rightarrow$ 0.0	0.5	1.0	1.5	2.0	
Background Due to $\gamma \rightarrow e^+e^-$				0.00	2.0
(number of tracks)			0.00	0.00	1.5
		0.00	0.00	0.00	1.0
	1.05	0.42	0.21	0.00	0.5
34.13	5.03	0.20	0.38	0.00	0.0 ↑ p_t
(fraction of total)				0.00	2.0
			0.00	0.00	1.5
		0.00	0.00	0.00	1.0
	0.03	0.01	0.01	0.00	0.5
0.25	0.05	0.00	0.01	0.00	0.0 ↑ p_t
$p \rightarrow$ 0.0	0.5	1.0	1.5	2.0	
Background Due to Taus				0.00	2.0
(number of tracks)			0.00	0.00	1.5
		0.01	0.01	0.00	1.0
	0.05	0.02	0.02	0.00	0.5
0.05	0.03	0.01	0.01	0.00	0.0 ↑ p_t
(fraction of total)				0.00	2.0
			0.00	0.00	1.5
		0.00	0.00	0.00	1.0
	0.00	0.00	0.00	0.00	0.5
0.00	0.00	0.00	0.00	0.00	0.0 ↑ p_t
$p \rightarrow$ 0.0	0.5	1.0	1.5	2.0	

REFERENCES

1. Assuming $\beta \approx 1$.
2. It is adequate in the sense that as far as it can be used to make definite predictions, these predictions agree with the experimental results.
3. M. Kobayashi and T. Maskawa, Prog. Theor. Phys. **49**, 652 (1973).
4. N. Cabibbo and L. Maiani, Phys. Lett. **87B**, 366 (1979).
5. M. Gaillard and L. Maiani, in *Proceedings of the 1979 Cargèse Summer Institute on Quarks and Leptons*, edited by M. Levy *et. al.* (Plenum, New York, 1979), p. 433.
6. A. Ali and E. Pietarinen, Nucl. Phys. **B154**, 519 (1979).
7. G. Corbo, Phys. Lett. **116B**, 298 (1982).
8. G. Corbo, Nucl. Phys. **B212**, 99 (1983).
9. N. Cabibbo and L. Maiani, Phys. Lett. **79B**, 109 (1978).
10. R. Behrends *et. al.*, Phys. Rep. **101**, 866 (1956).
11. S. Berman *et. al.*, Phys. Rep. **112**, 267 (1958).
12. T. Kinoshita and A. Sirlin, Phys. Rep. **113**, 1652 (1959).
13. G. Altarelli *et. al.*, Nucl. Phys. **B208**, 365 (1982).
14. A. Chen *et. al.*, Phys. Rev. Lett. **52**, 1084 (1984).
15. C. Klopfenstein *et. al.*, Phys. Lett. **130B**, 444 (1983).
16. J. Lee-Franzini, in *European Topical Conference on Flavor Mixing in Weak Interactions*, edited by Ling-Lie Chau (Plenum, New York, 1985), p.217.
17. B. Grinstein *et. al.*, Phys. Rev. Lett. **56**, 298 (1986).
18. B. Grinstein *et. al.*, California Institute of Technology - University of Toronto Report No. CALT-68-1311, UTPT-85-37, 1985 (unpublished).
19. D. Ouimette *et. al.*, IEEE Trans. Nucl. Sci. **29**, 290 (1982).
20. The thin beam pipe was in place during 1984 data taking only. Previous to this a 2 mm thick aluminum pipe was used.
21. G. Bowden and A. Johnston, Nucl. Inst. Meth. **222**, 610 (1984).
22. G. Bowden *et. al.*, Nucl. Inst. Meth. **228**, 207 (1984).

23. H. Yamamoto, Ph.D. thesis, California Institute of Technology Report No. CALT-68-1318, 1985 (unpublished).

24. D. Ouimette *et. al.*, IEEE Trans. Nucl. Sci. **30**, 328 (1983).

25. In addition to the ones described here, there are special classes for single electron events, selectron events, and Bhabha events where the tracks went into the pole tip counters.

26. A gap crossing is the amount of energy deposited by a single minimum ionizing particle crossing a single layer of scintillator.

27. Specifically, if $\epsilon_{ij} \rightarrow \epsilon_{ij} \pm \frac{1-\epsilon_{ij}}{2}$, then the final fitted b-lifetime changes by a negligible amount.

28. This ignores momentum mismeasurement of course. If one assumes that the detector resolution only slightly perturbs the momentum spectrum, then the track flipping will account for this also.

29. C. Peterson *et. al.*, Phys. Rev. **D 27**, 105 (1983).

30. At the risk of jumping ahead, if the fit to the electron spectrum is done using only events with $p > 1$ GeV, and the resulting fractions (see Chapter 5) and values of z_{ob} and z_{oc} used in the lifetime analysis, then the fitted value of the b-lifetime changes by an entirely negligible amount.

31. W. Bartel *et. al.*, Phys. Lett. **114B**, 71 (1982).

32. N. S. Lockyer *et. al.*, Phys. Rev. Lett. **51**, 1316 (1983).

33. E. Fernandez *et. al.*, Phys. Rev. Lett. **51**, 1022 (1983).

34. Since this cut is defined in terms of σ_δ, the fit must be done iteratively. The starting values are obtained from the widths of the distributions of tracks which are nearly vertical and nearly horizontal.

35. If this cut is allowed to vary between 2 and 3 σ, and if the corresponding corrections are applied, then the final σ_x, σ_y, and $\sigma_{\text{D.C.}}$ (see below) change by only about 2%.

36. C. Wohl *et. al.*, Rev. Mod. Phys. **56**, s1 (1984).

37. The sample used is expected to be mostly muons. Therefore, this test is most

sensitive to differences in the behavior of the detector due to the differing mass of pions and muons as compared to electrons. It is probably not very sensitive to any effects due to nuclear interactions from the pions.

38. V. Blobel, DESY Report No. 84-118, 1984 (unpublished).

39. It may be objected that the unfolding procedure is circular since it depends on τ_b. This is not the case because tracks from B-hadron decay make up only a small portion of the tracks considered. To within a factor of 2 or so, the contribution of B-decay to the $\bar{\delta}$ in hadronic events is $\frac{1}{11} \cdot 100\mu m$. (The first term comes from the production of b-events relative to all events and the second is the average δ for tracks from b-decay.) The result of this is $\approx 10\mu m$, which is small compared to the $\bar{\delta}$ for hadronic events. The relative independence of the unfolded resolution function on τ_b has been verified explicitly by recalculating the C_{ij}'s using different values of τ_b. Changing τ_b by a factor of 2 produces a negligible change in the final fitted b-lifetime.

40. G. J. Feldman *et. al.*, Phys. Rev. Lett. **48**, 66 (1982).

41. W. T. Ford *et. al.*, Phys. Rev. Lett. **49**, 106 (1982).

42. J. A. Jaros *et. al.*, Phys. Rev. Lett. **51**, 955 (1983).

43. E. Fernandez *et. al.*, Phys. Rev. Lett. **54**, 1624 (1985).

44. J. A. Jaros, in *Proceedings of the 1984 SLAC Summer Institute* edited by Patricia M. McDonough, SLAC-281, p.427.

45. This number, which is reported by the Mark II collaboration in reference 44, is used because it has the smallest errors.

46. M. Kendall and A. Stuart, *The Advanced Theory of Statistics, Volume 2, Inference and Relationship* (Macmillan, New York, 1979) p. 39.

47. D. E. Koop *et. al.*, Phys. Rev. Lett. **52**, 970 (1984).

48. T. Pal *et. al.*, Phys. Rev. **D 33**, 2708 (1986).

49. M. Piccolo, in *Proceedings of the 11th SLAC Summer Institute on Particle Physics*, edited by Patricia M. McDonough, SLAC-267, (1983), p. 673.

50. This last step is not strictly justifiable. It would require that each term in

the sum for χ^2 be Gaussianly distributed. This is true in the limit of large statistics but is clearly not the case here. It is very unlikely, however, that a rigorous determination of the confidence level would change the conclusion reached. If, for instance, the true confidence level were smaller by a factor of 10, one would be left with 4 % and 9 % which are still acceptable.

51. Note that one must require $\hat{s} \cdot \hat{p} > 0$.

52. E. Thorndike, Ann. Rev. Nucl. Part. Sci. **35**, 195(1985).

53. This number is from ref. 14. It is used because it avoids having to decide on a method of averaging the various measurements. Such an average is calculated in ref. 52 and is very close to the value used here. It is possible that different mixtures of b-hadrons are produced at the $\Upsilon(4S)$ and at a center of mass energy of 29 GeV. This could give rise to different average semileptonic branching ratios. Ref. 52 considers averages of $\Upsilon(4S)$ data and of data taken at 29 GeV and finds them to be consistent within the errors. In any event all these differences are small ($\approx 10\%$) compared to the uncertainty on τ_b.

54. Because equation 6.4 is substantially nonlinear over the range of τ_b allowed by equation 6.1, the errors on this equation have been obtained by moving τ_b by the appropriate amount, and then reevaluating equation 6.4. The systematic errors are obtained by adding the statistical and systematic errors from equation 6.1 linearly and then evaluating equation 6.4.

55. D. E. Klem *et. al.*, Phys. Rev. Lett. **53**, 1873 (1984).

56. W. Ford, in *Europhysics Topical Conference on Flavor Mixing in Weak Interactions*, edited by Ling-Lie Chou (Plenum, New York, 1984), p.77.

57. R. Prepost, in *Perspectives of Electroweak Interactions*, edited by Tran Thanh Van (Editions Frontières, Gif sur Yvette, France, 1985), p.219.

58. G. Wolf, in 22^{nd} *International Conference on High Energy Physics*, edited by A. Meyer and E. Wieczorek (Institut für Hochenergiephysik, Zeuthen, DDR, 1984), p.175.

59. M. Althoff *et. al.*, Phys. Lett. **149B**, 524 (1984).

60. J. Jaros, in *Proceedings of Physics in Collision 4*, edited by A. Seiden (Editions Frontières, Gif sur Yvette, France, 1984), p.257.

61. W. T. Eadie, D.Drijard, F. E. James, M. Roos and, B. Sadoulet, *Statistical Methods in Experimental Physics* (North-Holland, Amsterdam, 1971) p.155.

62. See ref. 38. This reference discusses a very general method for unfolding functions from data which has been smeared by detector resolution effects. This unfolding process is generally "ill-posed," which means that the solutions will often contain wild oscillations. This preprint describes a "regularization method" which removes these oscillations. The B-splines are very useful for this purpose because they make it possible to describe the curvature of the solution, $\int |f'(x)|^2 dx$, as a function only of the products of the amplitudes of the B-splines. In the present case such a regularization procedure turned out, after the fact, not to be necessary. This is the reason for representing the resolution function with the perhaps unnecessarily complicated B-splines.

63. T. Sjostrand, Comput. Phys. Commun. **27**, 243 (1982).

64. T. Sjostrand, Comput. Phys. Commun. **28**, 229 (1983).

65. J. Green, *et. al.*, Phys. Rev. Lett. **51**, 347 (1983).

66. S. E. Csorna, *et. al.*, Phys. Rev. Lett. **54**, 1894 (1985).

67. A. Chen, *et. al.*, Phys. Rev. **D 31**, 2386 (1985).

68. A. Giles, *et. al.*, Phys. Rev. **D 30**, 2279 (1984).

69. K. Abe, *et. al.*, Phys. Rev. **D 33**, (1986). They measure $\tau_{D^0} = 0.61 \pm 0.09 \pm 0.03$ psec and $\tau_{D^+} = 0.86 \pm 0.13^{+0.07}_{-0.03}$ psec.

70. L. Michel, Proc. Phys. Soc. **A63**, 514 (1949).

71. For a general review see: L.B. Okun, *Leptons and Quarks* (North Holland, Amsterdam, 1982), p.15.

72. Compare to ref. 8 equation 8 or to Appendix B of A. Ali, Z. Physik **C1**, 25 (1979).

73. H. Primakoff, in *Muon Physics, Volume II, Weak Interactions*, edited by V.

Hughes and C. Wu (Academic Press, New York, 1975), p.23.